EPJ manuscript
—

arXiv:1104.3708v2 [hep-lat] 9 Jun 2011

Transport Properties of the Quark-Gluon Plasma

A Lattice QCD Perspective

Harvey B. Meyer[1]

Institut für Kernphysik, Johannes Gutenberg Universität Mainz, 55099 Mainz, Germany

January 19, 2013

Abstract. Transport properties of a thermal medium determine how its conserved charge densities (for instance the electric charge, energy or momentum) evolve as a function of time and eventually relax back to their equilibrium values. Here the transport properties of the quark-gluon plasma are reviewed from a theoretical perspective. The latter play a key role in the description of heavy-ion collisions, and are an important ingredient in constraining particle production processes in the early universe. We place particular emphasis on lattice QCD calculations of conserved current correlators. These Euclidean correlators are related by an integral transform to spectral functions, whose small-frequency form determines the transport properties via Kubo formulae. The universal hydrodynamic predictions for the small-frequency pole structure of spectral functions are summarized. The viability of a quasiparticle description implies the presence of additional characteristic features in the spectral functions. These features are in stark contrast with the functional form that is found in strongly coupled plasmas via the gauge/gravity duality. A central goal is therefore to determine which of these dynamical regimes the quark-gluon plasma is qualitatively closer to as a function of temperature. We review the analysis of lattice correlators in relation to transport properties, and tentatively estimate what computational effort is required to make decisive progress in this field.

PACS. 12.38.Gc – 12.38.Mh – 25.75.-q

Contents

1 Introduction 1
2 Definition and Properties of Thermal Correlators . . 6
3 Retarded correlators: physical significance and analytic calculations 10
4 An Overview of Lattice Calculations 24
5 Euclidean Correlators and the Analytic Continuation Problem 35
6 Summary and Outlook 47

1 Introduction

The study of a bulk state of matter such as water begins with its equilibrium properties, such as the equation of state and the pair correlation function. However both to understand the nature of the state more deeply and to interpret the outcome of experiments, which necessarily involve time evolution at some level, it is essential to study the dynamic properties of the medium. A natural starting point is to focus on the response of the medium to long-wavelength and slow-frequency perturbations in energy density, momentum density and conserved charges. This is the realm of hydrodynamics. In addition one will at first restrict oneself to small-amplitude perturbations, and expand in them to first or perhaps second order. When studying a medium in which quantum and relativistic effects play a dominant role, the same approach proves useful. In this review we focus on the state of matter obtained when heating up ordinary nuclear matter to temperatures about 150'000 times the core temperature of the Sun. If the temperature is raised gradually, the system is thought to consist at first of a gas of hadrons (nucleons, pions, kaons, . . .). Around a temperature $T = T_c \approx$100–200MeV the hadrons 'melt', leading the system to go over to a phase where individual color charges can no longer be assigned to a unique hadron. At very high temperatures $T \gg T_c$, the color charge is transported by weakly interacting quasiparticles carrying either quark or gluon quantum numbers. This ultimate high-temperature behavior is a firm prediction of Quantum Chromodynamics (QCD), the fundamental theory that quantitatively describes the interactions of quarks and gluons, due to 'asymptotic freedom'. The latter property of the theory implies that the amplitude for large-angle scattering between two energetic particles is small. The phase above T_c is called the quark-gluon plasma. It equilibrium properties have been studied extensively using Monte-Carlo simulations [1].

Two research fields provide the main motivation to study the dynamic properties of the quark-gluon plasma:

early-universe cosmology and heavy-ion collisions. In the latter context, a bulk state of hadronic matter is formed for a time of the order of 5fm/c. Therefore dynamic properties of this hot phase are obviously important. An *a priori* open question is whether the relaxation times of the medium are short enough for it to be treated as being locally in equilibrium, thus enabling a hydrodynamic description of the system's evolution. In the context of the early universe, the strongly interacting particles were in the quark-gluon plasma phase up to a time of the order of a few microseconds, at which point the transition to the hadronic phase took place. While the universe's expansion was slow enough to allow the quark-gluon plasma to equilibrate, the production of weakly interacting particles depends on certain dynamic structure functions, as we will illustrate below, with potentially observable consequences.

Heavy ion collisions have been the experimental approach to study the quark-gluon plasma since the mid 1970's. In the standard interpretation of these reactions, a chunk is knocked out of each nucleus, and these two fragments undergo strong interactions and form a 'fireball', out of which many particles are produced. While the 'spectator' nucleons fly down the pipeline, the decay products of the fireball are recorded in particle detectors. The typically O(10^3) particles detected in the 'central rapidity region' are produced with a certain distribution in the azimuthal angle ϕ around the beam axis. The distribution is parametrized by Fourier coefficients, $dN/d\phi \propto [1 + 2\sum_n v_n \cos(2\phi)]$.

Undoubtedly one of the most striking observations from the Relativistic Heavy Ion Collider (RHIC) of Brookhaven National Laboratory is the very large elliptic flow v_2 [4,5,6,7]. The largest nuclei collided are gold nuclei, at a center-of-mass energy per nucleon of $\sqrt{s}/A = 200\text{GeV}$. Elliptical flow in peripheral heavy-ion collisions is a response of the system to the initial, anisotropic 'almond-shaped' region where the interactions take place, see Fig. (1). The measured size of elliptical flow suggests that the shear viscosity to entropy density ratio η/s of the formed system is smaller than ever observed in other systems [8]. In kinetic theory, the shear viscosity is proportional to the mean free path of the quasiparticles; a short mean free path corresponds to strongly interacting matter, which is the reason why the hot quark matter produced at RHIC has been called a strongly-coupled quark gluon plasma (sQGP).

The Pb-Pb collisions at the Large Hadron Collider (LHC) at CERN have very recently started to provide clues as to how sensitive the remarkable properties of the quark-gluon plasma are with respect to a change in temperature [9]. Inspite of an order-of-magnitude increase in the center-of-mass energy, $\sqrt{s}/A = 2.76\text{TeV}$, the charged-particle differential elliptic flow $v_2(p_t)$ is, within the uncertainties, identical to the flow observed in the Au-Au collisions at RHIC (see Fig. 2). Whatever the outcome of the ongoing analyses, the phenomenology of these collisions has generated a strong interest for transport properties in strongly coupled quantum systems [8].

Bounds on the shear viscosity can be extracted phenomenologically by comparing experimental elliptic-flow data to the dependence of v_2 on this parameter [10,11,12], as illustrated in Fig. (3). Viscous hydrodynamic calculations are technically rather involved, in particular because a naive implementation of the leading dissipative terms leads to unstable solutions. However, several groups have come up with numerical schemes (involving second-order terms) that cure this problem, and the results are in good agreement (see the review [3].) Since hydrodynamics is a good description at best for a part of the time evolution of the fireball, there are many sources of systematic uncertainty in constraining the values of η/s that are consistent with the data. The largest seems to be the sensitivity to the initial conditions. Nonetheless, the confidence in the hydrodynamic description can be increased by confronting the predictions for many correlation observables [13] to the experimental data.

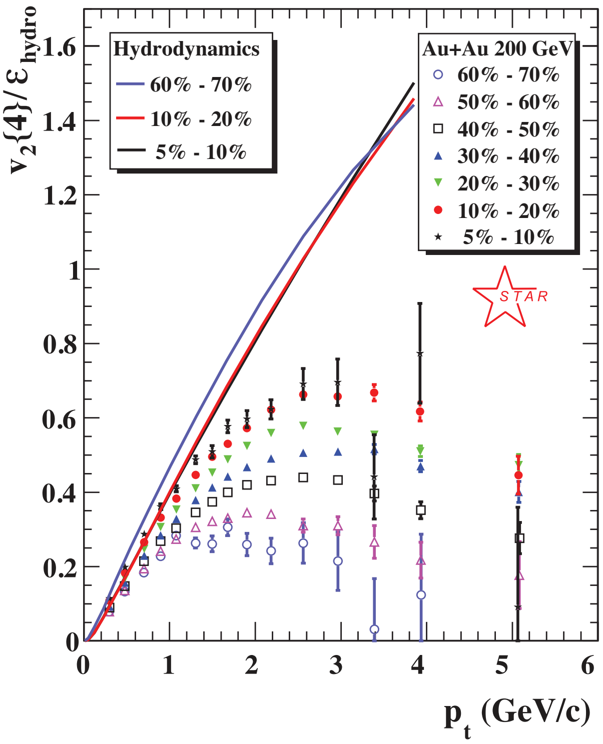

Fig. 1. The response of nuclear matter to an anisotropic initial condition in configuration space, expressed as the elliptic flow $v_2(p_t)$ per unit excentricity $\epsilon_{\text{hydro}} = \frac{\langle y^2 - x^2 \rangle}{\langle y^2 + x^2 \rangle}$, where averages are taken with respect to the number of participants in the transverse plane. The RHIC measurements (here by the STAR collaboration) are compared to the ideal hydrodynamic predictions. Figure from [2], presented in the review [3].

A conservative bound (see e.g. [3])

$$\left(\frac{\eta}{s}\right)_{\text{pheno}} \lesssim 0.40 \qquad (1)$$

has been inferred from the RHIC data as characterizing the produced medium. This number can be compared to the perturbative prediction, which in leading-logarithmic

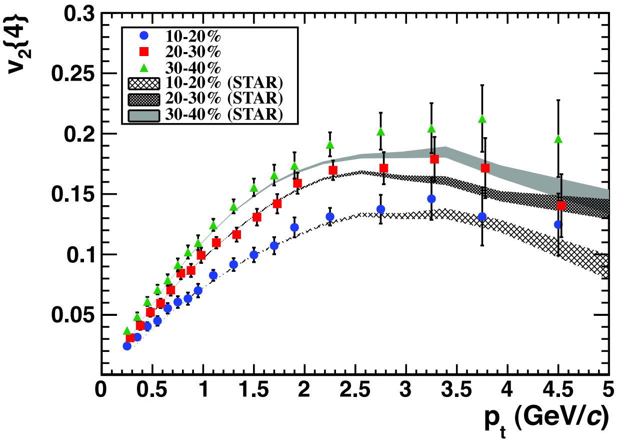

Fig. 2. Comparison of the elliptic flow measured at RHIC (Au-Au collisions at $\sqrt{s}/A = 200\text{GeV}$) and at the LHC (Pb-Pb collisions at $\sqrt{s}/A = 2.76\text{TeV}$) [9].

approximation reads

$$\left(\frac{\eta}{s}\right)_{\text{leading log}} = \frac{c}{g^4 \log(1/g)}\,, \tag{2}$$

c being a constant (see [14] and Refs. therein) and g the strong coupling constant. Numerically, $\frac{\eta}{s} \approx 2.0$ for $\alpha_s = 0.15$ at full leading order [15]. This value of the coupling is relevant to temperatures well above those reached in heavy-ion collisions, and it is uncertain how the numerical value extrapolates to lower temperatures. Since the phenomenological bound is small, it has become customary to also compare it to the value of η/s in the $\mathcal{N} = 4$ super-Yang-Mills (SYM) theory in the limit of infinite gauge coupling [16],

$$\left(\frac{\eta}{s}\right)_{\mathcal{N}=4,\lambda=\infty} = \frac{1}{4\pi}\,. \tag{3}$$

Due to the super-conformality of the $\mathcal{N} = 4$ SYM theory, the coupling constant does not evolve with the energy scale, instead it is a truly constant parameter of the theory, unlike in QCD. In fact the result (3) is much more general: it holds for a large class of field theories admitting a dual gravity description [17].

There are several other phenomenological indications that the medium created at RHIC is strongly interacting, see for instance [19]. The elliptic flow of charm quarks through the plasma is estimated experimentally via leptonic decays of D mesons [20,21]. The charm quarks exhibit a significant amount of elliptic flow, from which one infers that they kinetically thermalize on a time-scale which is small compared to the naively expected one, M/T^2 [22]. This aspect of relaxation in the quark-gluon plasma is reviewed in section (3.3).

Another indication comes from the study of jets, i.e. the passage of a fast parton through the medium which then fragments successively into the hadrons that are detected [23,24]. It is found that when triggering on a jet, the total transverse momentum is balanced not by a second back-to-back jet, but is balanced instead by a large number of particles of much lower momentum. This observation leads to the statement that the system is very ‘opaque’ to colored probes. Quantitatively it is expressed by saying that the medium admits a large jet quenching parameter $\hat{q}$. While the latter parameter is also a transport coefficient of the system, no method is known at present to connect it to Euclidean correlation functions, and we will therefore not discuss it further. We refer the reader to [25] for an introduction to the subject.

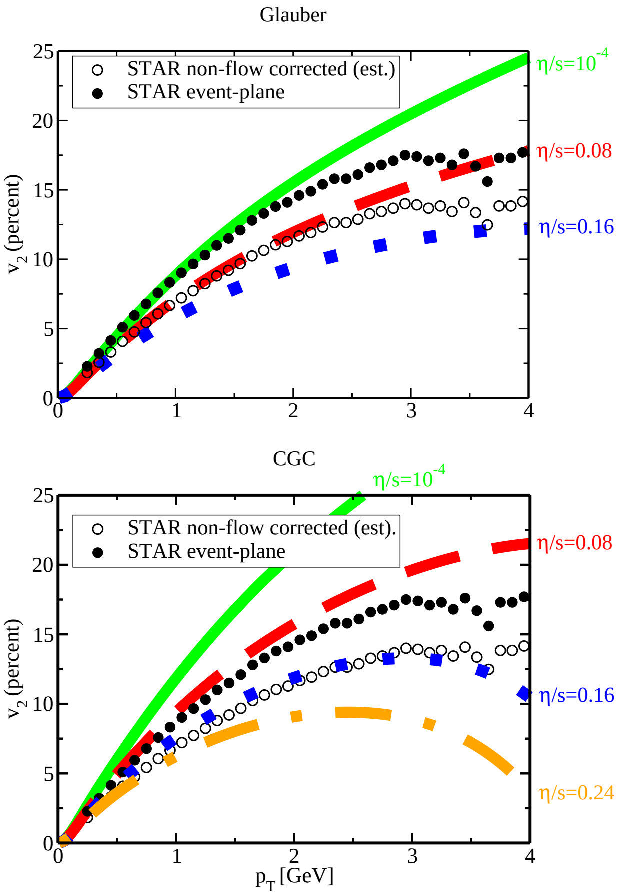

Fig. 3. The elliptic flow predicted by viscous hydrodynamics, for different values of the shear viscosity per unit entropy η/s and for Glauber (top) and color-glass condensate (bottom) initial conditions, compared to the measurements by the STAR collaboration at RHIC [18].

Before we discuss the calculation of equilibrium and transport properties of the quark-gluon plasma from first principles, we briefly remark on the relevance of transport properties of the quark-gluon plasma to early-universe cosmology. We recall that the precise understanding of primordial nucleosynthesis has repeatedly allowed cosmologists to put severe constraints on many new physics scenarios [26]. Controlling quantitatively the quark-gluon plasma era of the universe could potentially have analogous benefits.

The QCD phase transition, being a crossover at zero net baryon density [27], is not expected to lead to an observable signal in the gravitational wave background. Only an effective large baryon chemical potential could

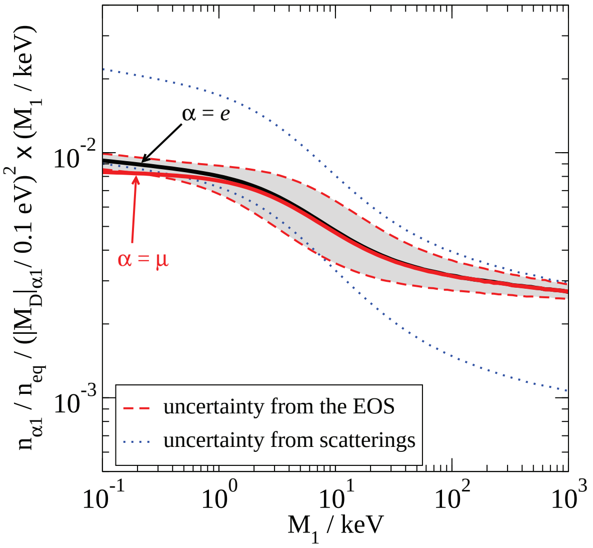

Fig. 4. Concentration of sterile neutrinos produced in the early universe [32]. The dominant uncertainty comes from the limited knowledge of the spectral function.

potentially turn it into a first order transition, where the inhomogeneous nucleation processes would make an imprint on the gravitational field (see e.g. [28] and Refs. therein). The probability per unit volume per unit time to nucleate a low-temperature phase bubble out of the high-temperature phase is proportional to a linear combination of the shear and bulk viscosities in the high-temperature phase [29]. In this way the transport properties would have an impact on cosmological observables.

A sterile, right-handed neutrino of mass $m \approx 10$keV has been proposed [30] as a candidate for warm dark matter in the context of the νMSM. In a given scenario the production of these particles happens to peak around temperatures of 0.1GeV..1GeV. Their distribution is then determined by the spectral functions of active neutrinos in a thermal QCD bath. The latter in turn can be expressed in terms of the thermal vector and axial-vector spectral functions of QCD [31]. Given the range of temperatures in which these spectral functions need to be calculated, non-perturbative methods are required for a precise and reliable result, see Fig. (4) reproduced from [32]. The example is specific, but it is likely that other particle physics models with cosmological implications can be constrained if the transport properties of QCD are determined reliably.

In order to understand the transport properties of the quark-gluon plasma, some prior familiarity with its equilibrium properties is required. We now summarize some of the essentials. The most recent published lattice QCD result for the entropy density as a function of temperature is depicted in Fig. (5) ([33]; see also [44]). The rapid rise between 150MeV and 250MeV in the number of degrees of freedom exerting pressure is clearly visible. The ratio s/T^3 then saturates and only very slowly tends towards the asymptotic 'Stefan-Boltzmann' value of

$$\left(\frac{s}{T^3}\right)_{\rm SB} = \frac{2\pi^2}{45}\left[2(N_c^2-1) + \frac{7}{8}\cdot 4N_c N_{\rm f}\right]. \tag{4}$$

One of the defining properties of a plasma is the existence of a finite correlation length over which (chromo-)electric fields are screened. Its inverse defines the Debye screening mass. In a weakly coupled plasma of quarks and gluons, the corresponding mass is calculable in perturbation theory,

$$m_D^2 = g^2\left(\frac{N_c}{3} + \frac{N_{\rm f}}{6}\right)T^2. \tag{5}$$

More generally, a widely accepted definition of m_D is that it is the smallest mass associated with a screening state odd under Euclidean time reversal [34], which corresponds to the product of time reversal and charge conjugation in Minkowski space. A unique feature of non-Abelian plasmas is that magnetic fields are also screened (unlike in the Sun), and at high temperature the corresponding lightest screening masses are parametrically of order g^2T. The smallest screening masses of states with a non-trivial flavor quantum number are close to $2\pi T$, which can be understood in terms of the minimal frequency πT associated with a fermion field in the imaginary-time formalism. Finally, as Eq. (2) illustrates, the mean path of a quark or gluon quasiparticle before it changes its direction of flight by an O(1) angle is $(g^4T)^{-1}$ [35]. These length scales associated with different physical phenomena are parametrically different at sufficiently high temperatures, but there are indications that at temperatures that can be reached in heavy-ion collisions, these scales are overlapping and even inverted in some cases, see the discussions in [36,37].

Without the RHIC and the LHC heavy-ion experiments, it would currently be unclear which of the strong or weak coupling paradigms is more appropriate to describe the quark-gluon plasma at temperatures of a few T_c. The answer must be expected to depend to some extent on the physical quantity. The convergence of perturbative calculations at $T \approx 2-3T_c$ (see for instance [38]) is in many cases poor, and these calculations are in tension with phenomenological bounds such as Eq. (1). It is therefore desirable to develop non-perturbative methods to compute transport properties of the quark-gluon plasma starting from the microscopic theory, QCD. This constitutes one of the central themes of this review. For illustration, we describe the recipe to calculate the shear viscosity in the next paragraph. The origin of this recipe will be described in detail in section (3.2).

The shear viscosity η parametrizes how efficiently the momentum of a layer of fluid (assume the momentum to be in the plane defined by that layer) diffuses in the direction orthogonal to the momentum. The diffusion constant is

$$D_{\rm sh} = \frac{\eta}{e+p}, \tag{6}$$

where $e+p$ is the enthalpy density. The time-evolution of transverse momentum is related to the transport of shear stress, T_{xy}, through the momentum conservation equation, $\partial_0 T^{0y} + \partial_x T^{xy} = 0$. A second key idea is that the response of the fluid to externally applied shear stress is encoded in the equilibrium ensemble, namely in the way the thermal fluctuations of shear-stress dissipate in real time. This is the outcome of the linear response formalism, reviewed in section (3.2). The time-correlation is encoded in

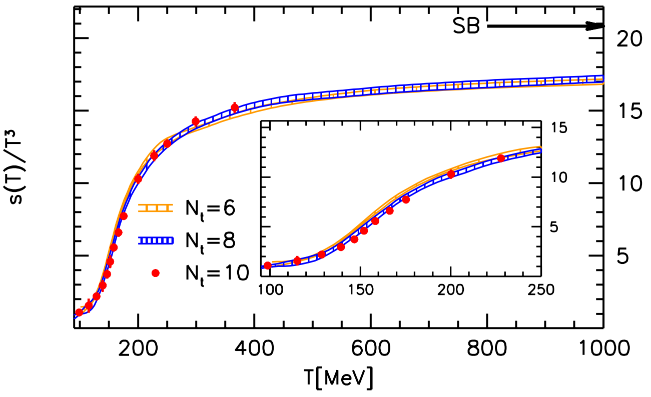

Fig. 5. The 2+1 flavor QCD entropy density in units of T^3 as a function of temperature [33].

the commutator-defined correlator $\langle [T_{xy}(t,\boldsymbol{x}), T_{xy}(0)]\rangle$. Its Fourier transform is given by the spectral function $\rho(\omega,\boldsymbol{k})$. One can then derive a 'Kubo formula', which gives the shear viscosity in terms of the low-frequency part of the spectral function,

$$\eta = \pi \lim_{\omega\to 0}\lim_{\boldsymbol{k}\to 0} \frac{\rho(\omega,\boldsymbol{k})}{\omega}. \tag{7}$$

Furthermore, the spectral function ρ is formally related to the Euclidean correlator by analytic continuation,

$$\pi\rho(\omega) = \mathrm{Im}\left(\tilde{G}_E(\omega_n \to -i[\omega + i\epsilon])\right), \tag{8}$$

where $\omega_n = 2\pi T n$ is one of the Matsubara frequencies. Alternatively, in the mixed time+spatial momentum representation, the connection is given by an integral transform,

$$G_E(t,\boldsymbol{k}) = \int_0^\infty \mathrm{d}\omega\, \rho(\omega,\boldsymbol{k})\, \frac{\cosh\omega(\frac{\beta}{2}-t)}{\sinh\beta\omega/2}\,, \tag{9}$$

where the kernel is the thermal propagator of a free scalar field. The computational recipe is thus formally straightforward: calculate the Euclidean correlator G_E, determine the spectral function by analytic continuation, and finally read off the shear viscosity from the slope of ρ at the origin. In practice however there are very significant difficulties in carrying out this program. The Euclidean correlator is normally only obtained in some approximation, either because it is expanded in powers of the coupling constant, or because it is obtained from Monte-Carlo simulations. In either case, an analytic continuation is not possible without further information or assumptions. In particular, while the Euclidean correlator can be expanded in powers of the strong coupling, the parametric dependence of the viscosity (2) makes it clear that some form of resummation of the perturbative series is required. In general it is not known how to implement the resummation in this way, and an effective kinetic theory treatment has been employed instead in [14]. In the representation (9), which is the form most commonly employed when the Euclidean correlator is determined by Monte-Carlo simulations, it is clear that the smoothness of the kernel implies that the fine features of $\rho(\omega)$ (particularly on scales $\Delta\omega \lesssim T$) are encoded in the correlator in a way which is numerically very suppressed.

We wish to illustrate the latter point somewhat more concretely. In the limit of zero-temperature, the kernel in (9) simply becomes $e^{-\omega t}$, so that the Euclidean correlator is simply the Laplace transform of the spectral function. Since Lorentz symmetry is restored in the limit $T \to 0$, the problem is simplified by going to four-momentum space. We will consider the case of the electromagnetic current correlator, $j_\mu(x) = \frac{2}{3}\bar{u}\gamma_\mu u - \frac{1}{3}\bar{d}\gamma_\mu d - \frac{1}{3}\bar{s}\gamma_\mu s + \ldots$ Current conservation and Lorentz invariance implies that a single function of four-momentum squared determines all correlation functions of the electromagnetic current,

$$\int \mathrm{d}^4x\, \langle j_\mu(x) j_\nu(0)\rangle\, e^{iq\cdot x} = (q_\mu q_\nu - q^2 g_{\mu\nu})\, \Pi(q^2). \tag{10}$$

In Euclidean four-momentum space, the spectral representation of the vacuum polarisation $\Pi(Q^2)$ reads

$$\Pi(0) - \Pi(q^2) = q^2 \int_0^\infty \mathrm{d}s \frac{\rho(s)}{s(s+q^2)}. \tag{11}$$

Via the Optical Theorem, the spectral density is accessible to experiments

$$\pi\rho(s) = \frac{s}{4\pi\alpha(s)}\sigma_{\mathrm{tot}}(e^+e^- \!\to \mathrm{hadrons}) \equiv \frac{\alpha(s)}{3\pi} R_{\mathrm{had}}(s), \tag{12}$$

where α is the QED coupling and the first equality holds up to QED corrections[1]. To illustrate the different character of a retarded correlator in the time-like and the space-like region, we reproduce in Fig. 6 the quantity R_{had}, as determined by experiments spanning several decades, as well as the corresponding vacuum polarization $\Pi(Q^2)$ in the space-like region. While many vector resonances show up in R_{had} (and therefore the spectral function), the vacuum polarisation in the space-like domain is a very smooth function. In the absence of auxiliary information, extracting the existence, position and width of each resonance from $\Pi(Q^2)$ in the space-like region is therefore a numerically ill-posed problem.

Returning to the physics of the quark-gluon plasma, it is not known precisely how far up in temperatures the sharp features of the vacuum spectral function depicted in Fig. (6) survive. However, in the case of conserved currents, the functional form of the spectral function in the region $\omega \ll \tau_{\mathrm{max}}^{-1}$, where τ_{max} is the longest relaxation time in the system, is completely determined by the continuous global symmetries of the theory[2]. The effective theory

---

[1] Neglecting the muon mass and up to QED radiative corrections, the quantity R_{had} can be expressed as $R_{\mathrm{had}}(s) \approx \frac{\sigma(e^+e^-\to\mathrm{hadrons})}{\sigma(e^+e^-\to\mu^+\mu^-)}$, which is convenient from an experimental point of view [39].

[2] At a phase transition, additional slow modes associated with an order parameter (possibly of a discrete symmetry) may play an important role.

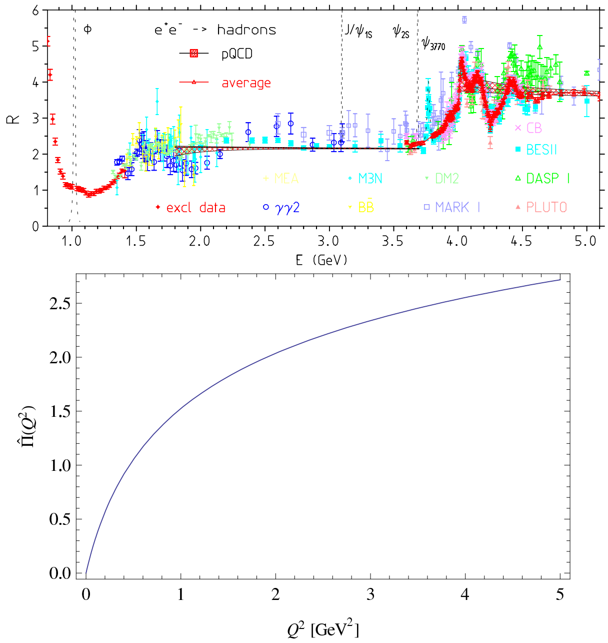

Fig. 6. The R ratio, Eq. (12), determined experimentally (Fig. from [39]), and the subtracted vacuum polarization $\widehat{\Pi}(Q^2) \equiv \Pi(0) - \Pi(Q^2)$ in the space-like domain calculated using Eq. (11,12) [40].

that describes this kinematical regime is hydrodynamics. This aspect is reviewed in section (3.2). The universality of these features means that they can be used as an ansatz for the spectral function in the small-ω region.

Beyond these universal features, the stronger assumption that the conserved charges are carried by quasiparticles leads to additional distinctive features of the spectral function around $\omega = 0$. The latter can be predicted in detail by using kinetic theory. However, thanks to the AdS/CFT correspondence, we now know of at least one theory where these features are absent (the strongly coupled $\mathcal{N} = 4$ SYM theory). We invite the reader to compare figures (11, black dashed curve) and (14, red curve), which illustrate the difference between the functional form of the shear stress spectral function in a kinetic description (Boltzmann equation) and in a theory which obviously does not admit any quasiparticles. The most important qualitative question about the quark-gluon plasma is whether, at the temperatures explored in heavy-ion collisions, it contains quasiparticles as assumed in kinetic theory. The alternative possibility is that there are instead no poles near the real axis in the retarded Green's function, other than those dictated by the symmetries of the theory; this possibility is realized in the strongly coupled SYM theory. To answer the question from first principles, we need to study the spectral functions of conserved currents in the small-frequency regime, in other words we need to study the transport coefficients.

This review is organized as follows. We start in section (Sec. 2) with a review of the analytic properties of thermal correlators, detailing in particular the relation between Euclidean and real-time correlators and giving the general tensor structure of correlators in the channels of interest (Sec. 2.5). We also describe the derivation of Kubo formulae and of the hydrodynamic predictions for spectral functions (Sec. 3.2), as well as the perturbative and kinetic theory treatments (Sec. 3.3). These results are contrasted with those obtained in strongly coupled theories via the AdS/CFT correspondence (Sec. 3.6). An overview of the state-of-the-art in lattice calculations of Euclidean correlators is given in Sec. (4), as well as of the scaling of their computational cost; we discuss the electric conductivity, the heavy-quark diffusion and shear & bulk viscosities. The analytic continuation problem is discussed from a numerical perspective in Sec. (5), where we show the advantages and disadvantages of linear and non-linear methods. We finish with a summary in Sec. (6).

There are a number of subjects closely related to those treated in this review, which are only briefly mentioned here. The extraction of a shear viscosity estimate from heavy-ion data is reviewed in [3]. The thermodynamic properties of the quark-gluon plasma [41,42,43,44,45] have been reviewed recently [1]. The behavior of spatial correlation lengths is discussed in [46,1]. For recent developments in hydrodynamics we refer to [47]. For introductions to relativistic hydrodynamics and the gauge/gravity duality, see [48,49,50]. Finally, the physics of shear viscosity and its perturbative calculation are succinctly reviewed in [51].

2 Definition and Properties of Thermal Correlators

In this section we review the different correlators relevant to calculations of transport properties. We introduce the Minkowski-space correlators and the Euclidean-space correlators, and describe how they are interrelated. Their spectral representation is given, from which the dispersion relation expressing the retarded correlator in terms of the spectral function is given. Finally, we summarize the tensor structure of the vector current and energy-momentum tensor correlators. In order to facilitate the initiation of the reader not accustomed to finite-temperature field theory, we begin with a reminder on vacuum correlators and then generalize the definitions for a thermal ensemble.

2.1 Vacuum correlation functions

We start with vacuum correlation functions, working in the metric $(-+++)$. The time-evolution operator

$$U(t) \equiv e^{-iHt} \tag{13}$$

is used to define the operators in the Heisenberg picture,

$$A(t) \equiv (U(t))^{-1} A(0) U(t). \tag{14}$$

We recall the time-ordering operation for operators,

$$T\big(A(t_1)B(t_2)\big) \equiv A(t_1)B(t_2)\,\theta(t_1-t_2) \pm B(t_2)A(t_1)\,\theta(t_2-t_1), \tag{15}$$

where the + (−) sign applies to bosonic (fermionic) operators. Time-ordered correlation functions,

$$G_T^{AB}(\omega) \equiv \int_{-\infty}^{\infty} \mathrm{d}t\, e^{i\omega t}\, \langle 0|T\big(A(t)B(0)\big)|0\rangle, \qquad (16)$$

have simple Lorentz invariance properties. For instance, the 'Feynman' propagator of a free scalar field reads

$$\langle 0|T\big(\hat\phi(t,\boldsymbol{x})\hat\phi(0)\big)|0\rangle = -i\int \frac{\mathrm{d}^D p}{(2\pi)^D}\frac{e^{ipx}}{p^2+m^2-i\epsilon}. \qquad (17)$$

Up to the factor i, the Euclidean space propagator has the same expression, but the scalar products are to be interpreted with the $(++++)$ metric, and the $i\epsilon$ prescription is unnecessary, since the integration region is well separated from the poles $p_0^2+\boldsymbol{p}^2=-m^2$.

The commutator $[A(t),B(0)]$ vanishes outside the light-cone in a relativistic causal theory. In the free scalar field theory,

$$i\theta(x_0)\langle 0|[\hat\phi(x),\hat\phi(0)]|0\rangle = \int \frac{\mathrm{d}^D p}{(2\pi)^D}\frac{e^{ipx}}{(p_0+i\epsilon)^2-\boldsymbol{p}^2-m^2}. \qquad (18)$$

The correlator

$$G_R^{AB}(\omega) = i\int_0^{\infty} \mathrm{d}t\, e^{i\omega t}\langle 0|[A(t),B(0)]|0\rangle, \qquad (19)$$

will play an important role in the following. In the vacuum it is related to the time-ordered correlator (16), which is familiar from time-dependent perturbation theory, through

$$G_R^{AB}(\omega) = \begin{cases} iG_T^{AB}(\omega) & \mathrm{Re}\,\omega > 0 \\ \big(iG_T^{B^\dagger A^\dagger}(\omega)\big)^* & \mathrm{Re}\,\omega < 0. \end{cases} \qquad (20)$$

Time-ordered products of fields appear when expressing the time-evolution operator, and in particular the S-matrix, in terms of the interaction-picture Hamiltonian. It is then natural to work with time-ordered propagators. Retarded correlation functions occur typically when coupling a field to an external source, which is switched on only for a finite time interval. A classic example is the calculation of the bremsstrahlung emitted by an electron passing near a nucleus. In the following we will deal mainly with this second type of situations, where the response comes however from a thermal medium rather than a single particle.

2.2 Finite-temperature correlation functions

In order to describe quantum statistical properties, the vacuum expectation values of operators are replaced by averages over an ensemble of states described by a density matrix $\hat\rho$. The finite-temperature, equilibrium density matrix is

$$\hat\rho \equiv \frac{1}{Z}e^{-\beta H}. \qquad (21)$$

with Z such that $\mathrm{Tr}\,\{\hat\rho\}=1$. At finite temperature, the Wightman correlation functions are defined as

$$G_>^{AB}(t) \equiv \mathrm{Tr}\,\{\hat\rho A(t)B(0)\}\,, \qquad (22)$$
$$G_<^{AB}(t) \equiv \mathrm{Tr}\,\{\hat\rho B(0)A(t)\}\,. \qquad (23)$$

Obviously, due to time-translation invariance of the equilibrium density matrix,

$$G_<^{AB}(t) = G_>^{BA}(-t). \qquad (24)$$

The reality property

$$G_>^{A^\dagger B^\dagger}(t) = G_>^{BA}(-t^*)^* \qquad (25)$$

is also easily proven. Last but not least, the definition (22) implies the Kubo-Martin-Schwinger (KMS) relation,

$$G_>^{AB}(t) = G_>^{BA}(-t-i\beta). \qquad (26)$$

In fact, it can be shown that this property uniquely characterizes the equilibrium density matrix. An obvious consequence of Eq. (26) is that the thermal correlation function of an anticommutator is periodic in the imaginary time direction.

The expectation value of a commutator,

$$G^{AB}(t) = i\mathrm{Tr}\,\{\hat\rho[A(t),B(0)]\} = i\left(G_>^{AB}(t)-G_<^{AB}(t)\right), \qquad (27)$$

is physically important. The commutator vanishes outside the light-cone, a reflection of the causality of the theory. Using Eq. (24) and (25), one obtains the properties

$$G^{AB}(-t) = -G^{BA}(t), \qquad (28)$$
$$G^{A^\dagger B^\dagger}(t) = G^{AB}(t^*)^*. \qquad (29)$$

The Euclidean correlator is defined as

$$G_E^{AB}(t) = G_>^{AB}(-it). \qquad (30)$$

As a special case of (26), it obeys the relation

$$G_E^{BA}(\beta-t) = G_E^{AB}(t)\,. \qquad (31)$$

The Fourier transform of $G^{AB}(t)$ defines the so-called spectral function [3]

$$\rho^{AB}(\omega) = \frac{1}{2\pi i}\int_{-\infty}^{+\infty} \mathrm{d}t\; e^{i\omega t}\; G^{AB}(t). \qquad (32)$$

It enjoys the symmetry properties

$$\rho^{AB}(-\omega) = -\rho^{BA}(\omega), \qquad (33)$$
$$\rho^{A^\dagger B^\dagger}(\omega) = \rho^{BA}(\omega)^*. \qquad (34)$$

The integral tranform over the positive half-axis

$$G_R^{AB}(\omega) = \int_0^{\infty} \mathrm{d}t\, e^{i\omega t} G^{AB}(t) \qquad (35)$$

---

[3] We use a small 'hat' on the density matrix to distinguish it from the spectral function.

is analytic in the half complex plane $\mathrm{Im}(\omega) > 0$. It is called the retarded correlator and plays a central role in linear response theory, as we shall see shortly. The Euclidean correlator can be expressed as a Fourier series on the interval $0 \le t < \beta$,

$$G_E(t) = T\sum_{\ell\in\mathbb{Z}} G_E^{(\ell)}\, e^{-i\omega_\ell t}\,, \tag{36}$$

$$G_E^{(\ell)} = \int_0^\beta dt e^{i\omega_\ell t} G_E(t)\,, \tag{37}$$

where $\omega_\ell = \omega_M \cdot \ell = 2\pi T\,\ell$ and we have dropped the label specifying the operators A, B.

For real ω and in finite volume, ρ is a distribution, namely a discrete sum of delta functions. However, in the infinite-volume limit of an interacting theory, it is typically a smooth function, except possibly at a finite number of points. The most useful relations among the correlators are those that survive the infinite-volume limit.

Using the KMS relation (26), one easily shows

$$\begin{aligned}\int_{-\infty}^{\infty}\frac{\mathrm{d}t}{2\pi}\,e^{i\omega t}\langle\{A(t),B(0)\}_\pm\rangle &= (1\pm e^{-\beta\omega})\cdot \\ &\cdot\int_{-\infty}^{\infty}\frac{\mathrm{d}t}{2\pi}\,e^{i\omega t}G_>^{AB}(t),\end{aligned} \tag{38}$$

whence it follows that the spectral function is related to the anticommutator-defined correlator via

$$\rho^{AB}(\omega) = \tanh\left(\tfrac{\beta\omega}{2}\right)\int_{-\infty}^{\infty}\frac{\mathrm{d}t}{2\pi}\,e^{i\omega t}\langle\{A(t),B(0)\}_+\rangle. \tag{39}$$

This relation is known as the fluctuation-dissipation theorem. Since the retarded propagator G_R^{AB} can be expressed in terms of ρ^{AB} via a dispersion relation, it so follows that the knowledge of the anticommutator-defined correlator also determines G_R^{AB}.

2.3 Spectral representation and relations between correlators

Using (28) and (29), one shows that

$$\rho^{AB}(\omega) = \frac{1}{2\pi i}\left(G_R^{AB}(\omega) - G_R^{B^\dagger A^\dagger}(\omega)^*\right). \tag{40}$$

In particular, for $B = A^\dagger$, the spectral function is identically related to the imaginary part of the retarded correlator,

$$\rho^{AA^\dagger}(\omega) = \frac{1}{\pi}\,\mathrm{Im}\,G_R^{AA^\dagger}(\omega) \in \mathbb{R}\,. \tag{41}$$

The spectral representation of the correlators is useful to prove further relations between the Euclidean and real-time correlators. Inserting two complete sets of energy eigenstates in the definitions of $G(t)$ and $G_E(t)$, one obtains

$$\begin{aligned}G^{AB}(t) &= \frac{2i}{Z}\sum_{m,n} A_{mn}B_{nm}e^{-\beta(E_n+E_m)/2} \\ &\qquad\cdot\sinh(\tfrac{\beta E_{nm}}{2})e^{-iE_{nm}t},\end{aligned} \tag{42}$$

$$G_E^{AB}(t) = \frac{1}{Z}\sum_{n,m} A_{mn}B_{nm}e^{-\beta E_m}e^{-E_{nm}t}\,, \tag{43}$$

where we employ the notation

$$E_{nm} = E_n - E_m\,, \qquad A_{nm} = \langle n|A(t=0)|m\rangle\,. \tag{44}$$

The expression for the retarded correlator reads

$$\begin{aligned}G_R^{AB}(\omega) &= \frac{2}{Z}\sum_{n,m}\frac{-A_{mn}B_{nm}}{\omega - E_{nm}} \\ &\qquad\cdot\; e^{-\beta(E_n+E_m)/2}\sinh(\tfrac{\beta E_{nm}}{2})\,,\end{aligned} \tag{45}$$

and the spectral function for $\omega\in\mathbb{R}$ takes the form

$$\begin{aligned}\frac{\rho^{AB}(\omega)}{2\sinh\frac{\beta\omega}{2}} &= \frac{1}{Z}\sum_{m,n}A_{mn}B_{nm} \\ &\qquad\cdot\; e^{-\beta(E_n+E_m)/2}\delta(\omega - E_{nm})\,.\end{aligned} \tag{46}$$

For $B = A^\dagger$, this formula can be obtained by taking the imaginary part of $G_R(\omega + i\epsilon)$ and using the standard representation of the delta function, $\delta(\omega) = \frac{1}{\pi}\frac{\epsilon}{\omega^2+\epsilon^2}$. After some algebraic manipulations, one finds for the Fourier coefficients (37)

$$G_E^{(\ell)} = \frac{2}{Z}\sum_{m,n}e^{-\beta(E_n+E_m)/2}\sinh(\beta E_{nm}/2)\frac{A_{mn}B_{nm}}{-i\omega_\ell + E_{nm}}. \tag{47}$$

Formulae (45) and (47) show in particular that

$$G_R(i\omega_\ell) = G_E^{(\ell)}\,, \quad \ell \neq 0\,. \tag{48}$$

Thus the frequency-space Euclidean correlator is the analytic continuation of the retarded correlator; the situation in the complex ω plane is illustrated in Fig. (7). For $\ell = 0$, one has to remember that the retarded correlator was initially defined for $\mathrm{Im}(\omega) > 0$. Therefore its value at the origin can only be defined as $\lim_{\epsilon\to 0_+} G_R(i\epsilon)$. This value differs from $G_E^{(0)}$ if the spectral function is singular at the origin. Specifically,

$$\frac{\rho(\omega)}{\omega} = A\delta(\omega) + \text{finite} \quad \Rightarrow \quad G_E^{(0)} - \lim_{\epsilon\to 0_+} G_R(i\epsilon) = A. \tag{49}$$

Finally, it is easy to verify, using Eq. (43) and (46), that the configuration-space Euclidean correlator can be obtained from ρ via

$$\begin{aligned}G_E^{AB}(t) + G_E^{AB}(\beta - t) &= \\ \int_{-\infty}^{\infty}\mathrm{d}\omega\rho^{AB}(\omega)&\frac{\cosh\omega(\frac{\beta}{2}-t)}{\sinh\beta\omega/2},\end{aligned} \tag{50}$$

$$\begin{aligned}G_E^{AB}(t) - G_E^{AB}(\beta - t)& \\ = \int_{-\infty}^{\infty}\mathrm{d}\omega\rho^{AB}(\omega)&\frac{\sinh\omega(\frac{\beta}{2}-t)}{\sinh\beta\omega/2}.\end{aligned} \tag{51}$$

These formulae show that the part of the Euclidean correlator that is even (odd) around $t = \beta/2$ is in correspondence with the odd (even) part of the spectral function. In particular, $B = A$ implies that the Euclidean correlator is symmetric around $t = \beta/2$ and that the spectral function is an odd function, while $B = A^\dagger$ implies that both $G_E^{AA^\dagger}(t)$ and $\rho^{AA^\dagger}(\omega)$ are real. In most cases of interest, $B = A = A^\dagger$, so that both properties are satisfied.

A simple calculation based on the explicit expression for the spectral density (46), or alternatively a contour integration, then leads to the Kramers-Kronig relation

$$\int_{-\infty}^{+\infty} d\omega\, \rho(\omega)\frac{\omega}{\omega^2+\omega_{\mathrm{I}}^2} = G_R(i\omega_{\mathrm{I}})\,, \qquad \forall \omega_{\mathrm{I}} > 0. \quad (52)$$

Starting from (52), it is easy to derive by recursion the following equalities,

$$\begin{aligned}(-1)^n \frac{d^{2n}}{d\omega_{\mathrm{I}}^{2n}} G_R(i\omega_{\mathrm{I}}) &= \int_{-\infty}^{\infty} d\omega \rho^{(2n)}(\omega)\,\frac{\omega}{\omega^2+\omega_{\mathrm{I}}^2}\,,\\ (-1)^{n+1}\frac{d^{2n+1}}{d\omega_{\mathrm{I}}^{2n+1}}G_R(i\omega_{\mathrm{I}}) &= \int_{-\infty}^{\infty} d\omega\rho^{(2n+1)}(\omega)\frac{\omega_{\mathrm{I}}}{\omega^2+\omega_{\mathrm{I}}^2}\\ &\overset{\omega_I\to 0}{=} \pi\rho^{(2n+1)}(\omega=0)\,. \quad (53)\end{aligned}$$

Thus at the origin, the even derivatives of the retarded correlator along the imaginary axis are given by integrals over the spectral density, while the odd derivatives are equal to the corresponding derivatives of the spectral function, see the bottom panel of Fig. (7).

2.4 Properties of the Euclidean correlator

We have seen that in configuration space, the Euclidean correlator is defined as the analytic continuation of the Wightman correlator, while in frequency space it turns out to be the analytic continuation of the retarded correlator. Here we discuss further relations between Euclidean and real-time correlators.

In our subsequent considerations, it will prove useful to express the Euclidean correlator in terms of the real-time correlator $G(t)$, in order to analyze the contribution of hydrodynamic modes. The relation between the Euclidean correlator and the real-time correlator is

$$G_E(t) = T\int_0^\infty \mathrm{d}u\, G(u)\,\frac{\sinh(2\pi T u)}{\cosh(2\pi T u) - \cos(2\pi T t)}. \quad (54)$$

The moments

$$\begin{aligned}\frac{d^{2n}}{dt^{2n}}G_E(t) &\overset{t=\frac{\beta}{2}}{=} \int_0^\infty \mathrm{d}\omega \frac{\omega^{2n}\rho(\omega)}{\sinh\frac{\beta\omega}{2}} \quad (55)\\ &= (-1)^n\int_0^\infty \mathrm{d}t\, G(t)\,\frac{d^{2n}}{dt^{2n}}\tanh(\pi T t)\end{aligned}$$

are thus expressed in terms of integrals of $G(t)$.

The positivity of $\rho(\omega)/\omega$ implies the positivity of certain linear combinations of the Euclidean correlator. For instance,

$$G_E^{(0)} - G_E^{(\ell)} = \omega_\ell^2\int_{-\infty}^\infty \frac{\mathrm{d}\omega}{\omega}\,\frac{\rho(\omega)}{\omega^2+\omega_\ell^2}\,, \quad (56)$$

$$3G_E^{(0)} - 4G_E^{(\ell)} + G_E^{(2\ell)} = 12\omega_\ell^4\int_{-\infty}^\infty \frac{\mathrm{d}\omega}{\omega} \quad (57)$$
$$\cdot\,\frac{\rho(\omega)}{(\omega^2+\omega_\ell^2)(\omega^2+4\omega_\ell^2)}\,.$$

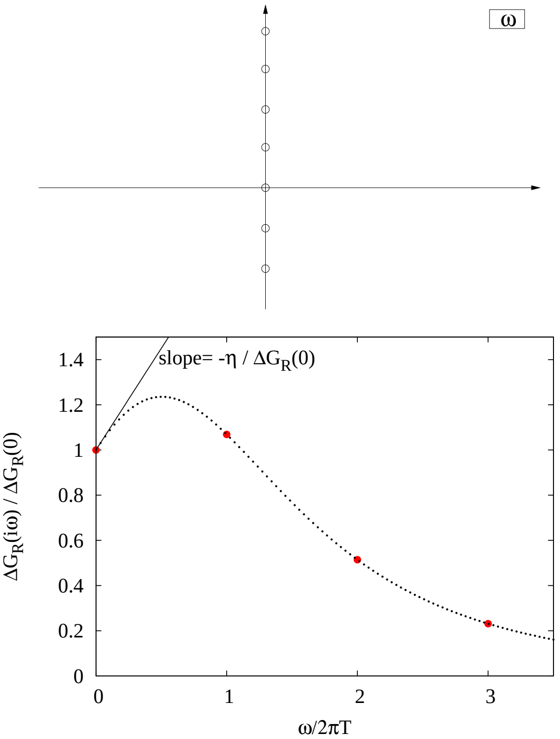

Fig. 7. Top: Analytic structure of the retarded correlator $G_R(\omega)$ in the complex ω plane. At the circled values of ω on the positive imaginary axis, it coincides with the Euclidean correlator (Eq. 48). Bottom: At the origin, the odd derivatives of G_R along the imaginary axis coincide with the corresponding derivatives of $\mathrm{Im}\, G_R$ along the real axis. These odd derivatives are given by transport coefficients (section 3.2). The figure illustrates a case where one subtraction has been made to make the dispersion integral converge.

We note that relations (54) and (56–57) only hold if the integrals converge in the ultraviolet. In the cases of interest, at least one subtraction (for example between two different temperatures) is necessary.

In a number of contexts, it is natural to study the difference between the finite-temperature and the zero-temperature spectral density. For that purpose it is convenient to define the so-called reconstructed Euclidean correlator by

$$G_E^{\mathrm{rec}}(t,T;T') \equiv \int_0^\infty d\omega\rho(\omega,T')\frac{\cosh\omega(\frac{\beta}{2}-t)}{\sinh\omega\beta/2}\,. \quad (58)$$

The identity $(0 \le t \le \beta)$

$$\frac{\cosh\omega(\frac{\beta}{2}-t)}{\sinh\omega\beta/2} = \sum_{m\in\mathbf{Z}} e^{-\omega|t+m\beta|} \quad (59)$$

allows us to derive in particular the exact relations

$$G_E^{\mathrm{rec}}(t,T;0) = \sum_{m\in\mathbb{Z}} G_E(|t+m\beta|, T=0)\,, \quad (60)$$

$$G_E^{\mathrm{rec}}(t,T;\tfrac{1}{2}T) = G_E(t,\tfrac{1}{2}T) + G_E(\beta-t,\tfrac{1}{2}T)\,. \quad (61)$$

2.5 Tensor Structure of Thermal Correlators

The tensor structure of current correlators and energy-momentum tensor correlators was worked out systematically in [52]. We simply report the results in the notation of section (2.1). Setting

$$A(t) \leftarrow \tfrac{1}{\sqrt{V}} \int \mathrm{d}\boldsymbol{x}\, e^{-i\boldsymbol{k}\cdot\boldsymbol{x}}\, J^{\mu}(t,\boldsymbol{x}) \tag{62}$$

and defining $B(t)$ analogously in terms of J^{ν}, we denote their retarded correlator by $G_R^{\mu\nu}(k)$, with $k=(k_0,\boldsymbol{k})$. Due to conservation of the current,

$$k_\mu G_R^{\mu\nu}(k) = 0. \tag{63}$$

Then one defines the tensors

$$P_{\mu\nu} = \eta_{\mu\nu} - \frac{k_\mu k_\nu}{k^2}\,; \quad P_{\mu\nu} = P^L_{\mu\nu} + P^T_{\mu\nu}\,, \tag{64}$$

$$P^T_{00} = 0, \quad P^T_{0i} = 0 \quad P^T_{ij} = \delta_{ij} - \frac{k_i k_j}{\boldsymbol{k}^2}. \tag{65}$$

The current-current correlator then has the generic tensor structure

$$G_{R,\mu\nu}(k) = P^T_{\mu\nu}\, \Pi^T(k_0,\boldsymbol{k}^2) + P^L_{\mu\nu}\, \Pi^L(k_0,\boldsymbol{k}^2). \tag{66}$$

Thus there are two independent functions of two variables $(k_0,\boldsymbol{k}^2)$ that characterize all possible current correlators at finite temperature. When $\Pi^T = \Pi^L = \Pi$, one recovers the familiar vacuum form of the correlators, which are characterized by a single function of k^2.

For the energy-momentum tensor, one proceeds similarly. Setting

$$A(t) \leftarrow \tfrac{1}{\sqrt{V}} \int \mathrm{d}\boldsymbol{x}\, e^{-i\boldsymbol{k}\cdot\boldsymbol{x}}\, T^{\mu\nu}(t,\boldsymbol{x}) \tag{67}$$

and defining $B(t)$ analogously in terms of $T^{\alpha\beta}$, we denote their retarded correlator by $G_R^{\mu\nu\alpha\beta}(k)$, with $k=(k_0,\boldsymbol{k})$. At zero temperature and in D spacetime dimensions,

$$G_R^{\mu\nu,\alpha\beta}(k) = P^{\mu\nu}P^{\alpha\beta}G_B(k^2) + H^{\mu\nu,\alpha,\beta}G_S(k^2), \tag{68}$$

$$H^{\mu\nu,\alpha,\beta} = \tfrac{1}{2}(P^{\mu\alpha}P^{\nu\beta} + P^{\mu\beta}P^{\nu\alpha}) - \tfrac{1}{D-1}P^{\mu\nu}P^{\alpha\beta}. \tag{69}$$

The tensor H is the polarization tensor of a spin-two particle. The correlators of the energy-momentum tensor are thus characterized by two independent functions. At finite temperature, the tensor H splits into three independent tensors, which one may choose as follows

$$H_{\mu\nu,\alpha,\beta} = S_{\mu\nu,\alpha\beta} + Q_{\mu\nu,\alpha\beta} + L_{\mu\nu,\alpha\beta}, \tag{70}$$

$$S_{\mu\nu,\alpha\beta} = \tfrac{1}{2}\big[P^T_{\mu\alpha}P^L_{\nu\beta} + P^L_{\mu\alpha}P^T_{\nu\beta} + P^T_{\mu\beta}P^L_{\nu\alpha} + P^L_{\mu\beta}P^T_{\nu\alpha}\big], \tag{71}$$

$$\begin{aligned} Q_{\mu\nu,\alpha\beta} = \tfrac{1}{D-1}\big[&(D-2)P^L_{\mu\nu}P^L_{\alpha\beta} + \tfrac{1}{D-2}P^T_{\mu\nu}P^T_{\alpha\beta} \\ &- (P^T_{\mu\nu}P^L_{\alpha\beta} + P^L_{\mu\nu}P^T_{\alpha\beta})\big]. \end{aligned} \tag{72}$$

The general tensor form of the correlators in a rotationally invariant average over states is

$$\begin{aligned} G_{R,\mu\nu,\alpha\beta}(k) = &\big(P^T_{\mu\nu}P^T_{\alpha\beta} + \tfrac{1}{2}(P^T_{\mu\nu}P^L_{\alpha\beta} + P^L_{\mu\nu}P^T_{\alpha\beta})\big)C_T(k_0,\boldsymbol{k}^2) \\ &+ \big(P^L_{\mu\nu}P^L_{\alpha\beta} + \tfrac{1}{2}(P^T_{\mu\nu}P^L_{\alpha\beta} + P^L_{\mu\nu}P^T_{\alpha\beta})\big)C_L(k_0,\boldsymbol{k}^2) \\ &+ S_{\mu\nu,\alpha\beta}G_1(k_0,\boldsymbol{k}^2) + Q_{\mu\nu,\alpha\beta}G_2(k_0,\boldsymbol{k}^2) + L_{\mu\nu,\alpha\beta}G_3(k_0,\boldsymbol{k}^2). \end{aligned}$$

There are thus five independent functions that specify all correlators of $T_{\mu\nu}$. The function G_1 describes the shear channel, G_3 describes the tensor channel, while G_2, C_L and C_T describe the sound channel and the bulk channel. When $C_L = C_T$ and $G_1 = G_2 = G_3$, one recovers the zero-temperature form (68).

3 Retarded correlators: physical significance and analytic calculations

In the previous section, we introduced the definitions of the Minkowski and Euclidean correlators, and described their basic analytic and tensorial structure. Here, using linear response theory, we want to show why the retarded correlator $G_R(\omega,\boldsymbol{q})$ is physically important. We then go through the most important analytic techniques to calculate the thermal spectral functions in different regimes. We describe how hydrodynamics makes a prediction for the low frequency and momentum dependence of $G_R(\omega,\boldsymbol{q})$, and thereby establish the Kubo formulae which allow one to compute transport coefficients *ab initio* (section 3.2). When the hydrodynamic regime arises from the many-body dynamics of weakly interacting quasiparticles, additional structures can be predicted in the spectral functions using kinetic theory (sections 3.3, 3.4). We also review the predictions of perturbation theory and the operator product expansion at high frequencies in section (3.5). Some important results on spectral functions obtained using AdS/CFT results are summarized in (3.6). Thermal sum rules provide useful constraints on the spectral functions, and those are discussed in section (3.7). Finally, certain aspects of spectral functions in finite volume (where lattice QCD simulations take place) are pointed out in section (3.8).

3.1 Linear response theory

When studying dynamical properties of a thermal medium, it is natural to start with small amplitude departures from equilibrium. The linear response of the system to ‘slow’ perturbations is sensitive to the first order transport coefficients, as well shall see in the next section.

We assume that the time-dependent perturbation of the system by an external classical field $f(t)$ coupling to operator B is described by a Hamiltonian of the form

$$H_f(t) = H - f(t)B(t), \tag{73}$$

H being the Hamiltonian of the unperturbed system. The perturbation leads to a ‘response’ of physical quantities, i.e. a change in their expectation values with respect to the unperturbed ensemble. The evolution equation of an operator A is given by

$$i\frac{\partial}{\partial t}A(t) = -[H_f(t), A(t)]. \tag{74}$$

One then finds that to linear order in f, the expectation value of A in the perturbed system minus its unperturbed value is [53]

$$\begin{aligned}\delta\langle A(t)\rangle &\equiv \langle A(t)\rangle_f - \langle A(0)\rangle \\ &= \int_{-\infty}^{t} \mathrm{d}t' G^{AB}(t-t')f(t') + \mathrm{O}(f^2).\end{aligned} \tag{75}$$

Equation (75) is the master formula of linear response theory. It shows that the correlator G^{AB} determines the response of an observable A to a time-dependent external field that couples to B.

A source term of the form

$$f(t) = e^{\epsilon t}\theta(-t) f_0 \tag{76}$$

is often adopted to study how the system relaxes back to equilibrium after having been perturbed adiabatically. The static susceptibility is defined as the expectation value of A at $t=0$,

$$\delta\langle A(t=0)\rangle_f = \chi_s^{AB}\, f_0. \tag{77}$$

From (75), it follows that

$$\chi_s^{AB} = \int_0^\infty \mathrm{d}t\, e^{-\epsilon t}\, G^{AB}(t) \;= G_R^{AB}(i\epsilon). \tag{78}$$

Looking back at Eq. (49), the zero-frequency Euclidean correlator is thus equal to the static susceptibility, barring any delta function at the origin in the spectral function.

Integrating both sides of (75), $\int_0^\infty \mathrm{d}\omega\, e^{i\omega t}(.)$, one obtains for the adiabatic perturbation (76)

$$G_R^{AB}(\omega) f_0 = \langle \delta A(0)\rangle_f + i\omega \int_0^\infty \mathrm{d}t\, e^{i\omega t}\langle \delta A(t)\rangle_f. \tag{79}$$

This formula shows that the relaxation of observable A back to its equilibrium value determines the retarded correlator $G_R^{AB}(\omega)$. Since the late-time relaxation is described by hydrodynamic evolution, this equation can be exploited to obtain a prediction of the small-ω functional form of G_R, thereby establishing the famous Kubo formulae for the transport coefficients (section (3.2)).

In the special case where B is a conserved charge, i.e. $[H,B]=0$, the situation described by $\epsilon = 0$ simply corresponds to looking at the system with a small 'chemical potential' f_0. Then $\delta\langle A(0)\rangle$ is given by the thermodynamic derivative

$$\delta\langle A(0)\rangle = \beta f_0 \left(\langle B(0)A(0)\rangle - \langle A\rangle\langle B\rangle\right), \tag{80}$$

which, by comparison with (78), shows that it is natural to assign to the retarded correlator at the origin the value

$$G_R^{AB}(0) = \beta\left(\langle A(0)B(0)\rangle - \langle A\rangle\langle B\rangle\right). \tag{81}$$

3.2 Hydrodynamic predictions and Kubo Formulas

There are recent excellent reviews on the modern point of view on hydrodynamics [47,3,48]. Therefore our goal here is simply to describe the important steps that lead to the Kubo formulae. Hydrodynamics can be thought of as a low-energy effective theory:

- it makes predictions for the low-momentum behavior of correlation functions.
- it has unknown 'low-energy constants', which are called the transport coefficients in this context: they are the coefficients of a derivative expansion.
- their values can be determined by a matching procedure with the underlying quantum field theory.
- the number of coefficients grows with the order of the expansion.

For illustration we choose as a simple example the case of the diffusion of a massive particle species in a thermal medium. In the hydrodynamic treatment, the conservation of the particle number is expressed by the classical equation

$$\partial_t n + \nabla\cdot \boldsymbol{j} = 0. \tag{82}$$

Second, a phenomenological 'constitutive equation' must be introduced to close the system of equations for $(n,\boldsymbol{j})$. To leading order in gradients, it takes the form of Fick's law,

$$\boldsymbol{j} = -D\nabla n. \tag{83}$$

The conjugate variable to particle density is the chemical potential. The particle number can be perturbed by

$$\begin{aligned} H_\mu &= H - \textstyle\int \mathrm{d}\boldsymbol{x}\, \mu(t,\boldsymbol{x}) n(t,\boldsymbol{x}), \qquad (84)\\ \mu(t,\boldsymbol{x}) &= \mu(\boldsymbol{x})\, e^{\epsilon t}\theta(-t),\end{aligned}$$

(see Eq. (73) with $f \leftarrow \mu$ and $B \leftarrow n$).

We define

$$\tilde n(\omega,\boldsymbol{k}) = \int_0^\infty e^{i\omega t}\int \mathrm{d}\boldsymbol{x}\, e^{-i\boldsymbol{k}\cdot\boldsymbol{x}} n(t,\boldsymbol{x}) \tag{85}$$

$$\mu(\boldsymbol{k}) = \int \mathrm{d}\boldsymbol{x}\, e^{-i\boldsymbol{k}\cdot\boldsymbol{x}}\, \mu(\boldsymbol{x}). \tag{86}$$

The conservation equation (82) becomes, with the help of Fick's law, the diffusion equation

$$\partial_t n(\boldsymbol{x}) = D\nabla^2 n(\boldsymbol{x}). \tag{87}$$

Upon Fourier transformation, the solution reads

$$\tilde n(\omega,\boldsymbol{k}) = \frac{n(0,\boldsymbol{k})}{-i\omega + D\boldsymbol{k}^2}. \tag{88}$$

The initial condition $n(0,\boldsymbol{k})$ is determined by the static susceptibility (see Eq. (77,78)),

$$n(0,\boldsymbol{x}) = \textstyle\int_0^\infty \mathrm{d}t\, e^{-\epsilon t} \int \mathrm{d}\boldsymbol{x}'\, G^{nn}(t,\boldsymbol{x}-\boldsymbol{x}')\,\mu(\boldsymbol{x}'), \tag{89}$$

$$G^{nn}(t,\boldsymbol{x}) = i\langle [n(t,\boldsymbol{x}), n(0)]\rangle, \tag{90}$$

or equivalently,

$$n(0,\boldsymbol{k}) = \chi_s(\boldsymbol{k})\mu(\boldsymbol{k}), \tag{91}$$

$$\chi_s(\boldsymbol{k}) = \textstyle\int_0^\infty \mathrm{d}t\, e^{-\epsilon t}\, G^{nn}(t,\boldsymbol{k}), \tag{92}$$

$$G^{nn}(t,\boldsymbol{k}) = \textstyle\int \mathrm{d}\boldsymbol{x} e^{-i\boldsymbol{k}\cdot\boldsymbol{x}} G^{nn}(t,\boldsymbol{x}). \tag{93}$$

This completes the prediction for the long-wavelength, late-time evolution of the particle number density. In Fourier space, the relaxation rate of a particle density perturbation of wave-vector $\boldsymbol{k}$ is encoded in the position of a pole in the lower-half of the complex ω plane, namely $\omega_{\rm pole}(\boldsymbol{k}^2) = -iD\boldsymbol{k}^2$. The residue of the pole is given by the initial condition of the relaxation process, which is determined by the static susceptibility.

We can now straightforwardly apply the general formula (79). In spatial Fourier space, this equation applies for each wave-vector $\boldsymbol{k}$. The result is

$$G_R^{nn}(\omega,\boldsymbol{k}) = \frac{1}{\mu(\boldsymbol{k})}\left(n(0,\boldsymbol{k}) + i\omega\tilde{n}(\omega,\boldsymbol{k})\right) \tag{94}$$

$$= \chi_s(\boldsymbol{k}) + i\omega\,\frac{\chi_s(\boldsymbol{k})}{-i\omega + D\boldsymbol{k}^2} \tag{95}$$

$$= \frac{(D\boldsymbol{k}^2)^2 + i\omega\, D\boldsymbol{k}^2}{\omega^2 + (D\boldsymbol{k}^2)^2}\,\chi_s(\boldsymbol{k}). \tag{96}$$

In particular, the imaginary part yields the spectral function,

$$\frac{\rho^{nn}(\omega,\boldsymbol{k})}{\omega} = \frac{\chi_s(\boldsymbol{k})}{\pi}\frac{D\boldsymbol{k}^2}{\omega^2+(D\boldsymbol{k}^2)^2}. \tag{97}$$

This equation describes how the transport properties are encoded in the low-frequency and low-momentum part of the spectral function. The Kubo formula is usually expressed in terms of the longitudinal part of the current correlator. The latter is related to the density correlator by the conservation equation, $\rho_L(\omega,\boldsymbol{k}) = \frac{\omega^2}{\boldsymbol{k}^2}\rho^{nn}(\omega,\boldsymbol{k})$ (see Eq. 66),

$$\frac{\rho_L(\omega,\boldsymbol{k})}{\omega} = \frac{\chi_s(\boldsymbol{k})}{\pi}\frac{D\omega^2}{\omega^2+(D\boldsymbol{k}^2)^2}, \tag{98}$$

implying in particular the Kubo formula

$$D\chi_s^N = \pi \lim_{\omega\to 0}\lim_{\boldsymbol{k}\to 0}\frac{\rho_L(\omega,\boldsymbol{k})}{\omega}. \tag{99}$$

Here $\chi_s^N = \beta\int \mathrm{d}\boldsymbol{x}\, n(t,\boldsymbol{x})n(0)$ is the particle number susceptibility.

3.2.1 Electric conductivity

The correlators of the electromagnetic current are of particular phenomenological interest. We will therefore study the operator

$$A(t) = \int \mathrm{d}\boldsymbol{x}\, e^{-i\boldsymbol{k}\cdot\boldsymbol{x}}\, j_\mu^{\rm em}(t,\boldsymbol{x}). \tag{100}$$

In QCD, the explicit expression of the electromagnetic current is

$$j_\mu^{\rm em}(x) = \tfrac{2}{3}\bar{u}\gamma_\mu u - \tfrac{1}{3}\bar{d}\gamma_\mu d - \tfrac{1}{3}\bar{s}\gamma_\mu s + \ldots \tag{101}$$

In the long-wavelength limit the current-current correlator is given by the diffusion equation, as described in the previous section, however here we wish to include the effects of coupling the current to an external electromagnetic field, $(\boldsymbol{E},\boldsymbol{B})$, and to promote the treatment to second order accuracy – we follow the treatment of [54]. For a linearized theory invariant under parity, Fick's law generalizes to

$$\boldsymbol{j} = -D\nabla n + \sigma\boldsymbol{E} - (\sigma\tau_J)\partial_t\boldsymbol{E} + \kappa_B\nabla\times\boldsymbol{B}. \tag{102}$$

However, a perturbation of the form $\mu(x)+A_0(x)=0$ does not affect the system at all, since both μ and A_0 couple to the charge density in the Hamiltonian. Therefore only the gradient of this combination can appear in the constitutive equation (102), and we conclude

$$\chi_s D = \sigma. \tag{103}$$

The conservation law $\partial_t n + \nabla\cdot\boldsymbol{j} = 0$ can be solved for $n(\omega,\boldsymbol{k})$ in the presence of a sinusoidal electric field. Teaney and Hong [54] find (for $\boldsymbol{k} = (0,0,k)$)

$$G_R^{zz}(\omega,\boldsymbol{k}) = D\chi_s\,\frac{\omega^2 + i\tau_J\omega^3}{-i\omega + D\boldsymbol{k}^2}, \tag{104}$$

$$G_R^{xx}(\omega,\boldsymbol{k}) = iD\chi_s\omega - D\chi_s\tau_J\omega^2 + \kappa_B\boldsymbol{k}^2. \tag{105}$$

From here, one can write out Kubo formulae for the second-order coefficients τ_J and κ_B,

$$D\chi_s\tau_J = -\frac{\partial}{\partial\omega^2}G_R^{xx}(\omega,\boldsymbol{k})_{\omega=\boldsymbol{k}=0}\,, \tag{106}$$

$$\kappa_B = \frac{\partial}{\partial k^2}G_R^{xx}(\omega,\boldsymbol{k})_{\omega=\boldsymbol{k}=0}\,. \tag{107}$$

The coefficient κ_B can thus be extracted directly by differentiating the static Euclidean correlator with respect to $\boldsymbol{k}$ at $\omega = 0$. An interesting fact about κ_B is that it vanishes in a theory whose transport properties are described by the Boltzmann equation [54]. Thus measuring a non-vanishing κ_B would exhibit a shortcoming of kinetic theory. The parameter κ_B is dimensionless and based on the constitutive equation for the current, it describes how a flux of particles $\int \mathrm{d}\boldsymbol{\sigma}\cdot\boldsymbol{j}$ appears through a surface around which there is a non-vanishing circulation of a magnetic field, $\oint \mathrm{d}\boldsymbol{\ell}\cdot\boldsymbol{B}$. Finally, using the conservation law, the spectral function for the charge density n is modified from Eq. (97) to

$$\frac{\rho^{nn}(\omega,\boldsymbol{k})}{\omega} = \frac{\chi_s}{\pi}\frac{D\boldsymbol{k}^2(1+\tau_J D\boldsymbol{k}^2)}{\omega^2+(D\boldsymbol{k}^2)^2}. \tag{108}$$

We conclude this section by noting that the vector spectral function determines the emission rate of photons by the thermal medium. Denoting the spectral function of components μ and ν of the electromagnetic current by $\rho_{\mu\nu}$, the real photon emissivity of the quark-gluon plasma at temperature T is related to the vector spectral function through (see [55] and Refs. therein)

$$\frac{\mathrm{d}\varGamma_\gamma}{\mathrm{d}^3\boldsymbol{k}} = \left(\textstyle\sum_{\rm f} Q_{\rm f}^2\right)\frac{\alpha_{\rm em}}{2\pi}n_B(\omega,T)\;\left.\frac{\rho^\mu_\mu(\omega,\boldsymbol{k},T)}{\omega}\right|_{\omega=|\boldsymbol{k}|}, \tag{109}$$

where $Q_{\rm f}$ are the fractional charges of the quarks. Thus the conductivity σ determines in particular the emission of soft photons. Similarly, the thermal production rate of dilepton pairs of invariant mass $M^2 = \omega^2 - \boldsymbol{k}^2$ reads

$$\frac{\mathrm{d}N_{\ell_+\ell_-}}{\mathrm{d}\omega\,\mathrm{d}\boldsymbol{k}^3} = \left(\textstyle\sum_{\rm f} Q_{\rm f}^2\right)\frac{\alpha_{\rm em}^2}{3\pi^2}\,n_B(\omega)\,\frac{\rho^\mu_\mu(\omega,\boldsymbol{k},T)}{\omega^2-\boldsymbol{k}^2}. \tag{110}$$

3.2.2 Kubo formulae for the transport of energy and momentum

In hydrodynamics the transport of energy and momentum is determined by the correlation functions of the energy-momentum tensor $T_{\mu\nu}$. It is a symmetric, $T_{\mu\nu} = T_{\nu\mu}$, and conserved operator, $\partial_\mu T_{\mu\nu} = 0$. The constituent equation, which is the analogue of Fick's law (83), reads

$$\begin{aligned} T^{\mu\nu} &= (e+P)u^\mu u^\nu + P g^{\mu\nu} \qquad (111)\\ &\quad - \eta P^{\mu\alpha}P^{\nu\beta}\left(\partial_\alpha u_\beta + \partial_\beta u_\alpha - \tfrac{2}{3} g_{\alpha\beta}\partial\cdot u\right) - \zeta P^{\mu\nu}(\partial\cdot u). \end{aligned}$$

where $u_\mu u^\mu = -1$. The energy-momentum conservation equations, together with Eq. (111), determine the evolution of the velocity and temperature fields, $u_\mu(x)$ and $T(x)$. To study the linearized modes of these equations, one writes $\boldsymbol{u}_\perp$, $\boldsymbol{u}_{||}$ and e in Fourier components as in (85), and decomposes the velocity field into a longitudinal and a transverse part with respect to $\boldsymbol{k}$, $\boldsymbol{u}_{||}$ and $\boldsymbol{u}_\perp$. The retarded correlator for the momentum density, $\boldsymbol{\pi} = (e+p)\boldsymbol{u}$ is then obtained along the same lines as Eq. (96). We refer to appendix C of [56] for the details and quote the leading-order result

$$G_R^{\pi_\perp\pi_\perp}(\omega,\boldsymbol{k}) = \frac{\eta\boldsymbol{k}^2}{-i\omega + \frac{\eta\boldsymbol{k}^2}{e+p}}\,, \qquad (112)$$

$$G_R^{\pi_{||}\pi_{||}}(\omega,\boldsymbol{k}) = \frac{i\omega\Gamma_s\boldsymbol{k}^2 - (c_s\boldsymbol{k})^2}{\omega^2 - (c_s\boldsymbol{k})^2 + i\omega\Gamma_s\boldsymbol{k}^2}\,. \qquad (113)$$

respectively for the transverse and longitudinal momentum density, where

$$\Gamma_s = \frac{\frac{4}{3}\eta + \zeta}{e+p} \qquad (114)$$

determines the damping of sound waves. The spectral functional is obtained by taking the imaginary part,

$$\frac{\rho^{\pi_\perp\pi_\perp}(\omega,\boldsymbol{k})}{\omega} = \frac{1}{\pi}\frac{\eta\boldsymbol{k}^2}{\omega^2 + (\frac{\eta\boldsymbol{k}^2}{e+p})^2}\,, \qquad (115)$$

$$\frac{\rho^{\pi_{||}\pi_{||}}(\omega,\boldsymbol{k})}{\omega} = \frac{e+p}{\pi}\frac{\omega^2\Gamma_s\boldsymbol{k}^2}{(\omega^2 - c_s^2\boldsymbol{k}^2)^2 + (\omega\Gamma_s\boldsymbol{k}^2)^2}\,. \qquad (116)$$

The first line corresponds to the shear channel, the second to the sound channel. The former admits a diffusive pole, similar to the pole appearing in the vector current correlator. The latter contains a pole at $\omega = \pm c_s k - \frac{1}{2}i\Gamma k^2$, which corresponds to the propagation of sound waves with velocity c_s with an attenuation $\propto e^{-\frac{1}{2}\Gamma_s k^2 t}$ for a plane wave of wavelength $\lambda = \frac{2\pi}{k}$. The sound channel spectral function is displayed for two different values of the wavelength in Fig. (8). Using the momentum conservation equations (see 73) and denoting the spectral function of $T_{\mu\nu}$ and $T_{\rho\sigma}$ by $\rho^{\mu\nu,\rho\sigma}$, one then obtains the Kubo formulae, for $\boldsymbol{k} = (0,0,k)$,

$$\eta(T) = \pi\lim_{\omega\to 0}\frac{\rho^{13,13}(\omega,\boldsymbol{0},T)}{\omega}, \qquad (117)$$

$$\zeta(T) = \frac{\pi}{9}\sum_{i,j=1}^{3}\lim_{\omega\to 0}\frac{\rho^{ii,jj}(\omega,\boldsymbol{0},T)}{\omega}. \qquad (118)$$

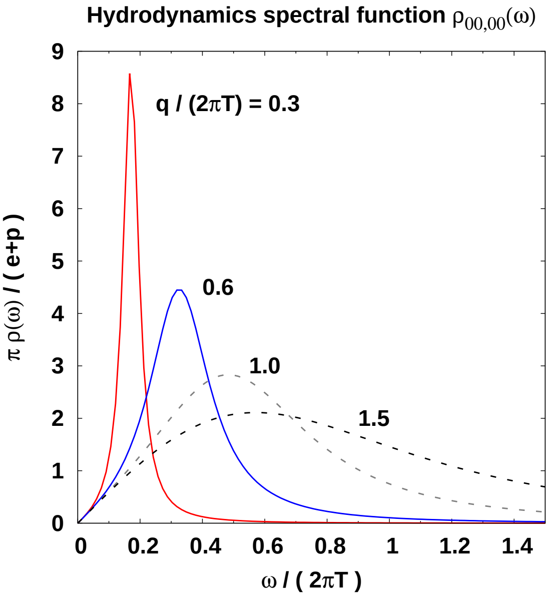

Fig. 8. The sound channel spectral function: correlator of T_{00} at finite spatial momentum $\boldsymbol{q}$. This is the functional form predicted by hydrodynamics at small momenta and frequencies, for $c_s^2 = \frac{1}{3}$ and $T\Gamma_s = \frac{1}{3\pi}$. For comparison with Fig. (15), the dashed curves are displayed, although they correspond to momenta well beyond the validity of hydrodynamics.

In numerical practice, it is convenient if $\rho(\omega)/\omega$ behaves smoothly at $\omega\to 0$. It is therefore important to study the spectral function in detail in this region [57,58]. One finds that

$$\frac{1}{9}\sum_{i,j=1}^{3}\frac{\rho_{ii,jj}(\omega,\boldsymbol{0},T)}{\omega} = \frac{\zeta}{\pi} + (e+p)c_s^2\delta(\omega) + \dots \qquad (119)$$

contains a delta function at the origin (see section 3.7). When studying the bulk (scalar) channel it is then preferable to work instead with the operator

$$T^{kk} + 3c_s^2 T^{00}, \qquad (120)$$

written here in Euclidean metric, whose spectral function at $\boldsymbol{k} = 0$ is identical to the spectral function of T^{kk}, except for not having the delta function at the origin.

The most general constitutive equation for $T^{\mu\nu}$ has been worked out to second order in gradients of the velocity fields for a conformal theory [59], and more recently even in the non-conformal case [47]. In the conformal case, there are five new transport coefficients, denoted $\tau_\Pi, \kappa, \lambda_1, \lambda_2, \lambda_3$. These second-order transport coefficients can be obtained from Kubo formulae,

$$\kappa = -\frac{\partial^2}{\partial k^2}G_R^{12,12}(\omega,\boldsymbol{k})_{\omega=k=0} \qquad (121)$$

$$\eta\tau_\Pi - \tfrac{1}{2}\kappa = \frac{1}{2}\frac{\partial^2}{\partial\omega^2}G_R^{12,12}(\omega,\boldsymbol{k})_{\omega=k=0}. \qquad (122)$$

still with the convention $\boldsymbol{k} = (0,0,k)$. A physically important effect is that at second order, the speed of sound receives a wavelength-dependent correction [59], $\omega = c_s(q)q$

with

$$c_s(q) = c_s \left\{ 1 + \frac{\Gamma_s}{2} q^2 \left(\tau_\Pi - \frac{\Gamma_s}{4c_s^2} \right) + \mathrm{O}(q^4) \right\} . \qquad (123)$$

This provides a way to determine the coefficient τ_Π if the leading-order speed of sound $c_s^2 = \frac{\partial p}{\partial e}$ and Γ_s are known. The coefficient κ can be extracted directly from the $\omega = 0$ Euclidean correlator[4]. The coefficients $\lambda_{1,2,3}$ influence the hydrodynamic evolution only at quadratic order in the amplitude of the perturbation. Kubo formulae have been derived for these second-order coefficients as well [60]. They involve three-point functions of the energy-momentum tensor. Among them we want to point out the expression for λ_3, which like κ can be extracted directly from a Euclidean correlator,

$$\lambda_3 = 6 \lim_{p,q\to 0} \frac{\partial^2}{\partial q \partial k} G_E^{11,01,01}(q,k), \qquad (124)$$

where $\boldsymbol{q}$ and $\boldsymbol{k}$ are aligned along the $\hat{3}$-direction. Both κ and λ_3 have a finite limit when the coupling constant goes to zero [59,60].

The physical interpretation of the second order coefficients is not always straightforward. The coefficients κ and λ_3 have been interpreted as a thermodynamic response to vorticity in the fluid velocity field [61,60]. The coefficient τ_Π has the unit of time and from its contribution to the constituent equation of $T_{\mu\nu}$, it implies a retardation in the response of the fluid to an change in the background metric. A relaxation time τ_R in the sense of the Israel-Stewart formalism is reflected in a pole in the retarded correlator at $\omega_{\rm pole} = -i\tau_R^{-1}$. Whether the retarded correlator actually admits such a pole cannot be answered within hydrodynamics, instead it must be answered at a more microscopic level, see the discussion in [62] and Refs. therein.

3.3 Quasiparticles and the Boltzmann Equation

In addition to the pole structure of certain spectral functions predicted by hydrodynamics, additional characteristic features show up if the conserved charges are transported by quasiparticles whose mean free path is long compared to the thermal scale. This is the subject of this section, where we first consider the technically simpler case of a diffusing heavy quark, and then discuss the transport of quark number, energy and momentum by the constituents of the quark-gluon plasma.

3.3.1 Diffusion of a heavy quark

The diffusion of a heavy quark (one has in mind the charm or bottom) in the quark-gluon plasma is characterized by a time scale M/T^2 which is long compared to the thermal time scale of $1/T$. For this reason it is widely believed that a classical Langevin equation should appropriately describe the thermalization of heavy quarks [22]. The equations of motion for the latter are

$$\frac{d\boldsymbol{x}}{dt} = \frac{\boldsymbol{p}}{M}, \qquad \frac{d\boldsymbol{p}}{dt} = \boldsymbol{\xi}(t) - \eta \boldsymbol{p}(t), \qquad (125)$$

$$\langle \xi^i(t) \xi^j(t') \rangle = \kappa \delta^{ij} \delta(t-t'). \qquad (126)$$

For a given $\xi(t)$, the equation is easily solved to give

$$\boldsymbol{p}(t) = e^{-\eta t}\big[\boldsymbol{p}(0) + \textstyle\int_0^t \mathrm{d}s \boldsymbol{\xi}(s) e^{\eta s}\big]. \qquad (127)$$

Then

$$\lim_{t\to\infty} \langle p_i(t) p_j(t) \rangle = \frac{\kappa}{2\eta} \delta_{ij}. \qquad (128)$$

The equipartition of energy requires $\frac{\boldsymbol{p}^2}{2M}$ to be $\frac{3}{2}T$ in equilibrium. The drag and fluctuation coefficients are then related by the fluctuation-dissipation relation (established by Einstein in 1905),

$$\eta = \frac{\kappa}{2MT}. \qquad (129)$$

Furthermore, the mean square distance is also easily worked out,

$$\begin{aligned} \tfrac{1}{3}\langle \boldsymbol{x}^2(t) \rangle = {} & \frac{\kappa}{\eta^2 M^2}\big[t - \tfrac{1}{\eta}(1-e^{-\eta t}) - \tfrac{1}{2\eta}(1-e^{-\eta t})^2\big] \\ & + \frac{\boldsymbol{p}^2(0)}{3M^2\eta^2}(1-e^{-\eta t})^2. \end{aligned} \qquad (130)$$

For large times, the first term dominates. Recall that the diffusion equation (87) yields a density of particles $n(t,\boldsymbol{k}) = n(0,\boldsymbol{k}) e^{-D\boldsymbol{k}^2 t}$, or $n(t,\boldsymbol{x}) \propto e^{-\frac{\boldsymbol{x}^2}{4Dt}}$ for an initial distribution localized at the origin. Therefore the mean square radius of the particles after time t is $\frac{1}{3}\langle \boldsymbol{x}^2 \rangle = 2Dt$, and comparing with (130), one finds that the Langevin process leads at late times to a diffusion with diffusion coefficient

$$D = \frac{T}{M\eta}. \qquad (131)$$

For a thermal initial distribution of momenta, $\langle p_i(0) p_j(0) \rangle = MT\delta_{ij}$, expression (130) simplifies to

$$\tfrac{1}{3}\langle \boldsymbol{x}^2(t) \rangle = 2D\big[t - \tfrac{1}{\eta}(1-e^{-\eta t})\big] \qquad (132)$$

This equation describes both the early-time directed motion, $\frac{1}{3}\langle \boldsymbol{x}^2(t)\rangle = \frac{1}{3}v^2t^2$, $\frac{1}{3}v^2 = \frac{T}{M}$, and the late-time diffusive motion, $\frac{1}{3}\langle \boldsymbol{x}^2(t)\rangle = 2Dt$ [63].

We follow the treatment of [63] to establish the connection between the distribution of heavy quarks after a time t and the retarded correlator of the heavy quark current. Let $P(t,\boldsymbol{x})$ be the probability that a heavy quark starts at the origin at $t=0$ and moves a distance $\boldsymbol{x}$ over a time t. If the distribution of heavy quarks at time zero is $N(0,\boldsymbol{x})$, at time t it will be given by the convolution

$$N(t,\boldsymbol{x}) = \int \mathrm{d}\boldsymbol{x}' \, P(t,\boldsymbol{x}-\boldsymbol{x}') \, N(0,\boldsymbol{x}'), \qquad (133)$$

---

[4] See Eq. (49), where in view of (188) no subtlety occurs when taking the limit $\omega \to 0$. Note however that a quartic divergence must be subtracted from $G_R^{12,12}$.

or equivalently

$$N(t,\boldsymbol{k}) = P(t,\boldsymbol{k})\, N(0,\boldsymbol{k}). \tag{134}$$

Applying the general rule (79), we thus find

$$G_R^{nn}(\omega,\boldsymbol{k}) = \chi_s(\boldsymbol{k}) \left[1 + i\omega \int_0^\infty \mathrm{d}t\, e^{i\omega t}\, P(t,\boldsymbol{k})\right] \tag{135}$$

If one assumes the noise to be Gaussian distributed, then the probability distribution $P(t,\boldsymbol{x})$ is Gaussian [63], with a width given by Eq. (132), and therefore so is $P(t,\boldsymbol{k})$. The static susceptibility $\chi_s(\boldsymbol{k})$ can be obtained by noting that the initial phase-space distribution of the heavy quarks is described by $f(\boldsymbol{x},\boldsymbol{p},t=0) = e^{\beta(\mu(\boldsymbol{x})-M-\boldsymbol{p}^2/2M)}$. Taking into account both quarks and antiquarks, the static susceptibility is independent of $\boldsymbol{k}$ to linear order in the perturbation $\mu(\boldsymbol{x}) = \mu_0 + \delta\mu(\boldsymbol{x})$,

$$\chi_s(\boldsymbol{k}) = \frac{\nu}{T}\left[\frac{MT}{2\pi}\right]^{3/2} e^{-\beta M}\cosh\beta\mu_0, \tag{136}$$

where $\nu = 4N_c$ is a multiplicity factor. Eq. (135) and (136) thus provide all the ingredients to compute the kinetic theory prediction of G_R at low frequencies and momenta. Fig. (9), from [63], displays the spectral function of the longitudinal current correlator ($\rho_L(\omega,\boldsymbol{k}) = \frac{\omega^2}{\pi k^2}\,\mathrm{Im}\,G_R^{nn}(\omega,\boldsymbol{k})$, denoted by ρ_{JJ} on the figure). In particular, the $\boldsymbol{k}=0$ spectral function takes the form

$$\frac{\rho_L(\omega,\mathbf{0})}{\omega} = \frac{\chi_s}{\pi}\frac{T}{M}\frac{\eta}{\omega^2+\eta^2}. \tag{137}$$

By comparison with the hydrodynamic prediction (98), we see that the kinetic treatment predicts not just the intercept of ρ_L/ω, but also its local functional form, a Lorentzian. The width has the interpretation of an inverse relaxation time. It is a long-known fact that kinetic theory establishes a connection between the diffusion coefficient $D = \frac{T}{M\eta}$ and the relaxation time η^{-1}. Already Drude's classical description of the electric conductivity in metals around 1900 showed that $\sigma/(\tau n) = \frac{e^2}{m}$, where n is the density of electrons and m their mass.

The spectral structure that is obtained from the Langevin equation is expected to arise for a sufficiently heavy diffusing particle. Conversely, the presence of a transport peak allows one to *define* the quantities appearing in the Langevin equation directly from the spectral function [64]. The effective mean-square velocity is then given by

$$\tfrac{1}{3}\langle\boldsymbol{v}^2\rangle \equiv \frac{1}{\chi_s}\int_{-\Lambda}^{\Lambda}\frac{\mathrm{d}\omega}{\omega}\rho_L(\omega), \tag{138}$$

where Λ is a cutoff that separates the scale η from the correlation time of the medium (which is typically of order T, or gT at weak coupling). The 'kinetic mass' $M_{\rm kin}$ is further defined so as to satisfy the equipartition theorem, $M_{\rm kin}\langle\boldsymbol{v}^2\rangle = 3T$. Finally, the momentum diffusion coefficient $\kappa(M)$ can be defined as

$$\kappa(M) = \frac{2\pi M_{\rm kin}^2}{\chi_s}\,\omega\rho_L(\omega)\Big|_{\eta\ll|\omega|\ll\Lambda}. \tag{139}$$

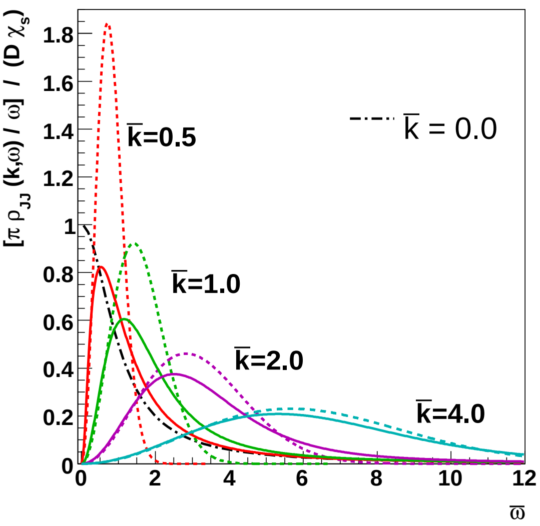

Fig. 9. Heavy-quark spectral function of the longitudinal current correlator as predicted by the Langevin equation [63] as a function of a scaled frequency $\bar\omega \equiv \omega D(M/T)$ for various values of a scaled momentum $\bar{\boldsymbol{k}} \equiv \boldsymbol{k}DM/T$. The solid lines are the predictions of the Langevin equations, while the dotted lines are the predictions of the free theory. The dash-dotted line shows the $\boldsymbol{k}=0$ result of the Langevin equation.

If one inserts the spectral function (137) derived from the Langevin equation, one recovers Einstein's relation (129). A weak-coupling calculation shows that while $\kappa(M)$ and D are only weakly dependent on M, the drag coefficient $\eta \sim T^2/M\times$ a power of the coupling constant is parametrically small compared to the medium time-scale. This justifies *a posteriori* the assumption that the transport peak is narrow. The momentum diffusion coefficient κ converges to a finite value when the static limit $M\to\infty$ is taken. Note that although the peak in $\rho_L(\omega)$ becomes arbitrarily narrow in that limit, the limit $M\to\infty$ cannot be interchanged with the limit $\omega\to0$ in the definition of κ.

The formula (139) can be understood heuristically as follows [64]: ρ_L is the spectral function for the operator j_k at vanishing spatial momentum. Classically, if the quark is heavy, this operator measures a single quark's velocity, $v_k = \int \mathrm{d}\boldsymbol{x}\, j_k$. Therefore the operator $M\int \mathrm{d}\boldsymbol{x}\,\frac{\mathrm{d}j_k}{\mathrm{d}t}$ measures the force acting on the quark. We now recall that κ measures the size of the force exerted by the medium on the quark, Eq. (126). We then have to evaluate the classical force-force correlator, whose quantum analog is the symmetrized correlator. Combining these ingredients, one reaches

$$\kappa = \frac{\beta}{6}\sum_{k=1}^{3}\lim_{\omega\to0}\left[\lim_{M\to\infty}\frac{M_{\rm kin}^2}{\chi_s}\int_{-\infty}^{\infty}\mathrm{d}t\, e^{i\omega(t-t')}\right. \tag{140}$$
$$\left.\int\mathrm{d}\boldsymbol{x}\langle\{\frac{\mathrm{d}\hat{j}_k(t,\boldsymbol{x})}{\mathrm{d}t},\frac{\mathrm{d}\hat{j}_k(t',\mathbf{0})}{\mathrm{d}t'}\}\rangle\right].$$

A second, rigorous derivation was given for this formula in [64]. Through the fluctuation-dissipation formula (39), the symmetrized correlator can be expressed in terms of the corresponding spectral function, which then leads back to formula (139) in the heavy-quark limit. As one might expect based on the classical argument laid out above, the correlator (140) can be expressed in the Heavy-Quark Effective Theory (HQET) as a force-force correlator, where the leading force is the chromo-electric force $g\boldsymbol{E}$,

$$\kappa = \frac{\beta}{6}\sum_{k=1}^{3}\lim_{M\to\infty}\frac{1}{\chi_s}\int \mathrm{d}t\,\mathrm{d}\boldsymbol{x}\,\Big\langle\Big\{\big(\hat\phi^\dagger gE^k\hat\phi-\hat\theta^\dagger gE^k\hat\theta\big)(t,\boldsymbol{x}),\; \big(\hat\phi^\dagger gE^k\hat\phi-\hat\theta^\dagger gE^k\hat\theta\big)(0,\boldsymbol{0})\Big\}\Big\rangle. \qquad (141)$$

where θ and ϕ are two-component spinors of HQET and the $\omega\to 0$ limit has now been taken. The corresponding Euclidean correlator reads, after evaluating the fermion line contractions,

$$G_E^{\rm HQET}(t) = \frac{\Big\langle \mathrm{Re\,Tr}\,\big(U(\beta,t)gE_k(t,\boldsymbol{0})U(t,\boldsymbol{0})gE_k(0,\boldsymbol{0})\big)\Big\rangle}{-3\,\langle \mathrm{Re\,Tr}\,U(\beta,0)\rangle}, \qquad (142)$$

where the color parallel transporters $U(t_2,t_1)$ in the fundamental representation are propagators of static quarks. In particular the denominator of (142) is the Polyakov loop. The momentum diffusion coefficient is given by the low-frequency limit of the corresponding spectral function via Eq. (50),

$$\kappa = \lim_{\omega\to 0}\frac{2\pi T}{\omega}\rho^{\rm HQET}(\omega). \qquad (143)$$

The obvious advantage of this formulation is that the large scale M has disappeared from the problem. The spectral function $\rho^{\rm HQET}$ has been studied in detail at next-to-leading order in perturbation theory [65]. Remarkably, even in the weak-coupling limit, the function is smooth as small frequencies. This is in contrast with the narrow transport peaks that are found at weak-coupling in e.g. the shear channel. This property is a clear advantage for numerical studies of the spectral function, as we will see in section (5).

3.3.2 Kinetic theory in other channels

When studying the diffusion of a light quark number, or the transport of transverse momentum, the applicability of kinetic theory is not *a priori* guaranteed. It is only valid if the medium admits quasiparticles that are sufficiently long-lived. In the heavy-quark diffusion case, the existence of a quasiparticle is guaranteed by the separation of scales M/T. Typically, although perhaps not necessarily, quasiparticles arise in weakly coupled systems. In ϕ^4 theory, the quasiparticle carries the same quantum numbers as the particles at zero-temperatures. At sufficiently high temperatures in QCD, due to asymptotic freedom, quasiparticles are expected to emerge, with the quantum numbers of quarks and gluons. At low temperatures, well below the crossover region, we expect the well-known hadron resonances to be good quasiparticles. In that regime the parameter $1/N_c$ can be used to provide an expansion around the non-interacting hadron gas (N_c is the number of colors).

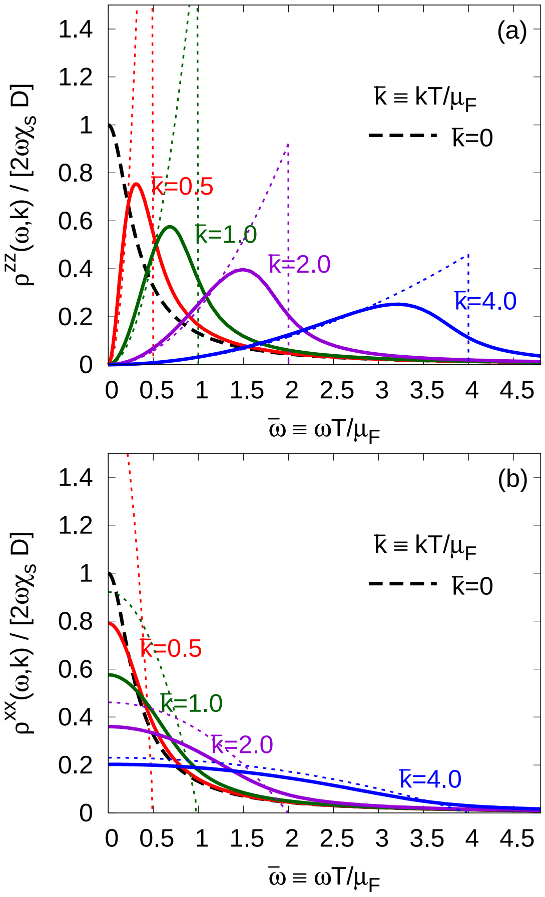

Fig. 10. Kinetic theory prediction for the vector current correlator in quenched QCD for massless quarks [54]. The momentum is directed in the z direction, $\boldsymbol{k}=(0,0,k)$, and $\mu_F = g^2C_Fm_D^2\log(T/m_D)/8\pi$ is the drag coefficient of a quark in leading-log approximation. The thick dashed curve corresponds to $\boldsymbol{k}=0$. The thin dashed lines show the result of the free Boltzmann equation [66,54]. Note that the normalization of ρ differs from our convention by a factor 2π.

The physical picture one has in mind is that of a particle propagating freely until it makes a ‘collision’ with a constituent of the medium, upon which its momentum or even its nature may be changed. The collision generally has to be described by a quantum-mechanical matrix element. The propagation of the quasiparticle between collisions can be treated as classical, provided the time until the next collision is long enough that any coherence effects can be neglected. The evolution of the quasiparticle can then be written as a convolution of transition probabilities, rather than amplitudes. In this approximation the evolution is described by the Boltzmann equation for the probability distribution $f(\boldsymbol{x},\boldsymbol{p},t)$.

To illlustrate these general remarks, we review a recent kinetic theory treatment of the diffusion of *light* quarks [54]. To treat this problem one needs the Boltzmann equation in the presence of an external field. Recalling that the Lorentz force on a charged particle is $F^i = QF^i{}_\mu v^\mu$, the Boltzmann equation (for a single flavor charged under the externally applied gauge field) reads

$$\frac{1}{E_{\boldsymbol{p}}}\left(p^\mu\partial_\mu + QF^{\mu\nu}p_\nu\frac{\partial}{\partial p_\mu}\right)f^a = C^a[f,\boldsymbol{p}]. \tag{144}$$

Here Q denotes the electric charge of the quark and below we will employ the notation

$$n^B(\omega) = \frac{1}{e^{\beta\omega}-1}, \tag{145}$$

$$n^F(\omega) = \frac{1}{e^{\beta\omega}+1}, \tag{146}$$

often with the understanding of an ultrarelativistic dispersion relation, i.e. $n^F_{\boldsymbol{p}} \equiv n^F(\omega = |\boldsymbol{p}|)$. Specializing to a spatial gauge potential, $A_\mu = (0,\boldsymbol{A})$, and linearizing the Boltzmann equation yields in Fourier space $(\omega,\boldsymbol{k})$

$$\begin{aligned}&(-i\omega + i\boldsymbol{v}_{\boldsymbol{p}}\cdot\boldsymbol{k})\delta f^a(\omega,\boldsymbol{k}) \\ &\quad -i\omega n(1-n)QA_i\frac{p^i}{E_{\boldsymbol{p}}} = C^a[\delta f,\boldsymbol{p}].\end{aligned} \tag{147}$$

Since the coupling of the gauge field is linear in the charge, it only influences the difference of quarks and antiquarks,

$$\begin{aligned}&(-i\omega + i\boldsymbol{v}_{\boldsymbol{p}}\cdot\boldsymbol{k})\delta f^{s-\bar{s}}(\omega,\boldsymbol{k}) \\ &\quad -i\omega n(1-n)2QA_i\frac{p^i}{E_{\boldsymbol{p}}} = C^{s-\bar{s}}[\delta f,\boldsymbol{p}].\end{aligned} \tag{148}$$

At this point one needs to specify the collision kernel $C^{s-\bar{s}}$. The quarks and gluons contribute a 'loss' term (1st line) and a 'gain' term [14,54],

$$\begin{aligned}(C^q_{qg} - C^{\bar{q}}_{qg}) &= -2\gamma\frac{n^F_p(1+n^B_p)}{p}[\chi^q(\boldsymbol{p}) - \chi^{\bar{q}}(\boldsymbol{p})] \\ &\quad + \frac{2\gamma}{\xi_{BF}}\frac{n^F_p(1+n^B_p)}{p}\int\frac{\mathrm{d}\boldsymbol{k}}{(2\pi)^3} \\ &\quad \frac{n^F_k(1+n^B_k)}{k}[\chi^q(\boldsymbol{k}) - \chi^{\bar{q}}(\boldsymbol{k})],\end{aligned} \tag{149}$$

$$\delta f(\boldsymbol{p}) = n^F_p(1-n^F_p)\chi(\boldsymbol{p}), \tag{150}$$

$$\gamma \equiv \frac{g^4C_F^2\xi_{BF}}{4\pi}\log\left(\frac{T}{m_D}\right), \tag{151}$$

$$\xi_{BF} \equiv \int\frac{\mathrm{d}\boldsymbol{k}}{(2\pi)^3}\frac{n^F_k(1+n^B_k)}{k} = \frac{T^2}{16}. \tag{152}$$

Hong and Teaney solved the Boltzmann equation (148) by expanding functions of momenta in real-valued linear combinations of spherical harmonics. The radial part of the momenta is discretized, and the problem is reduced to inverting a large matrix. The out-of-equilibrium expectation value of the current is determined from δf via

$$\langle J_i\rangle_A = Q\nu_s\int\frac{\mathrm{d}\boldsymbol{p}}{(2\pi)^3}\frac{p_i}{E_{\boldsymbol{p}}}\delta f^{s-\bar{s}}, \tag{153}$$

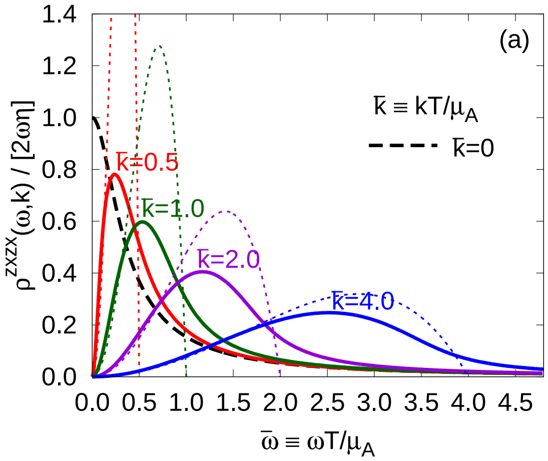

Fig. 11. Spectral function of T_{xy} in the shear channel, as predicted by the Boltzmann equation [54] in leading log approximation. The thick dashed curve corresponds to $\boldsymbol{k} = 0$, and $\mu_A = g^2C_Am_D^2\log(T/m_D)/8\pi$. The thin dashed curves represent the free theory result [67,54]. The normalization of ρ differs from our convention by a factor 2π.

and from there the retarded correlator is obtained via the frequency version of the linear response formula (75),

$$\langle J^\mu(\omega,\boldsymbol{k})\rangle_A = G_R^{\mu\nu}(\omega,\boldsymbol{k})A_\nu(\omega,\boldsymbol{k}). \tag{154}$$

The result is shown in Fig. (10). In the rescaled variables, the functional form of the curves corresponding to different momenta are similar to those obtained for heavy quarks, Fig. (9).

A similar approach was used in [54] to determine the correlators of $T_{\mu\nu}$. Now the perturbing field is gravitational rather than electromagnetic, and consequently the Boltzmann equation has to be generalized to non-flat background metrics. Another important aspect of the calculation is the selection of appropriate boundary conditions. Hong and Teaney argue that the appropriate boundary condition for $\chi(\boldsymbol{p})$ is a Dirichlet boundary condition at $\boldsymbol{p} = 0$. The reason is that the rate of soft gluon emission is parametrically high compared to the transport time scales. At high momenta the solution that grows exponentially is discarded by implementing the appropriate finite-difference scheme at the highest discretized momentum. The result for the shear channel is shown in Fig. (11). By the Kubo formula (117), the shear viscosity in leading logarithmic approximation can be read off from the intercept of the $\boldsymbol{k} = 0$ curve (parametrically, $\eta/s \sim [g^4\log(1/g)]^{-1}$).

3.4 Leading order results for the shear and bulk viscosities

The conductivity, as well as the shear and bulk viscosities, have been obtained beyond the leading-logarithmic order, namely to full leading order in the gauge coupling g [15,68]. The method follows the steps sketched in the previous section, namely a Boltzmann equation is written down and subsequently linearized. In addition to the ingredients necessary for a leading-logarithmic accuracy, the collision kernel must be treated more carefully at low momenta, and the Landau-Pomeranchuk-Migdal (LPM) effect, which involves collinear emissions and their destructive interferences, must be taken into account [51].

Arnold, Moore and Yaffe (AMY) solved these linear integral equations using a variational approach (a method introduced earlier in [69]). Numerical results for the shear and bulk viscosity are displayed in Fig. (12). The results are divided by the entropy density, effectively normalizing them by the number of degrees of freedom. The ratio η/s is about 30% lower in the pure gauge theory than in $N_{\rm f}=3$ QCD, primarily because the larger color charge carried by the gluons makes them equilibrate faster.

Numerically, η/s is about 2.0 for $\alpha_s = 0.15$, but the accuracy of the calculation deteriorates for larger values of the coupling. In the weak coupling regime, the bulk viscosity, of order g^4 in the gauge coupling, turns out to be negligible compared to the shear viscosity, see the bottom panel of Fig. (12).

Recently, the treatment of the inelastic process $gg \leftrightarrow ggg$ in the shear viscosity calculation has been scrutinized by Xu and Greiner (XG) [70]. They showed that at moderate values of α_s this process can numerically dominate the elastic $gg \leftrightarrow gg$ scattering due to soft, not necessarily collinear emissions. The calculation was revisited very recently by Chen et al. [71] without relying on the soft gluon bremsstrahlung approximation. The inclusion of gluon emissions appears to lower somewhat the ratio η/s, but a full next-to-leading order calculation has not been performed yet in a non-Abelian gauge theory.

3.5 Perturbative predictions for spectral functions and operator production expansion

We begin with the energy-momentum tensor correlators. At frequencies $\omega \gg T$, straightforward perturbation theory is expected to apply. Here we give some results for the SU(N_c) gauge theory in the limit of zero coupling. In the non-interacting limit, gluodynamics is of course a scale-invariant theory. There are thus three independent correlators of the stress-energy tensor, which were calculated in [67]. To describe them, we assume in the following expressions that $\omega, q > 0$, $\boldsymbol{q} = (0,0,q)$. We define the functional

$$\mathcal{I}[P] = \theta(\omega-q)\int_0^1 dz \frac{P(z)\,\sinh\frac{\omega}{2T}}{\cosh\frac{\omega}{2T}-\cosh\frac{qz}{2T}} + \theta(q-\omega)\int_1^\infty dz \frac{P(z)\,\sinh\frac{\omega}{2T}}{\cosh\frac{qz}{2T}-\cosh\frac{\omega}{2T}}. \quad (155)$$

Thus $\mathcal{I}[P]$ is a function of (ω, q, T). Then the spectral functions read, respectively in the shear channel, the sound channel and the tensor channel,

$$\rho_{13,13}(\omega,q,T) = \tfrac{d_A}{8\,(4\pi)^2}\,\omega^2(\omega^2-q^2)\,\mathcal{I}[1-z^4]\,, \quad (156)$$

$$\rho_{00,00}(\omega,q,T) = \tfrac{d_A}{4\,(4\pi)^2}\,q^4\,\mathcal{I}[(1-z^2)^2]\,, \quad (157)$$

$$\rho_{12,12}(\omega,q,T) = \tfrac{d_A}{32\,(4\pi)^2}\,(\omega^2-q^2)^2\,\mathcal{I}[1+6z^2+z^4], \quad (158)$$

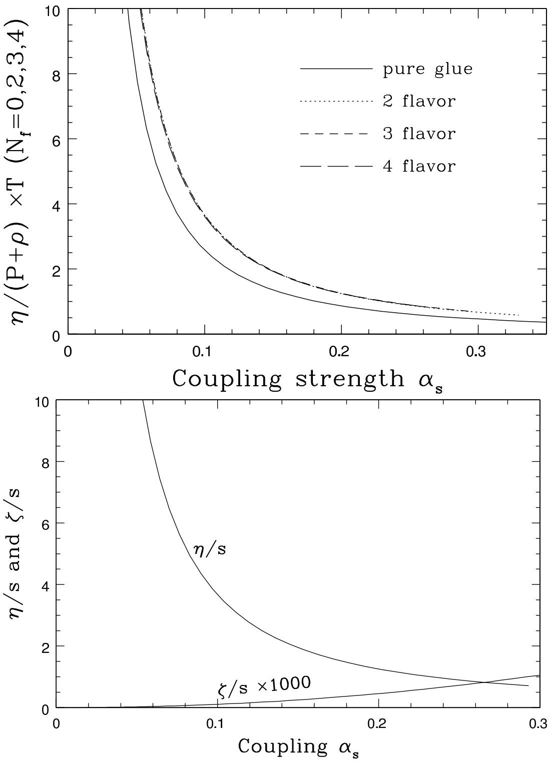

Fig. 12. The shear (η) and bulk (ζ) viscosities scaled by the entropy density, in full leading order of perturbation theory ([51,15] and [68] respectively).

where $d_A \equiv N_c^2-1$. In addition, the correlator of the trace anomaly reads

$$\rho_{\theta,\theta}(\omega,q,T) = \left(\tfrac{11\alpha_s N_c}{6\pi}\right)^2 \tfrac{d_A}{4\,(4\pi)^2}\,(\omega^2-q^2)^2 \Big[-\frac{\omega}{q}\theta(q-\omega) + \frac{2T}{q}\log\frac{\sinh(\omega+q)/4T}{\sinh|\omega-q|/4T}\Big]. \quad (159)$$

For P a polynomial, the quantity $I[P]$ can be expressed in terms of polylogarithms [67]. The correlators of $T_{\mu\nu}$ can be expressed in terms of polylogarithms up to order 5. The spectral functions are displayed for $q=\pi T$ in Fig. (13). Using expressions of this kind, the second-order transport coefficient κ can be extracted via the Kubo formula (121), yielding [57], after subtraction of the vacuum contribution,

$$\kappa = \frac{d_A}{18}T^2 = \frac{5s}{8\pi^2 T}. \quad (160)$$

Even in the non-interacting limit, the functional form of the spectral functions is relatively complicated, due to the three scales ω, q, T involved in the problem. The expressions simplify significantly when the spatial momentum q is set to zero, for instance (without summation over

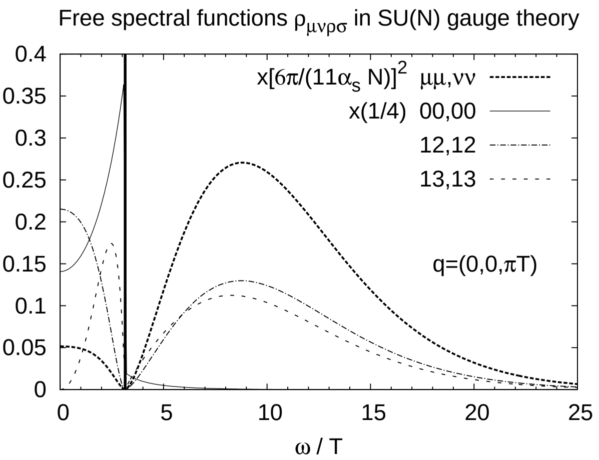

Fig. 13. Non-interacting spectral functions in the SU(N) gauge theory. More precisely, $q = \pi T$ and the functions plotted are $\frac{1}{d_A T^4}[\rho(\omega,\mathbf{q},T)/\tanh(\omega/2T) - \rho(\omega,\mathbf{q},0)]$ for four different channels. The sound channel $\rho_{00,00}$ admits a discontinuity at threshold, $\omega = q$.

the indices μ, ν)

$$\rho_{\mu\nu,\mu\nu}(\omega,0,T) = \frac{A_{\mu\nu}\ \omega^4}{\tanh\frac{1}{4}\omega\beta} + B_{\mu\nu}\beta^{-4}\ \omega\delta(\omega), \quad (161)$$

$$A_{12,12} = A_{13,13} = \frac{1}{10}\frac{d_A}{(4\pi)^2}, \quad (162)$$

$$B_{12,12} = B_{13,13} = \left(\frac{2\pi}{15}\right)^2 d_A; \quad (163)$$

$$A_\theta = d_A\left(\frac{11\alpha_s N}{3(4\pi)^2}\right)^2, \quad (164)$$

$$B_\theta = 0. \quad (165)$$

The δ-function at the origin corresponds to the fact that gluons are asymptotic states in the free theory and implies an infinite viscosity.

Next-to-leading order corrections are known in some cases. In the bulk channel $\rho_{\mu\mu,\nu\nu}$, they have been calculated recently [72], see Eq. (181). In the shear channel, the ω^4 term in the large-frequency behavior of the spectral function $\rho_{13,13}(\omega,\mathbf{0},T)$ is corrected by the factor $\left[1 - \frac{5\alpha_s N_c}{9\pi}\right]$ [73,74].

Expressions similar to Eq. (156) were obtained earlier by Aarts and Martinez Resco for the free spectral functions of dimension-three quark bilinears [66] in terms of polylogarithms. In this case polylogarithms up to order 3 appear. At $q = 0$, the expressions again simplify considerably. For the vector current, the result is for one flavor (see for instance [75,63])

$$\rho_{00}(\omega,0,T) = -\chi_s\omega\delta(\omega), \quad (166)$$

$$\sum_{i=1}^{3}\rho_{ii}(\omega,0,T) = \chi_s\langle v^2\rangle\omega\delta(\omega) \quad (167)$$
$$+ \frac{N_c}{4\pi^2}\theta(\omega-2m)\sqrt{1-(\frac{2m}{\omega})^2}$$
$$\left(1+\tfrac{1}{2}(\frac{2m}{\omega})^2\right)\omega^2\tanh\frac{\omega}{4T}.$$

The susceptibility and average velocities have simple expression in the massless and in the heavy-quark limits,

$$\chi_s,\ \langle v^2\rangle = \begin{cases} \frac{N_c}{3}T^2, & 1 \qquad m=0 \\ \frac{4N_c}{T}\left[\frac{mT}{2\pi}\right]^{\frac{3}{2}} e^{-\beta m}, & \frac{3T}{m} \qquad m \gg T. \end{cases} \quad (168)$$

At high frequencies $\omega \gg T$, the leading power in ω of the spectral function gets modified by radiative corrections. In this frequency regime, they are independent of the temperature and can be calculated in the vacuum. Famously, the vector-current spectral function ρ_{ii} is then modified by a factor $(1+\frac{\alpha_s}{\pi})$ [39]. The quark number susceptibility χ_s also receives calculable corrections at high temperature, $\chi_s = \frac{N_c}{3}T^2(1-\frac{g^2(T)}{2\pi^2})$ in the massless case [76]. The broadening of the delta function in ρ_{ii} into a peak of width on the order of the inverse relaxation time however requires either an explicit resummation procedure or a kinetic theory treatment, see section (3.3).

3.6 Thermal Correlators from the Gauge/Gravity Correspondence

In this section we summarize some of the results on spectral functions that have been obtained in the strong coupling regime using the holographic principle. We will restrict ourselves to presenting some of the spectral functions of the $\mathcal{N}=4$ SYM theory. Our main goal here is to contrast their analytic structure with the analytic structure found at weak coupling using kinetic theory. For the interested reader, the method of computing spectral functions based on the holographic principle [77,78,79,80,56] has been reviewed in [81,49,50].

The spectral function of the R-charge correlator at vanishing spatial momentum, remarkably, can be written in terms of elementary functions [82],

$$\rho(\omega) = \chi_s\left(\frac{\omega}{2\pi T}\right)^2\frac{\sinh\frac{\omega}{2T}}{\cosh\frac{\omega}{2T}-\cos\frac{\omega}{2T}}. \quad (169)$$

The static susceptibility is given by $\chi_s = \frac{N_c^2T^2}{8}$, and the diffusion constant $D = \frac{1}{2\pi T}$ can be read off from this formula by using the Kubo formula, Eq. (99). This function has a series of poles along the diagonals in the lower half of the ω complex plane,

$$\omega_p = n\cdot 2\pi T(\mp 1 - i). \quad (170)$$

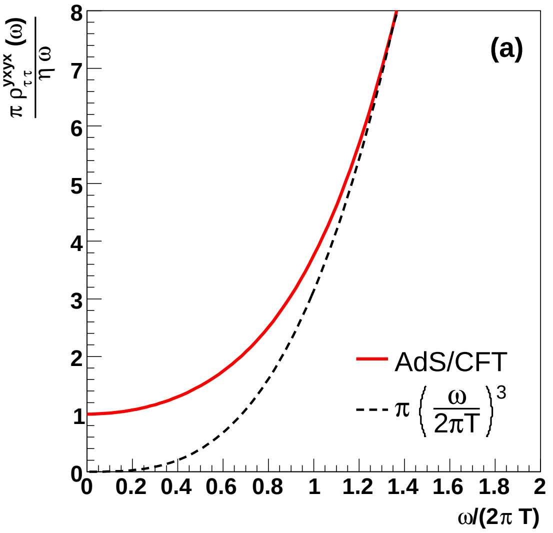

Fig. 14. Spectral function of shear stress at strong coupling in the $\mathcal{N} = 4$ SYM theory at vanishing spatial momentum. The dashed curve shows the zero temperature result (171) normalized by the same factors. Due to a non-renormalization theorem in these channels, the zero temperature spectral densities in the free and interacting theories are equal [83,84]. At finite temperature the kinetic theory peak observed in Fig. (11, $\boldsymbol{k} = 0$ curve) does not exist in the strongly interacting theory. Reproduced from [56].

The shear channel spectral function ($\rho(\omega)/\omega$) displayed in Fig. (14) [56,80] smoothly interpolates between the vacuum spectral function

$$\rho^{\rm SYM}_{12,12}(\omega, q = 0, T = 0) = \frac{N_c^2}{64\pi^2}\omega^4 \qquad (171)$$

at large frequencies and a finite value at $\omega = 0$, which yields the shear viscosity $\eta = \frac{\pi}{8}N_c^2T^3$ via the Kubo formula (117). Combining this with the entropy density of $s = \frac{\pi^2}{2}N_c^2T^3$, one obtains the ratio $\eta/s = 1/4\pi$ (see Eq. (3) in the Introduction).

Numerically no particular structure or excitation is visible in the spectral function at any frequency. This is in stark contrast with the peak structure predicted at the origin by the Boltzmann equation, see Fig. (11). One concludes from figure (14) that the conformal plasma of the $\mathcal{N} = 4$ SYM theory does not admit quasiparticles. There is no separation between the transport time scale τ_Π and the thermal scale πT. In fact, the second-order transport coefficients were calculated in the strongly coupled $\mathcal{N} = 4$ SYM theory ([59], see also [85] for τ_Π), with the result

$$\tau_\Pi = \frac{2 - \log 2}{2\pi T}, \qquad (172)$$

$$\kappa = \frac{\eta}{\pi T} = \frac{s}{4\pi^2 T}. \qquad (173)$$

The sound channel spectral function, namely the spectral function for the energy density T_{00} at finite spatial momentum, is diplayed in Fig. (15). Comparison with Fig. (8) shows that in this strongly coupled theory, hydrodynamics provides a good description of the spectral function up to momenta as large as πT. In a weakly-coupled theory, this range of validity is parametrically smaller.

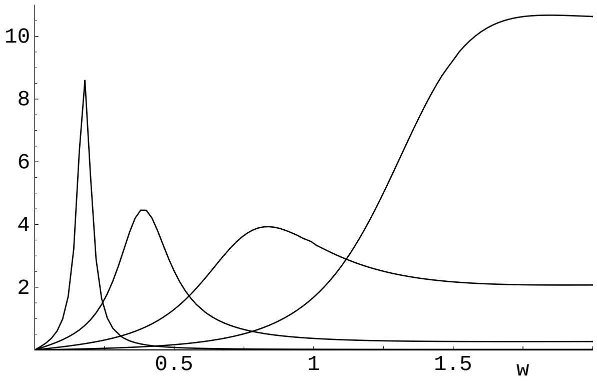

Fig. 15. Spectral function of the energy density at spatial momenta obtained from the AdS/CFT correspondence for the $\mathcal{N} = 4$ SYM theory. The quantity displayed is $\pi\frac{\rho(\omega)}{e+p}$ in infinite-coupling, large-N_c SYM theory, computed by AdS/CFT methods. The x-axis variable is $\mathtt{w} = \omega/2\pi T$ and the curves correspond to $q/2\pi T = 0.3, 0.6, 1.0$ and 1.5. Figure reproduced from [80].

Assuming the holographic principle to hold for other theories as well, non-conformal theories can also be studied by these methods. In the past few years, a program has been undertaken to tune the properties of the 'bulk' theory to reproduce the thermodynamic properties of QCD on the 'boundary', and then predict those properties such as transport coefficients that are difficult to extract from first principles [86,87,88]. These models can give qualitative insight into whether the shape of the spectral functions displayed in Fig. (14) and (15) are robust again modest modifications of the theory. A longer-term goal could be to understand the crossover between the functional form observed at weak coupling and that found at strong coupling.

We remark that in the 'AdS/QCD' models the shear viscosity to entropy density ratio remains $1/4\pi$ at all temperatures, which shows that the breaking of conformal invariance is not of the most general form. A bound that is found to be observed by these theories [88] is Buchel's conjectured bound [89],

$$\frac{\zeta}{\eta} \geq 2\left(\frac{1}{3} - c_s^2\right). \qquad (174)$$

It implies that the bulk viscosity must become at least comparable to the shear viscosity when the speed of sound becomes small, as happens for instance at certain phase transitions.

3.7 Thermal Sum Rules

We briefly remind the reader of the derivation of sum rules. The first step is to derive a dispersion relation [90]. For this purpose it is useful to introduce the function

$$\mathcal{G}(\omega) = \begin{cases} G_R(\omega) \equiv \int_0^\infty \mathrm{d}t\, e^{i\omega t}\, G(t) & \mathrm{Im}(\omega) > 0 \\ G_A(\omega) \equiv -\int_{-\infty}^0 \mathrm{d}t\, e^{i\omega t}\, G(t) & \mathrm{Im}(\omega) < 0 \end{cases} \tag{175}$$

It is analytic in ω everywhere except along the real axis. We now apply Cauchy's theorem for a contour $\mathcal{C}$ which is the sum of two large semi-circles, as depicted on Fig. (16). In order for the contributions at infinity to vanish, the theorem is applied to $\mathcal{G}(\omega)/P(\omega)$, where $P(\omega)$ is a polymonial of sufficiently high order n with simple zeros at $\omega = \omega_\nu$. The contour integral then yields

$$\frac{1}{2\pi i} \oint_{\mathcal{C}} \frac{\mathcal{G}(z)\,\mathrm{d}z}{(z-\omega)P(z)} = \frac{\mathcal{G}(\omega)}{P(\omega)} + \sum_\nu \frac{\mathcal{G}(\omega_\nu)}{(\omega_\nu - \omega)P'(\omega_\nu)}, \tag{176}$$

By construction, the contribution of the semi-circles vanishes in the limit of infinite radius. Now recalling the definition of the spectral function, the left-hand side is equal to

$$\int_{-\infty}^{\infty} \frac{\mathrm{d}z\,\rho(z)}{(z-\omega)P(z)}. \tag{177}$$

Therefore, noticing that $\mathcal{G}(\omega) = G_R(\omega)$ for $\mathrm{Im}(\omega) > 0$, we obtain

$$G_R(\omega) = P(\omega) \int_{-\infty}^{\infty} \frac{\mathrm{d}z\,\rho(z)}{(z-\omega)P(z)} + Q(\omega), \tag{178}$$

where

$$Q(\omega) \equiv -P(\omega) \sum_\nu \frac{\mathcal{G}(\omega_\nu)}{(\omega_\nu - \omega)P'(\omega_\nu)}. \tag{179}$$

is a polynomial of degree $n-1$. In practice it means that n constants have to be calculated before formula (178) determines the retarded correlator For instance, for the vector correlator, Eq. (11), one subtraction is sufficient to make the dispersion integral converge. We reserve the name sum rule to the case where $G_R(\omega)$ can be calculated in an independent way, for instance in terms of thermodynamic potentials. Eq. (178) can then be interpreted as a global constraint on the spectral function $\rho(\omega)$, which may help to parametrize it in a consistent way.

Since the derivation of a sum rule involves integrating the spectral function over all frequencies, it is necessary to know its large frequency behavior in order to ensure the integral's UV convergence. This leads us to the subject of the operator product expansion (OPE). In thermal field theory, the spectral functions typically rise at large frequencies with a positive power of frequency. The simplest subtraction to implement is then to take the difference between two temperatures. This reduces the asymptotic power by four units, due to the absence of gauge invariant operators of lower dimension (chiral symmetry implies that the operator $\bar\psi\psi$ appears accompanied by a power of the quark mass).

Correlation functions deep in the Euclidean region admit an operator-product expansion. Through the dispersion relation, this leads to a large frequency expansion for the spectral function [91]. Leading-order results for the OPE of current and energy-momentum tensor correlators were obtained in [92]. Recently, a full two-loop calculation of the correlator of $\theta \equiv T_{\mu\mu}$ has been performed [72] in Yang-Mills theory (see also the closely related work [93]). In addition to giving the radiative corrections to the leading ω^4 power, this calculation provides the Wilson coefficients of the θ and $\theta_{00} \equiv T_{00} - \frac{1}{4}\theta$ operators in the operator product expansion of the trace anomaly correlator. We quote the $\omega \gg \pi T$ result,

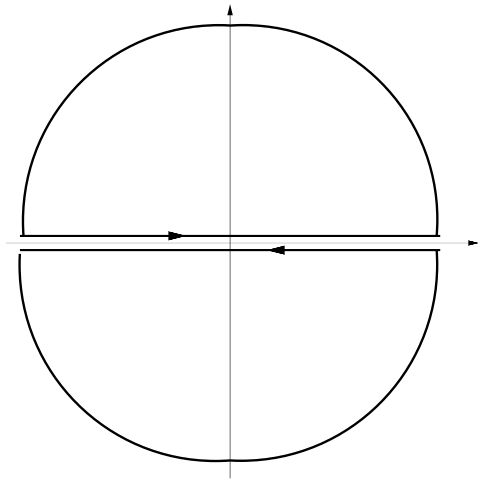

Fig. 16. Contour chosen in the derivation of thermal sum rules, see Eq. (178).

$$\begin{aligned} \frac{\rho_\theta(\omega)}{4c_\theta^2} &= \frac{d_A\omega^4}{(4\pi)^2}\,\tilde\gamma_{\theta;1}(\omega) \qquad (180)\\ &\quad - 2(e+p)\,\tilde\gamma_{\theta;\,e\,+\,p}(\omega) \\ &\quad - 2(e-3p)\,\tilde\gamma_{\theta;\,e\,-\,3p}(\omega) \;+\; \mathrm{O}\left(\frac{T^6}{\omega^2}\right), \\ \tilde\gamma_{\theta;1}(\omega) &= g^4 + \frac{g^6 N_c}{(4\pi)^2}\left(\frac{22}{3}\ln\frac{\bar\mu^2}{\omega^2} + \frac{73}{3}\right) \qquad (181)\\ &\quad + \mathrm{O}(g^8)\,, \\ \tilde\gamma_{\theta;\,e\,+\,p}(\omega) &= \frac{11 g^6 N_c}{(4\pi)^2} + \mathrm{O}(g^8)\,, \qquad (182)\\ \tilde\gamma_{\theta;\,e\,-\,3p}(\omega) &= g^4 + \mathrm{O}(g^6)\,, \qquad (183) \end{aligned}$$

where $c_\theta = -\frac{b_0}{2} - \frac{b_1}{4}g^2$, $b_0 = \frac{11N_c}{3(4\pi)^2}$ and $b_1 = \frac{34N_c^2}{3(4\pi)^4}$, and g^2 is the dimensionless renormalized coupling constant, evaluated at the $\overline{\mathrm{MS}}$ scheme renormalization scale $\bar\mu$ ($\mu^2 = \bar\mu^2 e^{\gamma_{\mathrm{E}}}/4\pi$). Expressions such as Eq. (181) are very useful to constrain the form of the spectral function at high frequencies, particularly since the thermodynamic potentials e and p can be evaluated non-perturbatively. In particular, if the vacuum correlator is subtracted from the thermal correlator, then the leading asymptotic behavior is determined by two linear combinations of energy density and pressure. This has recently been exploited to constrain the spectral function ρ_θ [58], at which time however only the leading order behavior of the Wilson coefficients was known [92].

The calculation shows that (a) the scalar and pseudoscalar correlators do not have contact terms (the correlators vanish in the limit $\omega \to \infty$) and (b) the integral of $\varDelta\rho/\omega$ is UV-finite. Using these facts, one can derive a sum rule in the $\mathrm{SU}(N_c)$ Yang-Mills theory [94,95]. First, the following expression

$$G^{(0)}_{E,\theta}(T) - G^{(0)}_{E,\theta}(T=0) = T^5 \frac{\partial}{\partial T} \frac{e-3p}{T^4}\,, \qquad (184)$$

is obtained for the $(\omega, \boldsymbol{q}) = 0$ Euclidean correlator, where e and p are the energy density and pressure of the finite-temperature system. We now convert identity (184) into a sum rule for the bulk spectral function with the goal to constrain the latter. Combining equations (184) and (9), we obtain

$$\int_{-\infty}^{\infty} \frac{d\omega}{\omega} [\rho_\theta(\omega, T) - \rho_\theta(\omega, 0)] = T^5 \partial_T \frac{e-3p}{T^4}\,. \qquad (185)$$

Next, we separate an infrared contribution of the form $\omega\delta(\omega)$ in ρ_θ from the rest of the spectral function [57]. Starting from Eq. (116), we recall that for any smooth function such that $\int_{-\infty}^{\infty} f(x)dx = 1$, $\frac{1}{\epsilon} f(x/\epsilon)$ provides a representation of the delta function. Here we will exploit this fact for the function

$$f(x) = \frac{1}{\pi(b^2-1)} \left[\frac{x^4}{(x^2-b^2)^2 + x^2} - 1\right] \qquad (186)$$

and $b = c_s/(\varGamma_s k)$ and $\epsilon = \varGamma_s k^2$. In this way one finds that, in the sense of distributions,

$$\lim_{\boldsymbol{k}\to 0} \frac{\rho_{33,33}(\omega, \boldsymbol{k}, T)}{\omega} = \frac{e+p}{\pi} \varGamma_s + (e+p) c_s^2 \delta(\omega) + \ldots \qquad (187)$$

In the shear channel on the other hand,

$$\begin{aligned} \frac{\rho_{13,13}(\omega, \boldsymbol{k}, T)}{\omega} &= \frac{\eta}{\pi} \frac{\omega^2}{\omega^2 + \left(\frac{\eta k^2}{e+p}\right)^2} \qquad (188) \\ &\overset{\boldsymbol{k}\to 0}{\sim} \frac{\eta}{\pi} - \frac{\eta^2 k^2}{e+p}\delta(\omega) \end{aligned}$$

and the delta function is suppressed by a power of $\boldsymbol{k}^2$. Thus combining the shear and sound channels,

$$\begin{aligned} \frac{1}{9}\frac{\rho_{ii,kk}(\omega, \boldsymbol{0}, T)}{\omega} &= \frac{\rho_{33,33}(\omega, \boldsymbol{0}, T)}{\omega} - \frac{4}{3}\frac{\rho_{13,13}(\omega, \boldsymbol{0}, T)}{\omega} \\ &= \frac{\zeta}{\pi} + (e+p) c_s^2 \delta(\omega) + \ldots \qquad (189) \end{aligned}$$

Using the exact relations

$$\rho_{00,00}(\omega, \boldsymbol{0}, T) = \frac{e+p}{c_s^2} \omega\delta(\omega)\,, \qquad (190)$$

$$\rho_{00,kk}(\omega, \boldsymbol{0}, T) = -3(e+p)\omega\delta(\omega)\,, \qquad (191)$$

one finds

$$\frac{\rho_\theta(\omega, \boldsymbol{0}, T)}{\omega} = \frac{9\zeta}{\pi} + \frac{e+p}{c_s^2}(3c_s^2 - 1)^2 \delta(\omega) + \ldots$$

We introduce the operator

$$\mathcal{O}_\star = L^{-3/2} \int d^3\boldsymbol{x} \, \left(T_{\mu\mu}(x) + (3c_s^2 - 1) T_{00}(x)\right)\,. \qquad (192)$$

Its spectral function, which we denote by $\rho_\star$, satisfies

$$\rho_\theta(\omega, \boldsymbol{0}, T) = \rho_\star(\omega, \boldsymbol{0}, T) + \frac{e+p}{c_s^2}(3c_s^2 - 1)^2 \,\omega\, \delta(\omega) \qquad (193)$$

and, in view of Eq. (192), is free of the delta function at the origin.

We are now ready to turn Eq. (185) into a sum rule for $\rho_\star$, the spectral function of the operator $\mathcal{O}_\star$ (192), which is smooth at the origin. Using Eq. (193), one finds

$$2\int_0^{\infty} \frac{d\omega}{\omega} [\rho_\star(\omega, T) - \rho_\star(\omega, 0)] = 3(1-3c_s^2)(e+p) - 4(e-3p)\,. \qquad (194)$$

Eq. (185) was already obtained in [95], but the presence of the $\omega\delta(\omega)$ term in ρ_θ was missed. In [57], a finite spatial momentum $\boldsymbol{k}$ was used as an infrared regulator and the contribution of the zero-frequency delta function correctly identified for the first time. If one insists on expressing Eq. (194) in terms of ρ_θ, one should strictly write $\lim_{\epsilon\to 0} \int_{-\infty}^{\infty} \frac{\omega\, d\omega}{\omega^2+\epsilon^2} \varDelta\rho_\theta(\omega, T) = 3(1-3c_s^2)(e+p) - 4(e-3p)$.

In the shear channel, a similar sum rule applies in the Yang-Mills theory, as first pointed out in [57]. It was later also studied in lattice regularization [96]. There it was given in the form

$$\begin{aligned} \int_{-\infty}^{\infty} \frac{\mathrm{d}\omega}{\omega}\, \varDelta\rho_{12,12}(\omega, \boldsymbol{p} = 0, T) &= \frac{2}{3} e(T) \qquad (195) \\ &\quad - \lim_{\omega\to\infty} \varDelta G(\omega, T)\,, \end{aligned}$$

where

$$\begin{aligned} \varDelta G(\omega, T) \equiv \int \mathrm{d}^4x\, e^{i\omega x_0} \Big\langle &-\tfrac{2}{3} T_{00}(x)\, T_{00}(0) \qquad (196) \\ &+ \tfrac{1}{4}(T_{11}(x) - T_{22}(x))(T_{11}(0) - T_{22}(0))\Big\rangle_{T-0}. \end{aligned}$$

was proved to be finite. The form (195) is equivalent to the form given in [57]. The sum rule remains incomplete, because a finite, but yet undetermined contribution of the trace anomaly can affect $\varDelta G(\omega \to \infty, T)$. The determination of its OPE coefficient requires a two-loop calculation. To our knowledge, this contact term can not be determined by Ward identities.

Another important example is the difference of thermal vector and axial-vector current correlators, which generalizes the Weinberg sum rules of the sixties. The difference of the corresponding spectral functions obeys sum rules $\forall \boldsymbol{k}$ in the chiral limit [97],

$$\int_0^{\infty} \frac{\mathrm{d}\omega\, \omega}{\omega^2 - \boldsymbol{k}^2} \left(\rho_L^V(\omega, \boldsymbol{k}) - \rho_L^A(\omega, \boldsymbol{k})\right) = 0. \qquad (197)$$

$$\int_0^{\infty} \mathrm{d}\omega\, \omega \left(\rho_L^V(\omega, \boldsymbol{k}) - \rho_L^A(\omega, \boldsymbol{k})\right) = 0. \qquad (198)$$

$$\int_0^{\infty} \mathrm{d}\omega\, \omega \left(\rho_T^V(\omega, \boldsymbol{k}) - \rho_T^A(\omega, \boldsymbol{k})\right) = 0. \qquad (199)$$

A remarkable point is that the difference of the vector and axial-vector spectral functions falls off rapidly at large frequencies. In the OPE analysis, the correlators first differ by a four-quark operator, which means that the difference of spectral functions falls off as ω^{-4} at high frequencies.

3.8 Correlators in Finite-volume

All the analytic treatments covered in this section are performed in infinite spatial volume. However, the Monte-Carlo calculations reviewed in section (4) are necessarily performed in finite volume $V = L^3$. The boundary conditions are normally taken to be periodic. As is manifest from the formal spectral expression (46) of the spectral density, the latter is a distribution, which consists of a collection of delta functions with a weight given by the matrix elements of the current under investigation between energy eigenstates. The spectral weight at the origin $\omega = 0$ is thus determined by transition matrix elements of the current between states whose energy differs only infinitesimally. Symmetry considerations thus do not result in as stringent restrictions as at zero temperature. For instance, for any energy eigenstate above the two-particle threshold, there typically exist energy eigenstates whose energy differs only by an amount of order $1/L$ and which are connected to it by a non-vanishing matrix element.

Clearly one cannot literally apply the Kubo formula to the finite-volume spectral function, since this would given a undefined value. The situation is similar in this respect to the discussion of the spectrum of the Dirac operator. In that context, the spectral density at threshold in infinite volume is equal to the chiral condensate $-\langle\bar\psi\psi\rangle$. In finite volume, the Dirac spectrum is discrete and therefore it is necessary to send the volume to infinity (before setting the quark mass m to zero) in order to extract the value of the chiral condensate. However, if the density is given by

$$\rho(\lambda, m) = \sum_{k=1}^{\infty} \delta(\lambda - \lambda_k), \qquad (200)$$

the difficulty can be dealt with by working with the integrated spectral density [98],

$$\nu(M, m) = V \int_{-\Lambda}^{\Lambda} \mathrm{d}\lambda\, \rho(\lambda, m), \qquad \Lambda = \sqrt{M^2 - m^2}. \qquad (201)$$

A finite spectral density manifests itself by a linearly rising $\nu(M, m)$ as a function of M on a scale much larger than the typical eigenvalue interspacing, but much smaller than the scale on which a curvature arises. This behavior is readily seen in simulations of QCD in large but finite volume [98]. In the case at hand of thermal spectral functions of gauge invariant operators, a natural way to deal with the singular nature of the spectral functions is to work with the coordinate-space retarded correlator $G^{AB}(t)$. For $B = A = A^\dagger$, inverting the Fourier transform (32) yields

$$G(t) = 2\int_0^\infty \mathrm{d}\omega\, \sin(\omega t)\, \rho(\omega). \qquad (202)$$

Consider for illustration the quantum Hamiltonian of a free particle coupled to an assembly of harmonic oscillators ($[q, p] = i$, $[q_n, p_m] = i\delta_{nm}$) [99,100],

$$\hat H = \frac{\hat p^2}{2m} + \tfrac{1}{2}\sum_n \{(\hat p_n - \kappa_n \hat q)^2 + \omega_n^2 \hat q_n^2\}. \qquad (203)$$

The Heisenberg equations of motion $\dot{\hat Y} = i[\hat H, \hat Y]$ are easily obtained (first for the annihilation operators $\hat a_n \equiv \frac{\omega_n \hat q_n + i\hat p_n}{\sqrt{2\omega_n}}$, then for $\hat p$ and $\hat q$) and cast in the form

$$\dot{\hat q}(t) = \hat p(t)/m\,, \qquad (204)$$

$$\dot{\hat p}(t) = \hat\xi(t) - \int_0^t \mathrm{d}s\, f(t-s)\, \dot{\hat q}(s)\,, \qquad (205)$$

$$\hat\xi(t) \equiv \sum_n \kappa_n \frac{\omega_n}{2i}\Big[\hat a_n(0) e^{-i\omega_n t} - \hat a_n^\dagger(0) e^{i\omega_n t}\Big], \qquad (206)$$

$$f(t) = \sum_n \kappa_n^2 \cos\omega_n t. \qquad (207)$$

The operator equations for $\hat q$ and $\hat p$ resemble formally the classical Langevin equation with a memory kernel given by $f(t)$. The commutator-defined correlator of the operator $\hat\xi(t)$, which plays the role of the random force term, is given by

$$G^{\xi\xi}(t) \equiv i[\xi(t), \xi(0)] = -\frac{df(t)}{dt} \qquad (208)$$

and, based on Eq. (202), the spectral function by

$$\frac{2\rho(\omega)}{\omega} = \sum_n \kappa_n^2 \delta(\omega - \omega_n). \qquad (209)$$

It has the expected form for a spectral function (Eq. 46).

Imagine now that the frequencies ω_n correspond to differences of photon or phonon modes in a box of size L,

$$\omega_n = 2\pi n/L, \qquad n \in \mathbb{Z}, \qquad (210)$$

and that

$$\kappa_n^2 = \frac{1}{L}\frac{2\Gamma\chi}{\Gamma^2 + \omega_n^2}, \qquad (211)$$

then one finds

$$G^{\xi\xi}(t) = -\chi\Gamma \frac{\sinh \Gamma(t - L/2)}{\sinh \Gamma L/2}\,. \qquad (212)$$

In the limit of infinite volume, linear response predicts that the retarded correlator falls off exponentially and the spectral function has the form of a Lorentzian[5],

$$G^{\xi\xi}(t) = \chi\Gamma e^{-\Gamma|t|} \qquad (213)$$

$$\rho^{\xi\xi}(\omega) = \frac{\chi}{\pi}\frac{\Gamma\omega}{\Gamma^2 + \omega^2}. \qquad (214)$$

---

[5] Non-linear effects in general dominate at large times with $G(t) \sim t^{-3/2}$. The cross-over time from the exponential to the power-law behavior is however parametrically of order N_c^2 in SU(N_c) gauge theories [101].

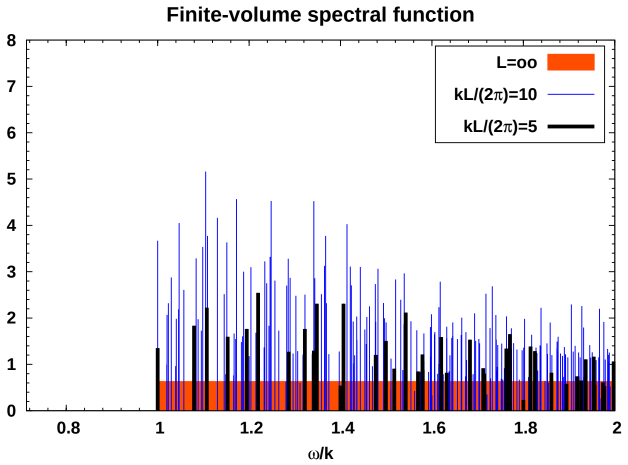

Fig. 17. Comparison of spectral functions in finite and infinite volume, in a free (3+1)-dimensional massless scalar field theory at zero temperature. The infinite-volume spectral function is a step function at threshold, $\omega = |\boldsymbol{k}|$. Two different volumes are shown.

The lesson we draw from this example is that in infinite volume, the parameters of a transport peak could be read off the asymptotic $t \to \infty$ behavior of $G^{\xi\xi}(t)$. In finite volume on the other hand, Eq. (212), these parameters have to be read off for $t \ll L$, but large enough for contributions from higher frequencies to have died off. The window of real-time in which the transport properties can be extracted thus only exists for a sufficiently large volume.

To conclude with this example, when $\Gamma \to \infty$, $\rho(\omega) = \frac{\chi}{\pi}\frac{\omega}{\Gamma}$, the memory function becomes a delta function, $f(t) = 2\gamma\delta(t)$, $\gamma \equiv \frac{\chi}{\Gamma}$ and Eq. (205) takes the form of the memory-free Langevin equation [100]. If one then attributes a thermal distribution to the occupation numbers of the photonic energy levels, $\langle \hat{a}_n^\dagger \hat{a}_m \rangle = \delta_{nm} n_B(\omega_n)$, $n_B(\omega) = (e^{\beta\omega} - 1)^{-1}$, one recovers familiar results (see section 4.6) such as

$$\frac{1}{2m}\langle \hat{p}^2(t)\rangle \overset{t\to\infty}{=} \frac{\gamma}{\pi m}\int_0^\infty \mathrm{d}\omega\, \frac{\omega n_B(\omega)}{(\gamma/m)^2 + \omega^2} + \dots \qquad (215)$$

where the dots represent a temperature-independent term. For $\gamma/m \to 0$, the first term reproduces the equipartition result $\frac{1}{2}k_B T$.

To familiarize oneself with the infinite-volume limit further it may be useful to look at a specific example in 3+1 dimensions. Consider a free massless scalar field theory at $T = 0$ and the correlator of the mass operator,

$$G_E(t, \boldsymbol{k}) = \int \mathrm{d}\boldsymbol{x}\, e^{i\boldsymbol{k}\cdot\boldsymbol{x}}\, \langle \phi^2(t, \boldsymbol{x})\, \phi^2(0)\rangle. \qquad (216)$$

One easily finds the expressions for the Euclidean correlator

$$G_E(t, \boldsymbol{k}) = \frac{e^{-|\boldsymbol{k}|t}}{(4\pi)^2 t}\,, \qquad (217)$$

and the associated spectral function,

$$\rho(\omega, \boldsymbol{k}) = \frac{1}{(4\pi)^2}\,\theta(\omega - |\boldsymbol{k}|). \qquad (218)$$

In a finite periodic box on the other hand,

$$G_E(t, \boldsymbol{k}) = \frac{1}{L^3}\sum_{\boldsymbol{p}} \frac{e^{-|\boldsymbol{p}|t}}{2|\boldsymbol{p}|}\, \frac{e^{-|\boldsymbol{k}-\boldsymbol{p}|t}}{2|\boldsymbol{k}-\boldsymbol{p}|}\,, \qquad (219)$$

and the corresponding spectral function

$$\rho(\omega, \boldsymbol{k}) = \frac{1}{L^3}\sum_{\boldsymbol{p}} \frac{\delta(\omega - |\boldsymbol{p}| - |\boldsymbol{k}-\boldsymbol{p}|)}{4|\boldsymbol{p}|\,|\boldsymbol{k}-\boldsymbol{p}|} \qquad (220)$$

is, as expected, a collection of delta functions accompanied by a weight factor. The spectral functions are displayed in Fig. (17) for illustration. The 'spikes' in the finite-volume spectral function have been drawn with a height proportional to the weight of the corresponding delta function. It is clear that the finite-volume spectral function does not converge towards the infinite spectral function point-by-point in ω, but rather in the sense of distributions. In infinite volume the convolution of the spectral function with a Gaussian 'resolution function',

$$F(\omega_0, \Gamma) \equiv \int_0^\infty \mathrm{d}\omega\, \rho(\omega, \boldsymbol{k} = 0)\frac{e^{-(\omega-\omega_0)^2/2\Gamma^2}}{\sqrt{2\pi}\Gamma}\,, \qquad (221)$$

amounts to $\frac{1}{4\pi^2}$, for $\Gamma \ll \omega_0$. In finite volume, on the other hand, the corresponding integral amounts to (using the Poisson summation formula)

$$\begin{aligned} F_L(\omega_0, \Gamma) = \frac{1}{(4\pi)^2}\sum_{\boldsymbol{m}\in\mathbb{Z}^3} &\frac{2\sin\frac{\omega_0|\boldsymbol{m}|L}{2}}{\omega_0 L|\boldsymbol{m}|} \\ &\exp\left(-\frac{\boldsymbol{m}^2 L^2 \Gamma^2}{8}\right), \quad \Gamma \ll \omega_0,\ \Gamma^2 L \ll \omega_0. \end{aligned} \qquad (222)$$

Thus one sees that on a resolution scale Γ which is not too small compared to $1/L$, $F_L(\omega_0, \Gamma)$ is a good approximation to its infinite-volume counterpart. This point was already made a long time ago in the study of non-relativistic systems [102]. The volume thus intrinsically limits the resolution in ω at which one can determine properties of the infinite-volume spectral function with good accuracy. The simple formula (222), displayed in Fig. (18), also illustrates that the convergence of F_L to F is rather 'erratically' dependent on ω_0; for instance, if ω_0 is a multiple of $2/L$, all contributions of the type $\boldsymbol{m} = (0, 0, m)$ vanish.

4 An Overview of Lattice Calculations

In this section we give an overview of the technical aspects of lattice QCD relevant to the calculations of Euclidean correlators, and review the latest of these calculations; the discussion of their analysis in terms of the spectral function is postponed till section (5). We begin by reminding the reader of the Matsubara formalism in section (4.1). The basics of lattice regularized QCD are given in section (4.2). The question of the renormalization of correlation functions is briefly discussed in section (4.3), and their discretization effects are investigated perturbatively

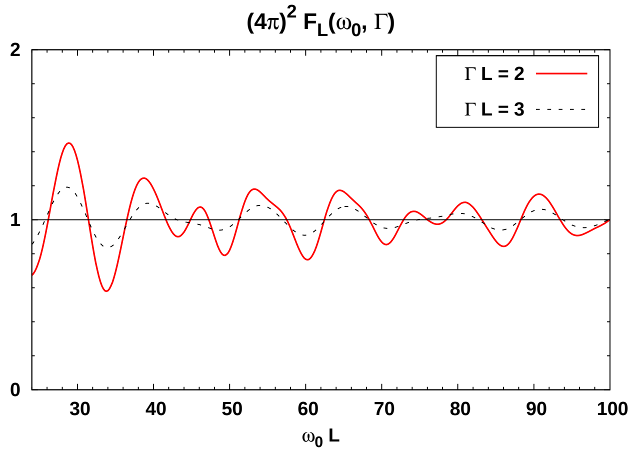

Fig. 18. The function F_L as given by Eq. (222), normalized to converge to 1 in the limit $L \to \infty$. It represents the convolution of the finite-volume spectral function with a Gaussian of width Γ centered at ω_0. At fixed L, increasing the resolution in frequency comes at the cost of enhancing the finite-volume effect.

in section (4.4). We then review the lattice calculations of light-quark vector current correlators, HQET correlators and energy-momentum tensor correlators (sections 4.5 to 4.7 respectively). An important question for the field is how the accuracy of the calculations scale with the lattice spacing and volume, and this question is addressed in section (4.8). Finally, we briefly mention the possibility of probing the relaxation of conserved charge densities through off-diagonal correlators, G^{AB} with A different from B.

4.1 Path-integral representation of the partition function

In this subsection we briefly sketch the origin of the imaginary time path-integral formalism of thermal field theory. To arrive at the path integral formula for the partition function (see Eq. 21) of a scalar field theory, we evaluate the trace using the eigenvectors of the field operator

$$\hat{\phi}(0,\boldsymbol{x})|\phi\rangle = \phi(\boldsymbol{x})|\phi\rangle. \qquad (223)$$

Then the partition function can be written as

$$\begin{aligned} Z = \mathrm{Tr}\,\{e^{-\beta H}\} &= \textstyle\int \prod_{\boldsymbol{x}} (d\phi_a(\boldsymbol{x}))\langle\phi_a|e^{-\beta H}|\phi_a\rangle \qquad (224)\\ &= \textstyle\int \prod_{\boldsymbol{x}} (d\phi_a(\boldsymbol{x}))\langle\phi_a|U(-i\beta)|\phi_a\rangle \end{aligned}$$

We can then use the standard path integral formula for the matrix elements of $U(t)$ (see for instance [53]),

$$\begin{aligned} \langle\phi_b|U(t)|\phi_a\rangle = &\textstyle\int_{\phi_a}^{\phi_b}[\,\mathrm{d}\phi] \qquad (225)\\ &\exp\left\{-\,i\textstyle\int_0^t \mathrm{d}t' \int \mathrm{d}\boldsymbol{x}\,\mathcal{L}(\partial_t\phi(t',\boldsymbol{x}),\phi(t',\boldsymbol{x}))\right\}. \end{aligned}$$

Now setting $t \doteq -i\beta$, $b = a$ and summing over a yields

$$\begin{aligned} Z_{\mathrm{boson}} = &\textstyle\int_{\mathrm{periodic}}[d\phi] \qquad (226)\\ &\exp\left\{-\textstyle\int_0^\beta \mathrm{d}t \int \mathrm{d}\boldsymbol{x}\,\mathcal{L}_E(\partial_t\phi(t,\boldsymbol{x}),\phi(t,\boldsymbol{x}))\right\}, \end{aligned}$$

where

$$\mathcal{L}_E(\partial_t\phi(t,\boldsymbol{x}),\phi(t,\boldsymbol{x})) = -\mathcal{L}(i\partial_t\phi(t,\boldsymbol{x}),\phi(t,\boldsymbol{x})). \qquad (227)$$

For fermions, the representation of the partition function using Grassmann variables leads to

$$\begin{aligned} Z_{\mathrm{fermion}} = &\textstyle\int_{\mathrm{antiperiodic}}[d\psi] \qquad (228)\\ &\exp\left\{-\textstyle\int_0^\beta \mathrm{d}t \int \mathrm{d}\boldsymbol{x}\,\mathcal{L}_E(\partial_t\psi(t,\boldsymbol{x}),\psi(t,\boldsymbol{x}))\right\}. \end{aligned}$$

Without reproducing the proof in detail, we illustrate where the antiperiodic boundary condition comes from in a two-state system, $\{|0\rangle, |1\rangle\}$. Coherent fermionic states are defined by

$$|\eta\rangle = e^{-\eta a^\dagger}|0\rangle, \qquad \langle\eta| = \langle 0|e^{-a\eta^*}. \qquad (229)$$

where η and η^* are Grassmann variables. The definition

$$\textstyle\int \mathrm{d}\eta^*\,\mathrm{d}\eta\,\eta\,\eta^* = 1 \qquad (230)$$

furthermore implies the 'completeness relation'

$$\textstyle\int \mathrm{d}\eta^*\,\mathrm{d}\eta\,e^{-\eta^*\eta}|\eta\rangle\langle\eta| = \mathbf{1}. \qquad (231)$$

Some algebraic manipulations then lead to

$$\begin{aligned} \mathrm{Tr}\,\{e^{-\beta H}\} &= \sum_{0\le k<2} \langle k|\,e^{-\beta H}|k\rangle \qquad (232)\\ &= \textstyle\int \mathrm{d}\eta^*\,\mathrm{d}\eta\,e^{-\eta^*\eta}\langle -\eta|e^{-\beta H}|\eta\rangle, \qquad (233) \end{aligned}$$

where the minus sign in $\langle -\eta|$ translates into the antiperiodic boundary condition. See for instance the appendix of Ref. [103] for the generalization to multiple degrees of freedom.

4.2 Common actions in lattice QCD

For definiteness we write out the simplest action for lattice QCD [104]. We restrict ourselves to a four-dimensional cubic lattice, and the lattice spacing is denoted by a. The unit vectors $\hat{\mu}$ are aligned along the four directions of the lattice of highest symmetry. The dynamical variables are (a) the 'link' variables $U_\mu(x) \in SU(3)$, which can be thought of as living on the link from x to $x + a\hat{\mu}$, and (b) the Grassmann variables $\psi(x)$, which are Dirac spinors in the fundamental color representation and live on the lattice sites. The latter correspond to the quarks, while the 'link variables' are classically related to the gauge potential by $U_\mu(x) = e^{iaA_\mu(x)}$.

The Wilson gauge action reads

$$S_{\mathrm{g}} = \frac{1}{g_0^2}\sum_{x,\mu,\nu} \mathrm{Re}\,\mathrm{Tr}\,\{1 - P_{\mu\nu}(x)\}\,, \qquad (234)$$

$$P_{\mu\nu}(x) = U_\mu(x)U_\nu(x+a\hat{\mu})U_\mu(x+a\hat{\nu})^{-1}U_\nu(x)^{-1}. \qquad (235)$$

The Wilson fermion action reads

$$S_{\mathrm{f}} = a^4\sum_x \bar{\psi}(x)\left(\widetilde{\nabla}_\mu\gamma_\mu + m + \tfrac{1}{2}a\triangle\right)\psi(x), \qquad (236)$$

where the summation over μ is understood. Here $\widetilde{\nabla}_\mu = \frac{1}{2}(\nabla_\mu + \nabla_\mu^*)$ is the symmetric covariant derivative and $\triangle = \partial_\mu \partial_\mu^*$ the covariant Laplacian,

$$\nabla_\mu \psi(x) = \frac{1}{a}\big(U_\mu(x)\psi(x+a\hat{\mu}) - \psi(x)\big), \qquad (237)$$

$$\nabla_\mu^* \psi(x) = \frac{1}{a}\big(\psi(x) - U_\mu(x)^{-1}\psi(x-a\hat{\mu})\big). \qquad (238)$$

In numerical implementations, the hopping parameter κ, defined by

$$\kappa^{-1} = 2am + 8, \qquad (239)$$

is used to parametrize the bare quark mass, and the quark field is rescaled so as to give the $\bar{\psi}(x)\psi(x)$ term in Eq. (236) a unit coefficient. The discretization errors of the Wilson action are $\mathrm{O}(a)$, even at the classical level. Therefore it is useful to improve the action by adding dimension-five operators with coefficients tuned to remove the leading cutoff effects on the spectrum of the theory [105]. Fortunately, having made use of the equations of motion, a single operator needs to be considered, a Pauli term $ac_{\rm sw}\bar{\psi}(x)\frac{i}{4}\sigma_{\mu\nu}F_{\mu\nu}(x)\psi(x)$ [106]. The coefficient $c_{\rm sw} = 1 + \mathrm{O}(g_0^2)$ has been determined non-perturbatively for a wide range of bare couplings in the $N_{\rm f} = 0$ [107], 2 [108] and 3 theories [109].

The Wilson action (improved or not) preserves the vector flavor symmetry $\mathrm{SU}(N_{\rm f})$, while the axial symmetry is broken. The space-time symmetries are of course broken down to discrete groups on the lattice. The discrete symmetries P and C are preserved. In general, it is the exact gauge invariance of lattice QCD actions and the compactness of the gauge degrees of freedom make non-perturbative calculations possible.

For a brief introduction to Kogut-Susskind (also called staggered) quarks [110], see [111], section (3.F). An introduction to Domain-Wall [112,113] and Overlap [114] fermions, which preserve chiral symmetry on the lattice, is given in [1,115].

Since the quark action is quadratic, the Grassmann variables can be integrated out exactly, yielding in the *numerator* the determinant of the Dirac operator D (or equivalently, of $Q \equiv \gamma_5 D = Q^\dagger$). In the simplest form, the determinant is then represented as a Gaussian integral over a 'pseudofermion' field ϕ, which is a c-number field on which the Dirac operator acts in the same way as on a fermion field. The action reads

$$S_{\rm g}[U] + \phi^\dagger |Q|^{-N_{\rm f}}\phi. \qquad (240)$$

It is manifestly positive-definite for an even number of mass-degenerate flavors, while the absolute value of Q is taken for an odd number of flavors. The 'Boltzmann' factor e^{-S} is a real, positive definite integrand in the path integral, and can therefore be interpreted as a probability distribution for the gauge fields. This property allows one to apply importance sampling methods to generate gauge field configuration which dominate the path integral. The best known algorithm to generate these configurations is the Hybrid Monte-Carlo algorithm [116]. In the past decade many improvements have been made to its earliest implementation. Of particular relevance are the more faithful representations of the quark determinant through several pseudofermions (instead of just one), where the long wavelength modes are separated from short wavelength modes. The most widely used realizations of this idea are the mass preconditioning (MPHMC [117]), the domain-decomposition (DDHMC [118]) and the rational HMC (RHMC [119]) algorithms.

The calculation of correlation functions amounts to calculating quark propagators on background gauge fields, i.e. solving the equation $D[U]\psi = \eta$ for a given spinor field $\eta(x)$ carrying Dirac and color indices. Much progress has been made in speeding up the solution of this equation, which results in an improved scaling of the cost towards the chiral limit [120,121,122]. In the simplest implementation, gluonic correlators are evaluated by computing the correlation on the generated ensemble of gauge field configurations. However, in the absence of fermions the locality of the action can be exploited to sample the fields more efficiently (multi-level algorithms [123,124]).

The 'quenched' approximation consists in neglecting the gauge-field dependence of the fermion determinant altogether. The fermions then only appear at the level of the correlation functions. As a consequence, the weighting factor of configurations e^{-S_g} is local, and a heat-bath update algorithm can be employed, resulting in an update speedup factor on the order of 100. See [125] for a review of the state-of-the-art in simulation algorithms.

4.3 Renormalization of lattice correlation functions

Most lattice calculations are restricted to on-shell correlators. An on-shell correlator avoids any contact terms in coordinate space, so that the equations of motion can be used to simplify its renormalization. In the case of the vector and the axial-vector current only a finite multiplicative renormalization is then necessary. For instance, the renormalization factors $Z_A(g_0)$ and $Z_V(g_0)$ have been determined non-perturbatively in the $N_{\rm f} = 2$ $\mathrm{O}(a)$-improved Wilson theory [126,127].

The renormalization of the lattice energy-momentum tensor is more complicated already in the continuum, due to the trace anomaly. In addition, the lattice regulator breaks continuous translation invariance, resulting in additional (finite) renormalization effects. In the continuum, a symmetric and gauge invariant form of the energy-momentum tensor is

$$\begin{aligned}
T_{\mu\nu} &\equiv \theta^{\rm g}_{\mu\nu} + \theta^{\rm f}_{\mu\nu} + \tfrac{1}{4}\delta_{\mu\nu}(\theta^{\rm g} + \theta^{\rm f}), \qquad (241)\\
\theta^{\rm g}_{\mu\nu} &= \tfrac{1}{4}\delta_{\mu\nu}F^a_{\rho\sigma}F^a_{\rho\sigma} - F^a_{\mu\alpha}F^a_{\nu\alpha},\\
\theta^{\rm f}_{\mu\nu} &= \tfrac{1}{4}\textstyle\sum_f \bar{\psi}_f \overset{\leftrightarrow}{D}_\mu \gamma_\nu \psi_f + \bar{\psi}_f \overset{\leftrightarrow}{D}_\nu \gamma_\mu \psi_f - \tfrac{1}{2}\delta_{\mu\nu}\bar{\psi}_f \overset{\leftrightarrow}{D}_\rho \gamma_\rho \psi_f,\\
\theta^{\rm g} &= \beta(g)/(2g)\ F^a_{\rho\sigma}F^a_{\rho\sigma}, \quad \theta^{\rm f} = \textstyle\sum_f m_f \bar{\psi}_f \psi_f\ ,
\end{aligned}$$

where $\overset{\leftrightarrow}{D}_\mu = \vec{D}_\mu - \overset{\leftarrow}{D}_\mu$. This form has finite matrix elements between physical states (but divergences appear in offshell correlation functions). The term $\theta^{\rm g}$ is the trace anomaly [128,129]. On the lattice, there is a lot of freedom as to how to discretize these expressions [130]. An important consideration is that the traceless part $\theta_{\mu\nu}$ for $\mu = \nu$ belongs to a three-dimensional irreducible representation of the H(4) group [131], while $\theta_{\mu\nu}$ for $\mu \neq \nu$ belongs to a six-dimensional representation and θ belongs to the trivial representation. Because there are no other gauge invariant operators of dimension four in these representations, their renormalization is multiplicative. The renormalization of θ is particularly simple when its discretization is based on the action itself, in which case the renormalization factor is expressed in terms of the lattice beta function, $dg_0^{-2}/d\log a$. For $\theta_{\mu\nu}$ ($\mu = \nu$), the renormalization factor of $\theta_{\mu\nu}$ for $\mu = \nu$ of the discretization based on plaquettes can be related to anisotropy coefficients [132,133].

A number of quantities of interest are defined through frequency-space correlation functions, which are not on-shell quantities. These include the static susceptibility of the quark number density,

$$\chi_s(\boldsymbol{k}) = \int_0^\beta \mathrm{d}t \int \mathrm{d}\boldsymbol{x}\, e^{-i\boldsymbol{k}\cdot\boldsymbol{x}}\, \langle n(-it,\boldsymbol{x})\, n(0)\rangle. \qquad (242)$$

At $\boldsymbol{k} = 0$, this corresponds to the derivative of the free energy with respective to the chemical potential. Another example is the static susceptibility of the axial current, which was shown to be related to the finite-temperature dispersion relation of the 'pion' quasiparticle [134],

$$\chi_5\delta^{ab} = \int \mathrm{d}t\ \mathrm{d}\boldsymbol{x}\, \langle A_0^a(-it,\boldsymbol{x})\, A_0^b(0)\rangle, \qquad (243)$$

$$A_\mu^a(x) = \bar{\psi}\gamma_\mu\gamma_5\tfrac{\tau^a}{2}\psi. \qquad (244)$$

Care has to be taken to renormalize these correlation functions. Using a conserved current greatly simplifies this task, but this requires an exact chiral symmetry on the lattice. Formulations preserving an exact chiral symmetry exist but are computationally expensive [135].

We illustrate in the case of the vector current how off-shell correlation functions on the lattice can be given the same structure as in the continuum [136]. By performing a non-anomalous change of variables in the path integral, one obtains the identity $\langle\delta S\mathcal{O}\rangle = \langle\delta\mathcal{O}\rangle$ for a general operator $\mathcal{O}$. We now consider the case of Wilson fermions for simplicity. From the transformation

$$\delta\psi(x) = \omega(x)\psi(x), \quad \delta\bar{\psi}(x) = -\omega(x)\bar{\psi}(x), \qquad (245)$$

one obtains, for $\mathcal{O} = j_\nu(0)$,

$$\sum_\mu \hat{k}_\mu \Pi_{\mu\nu}(k) = 0, \quad (\hat{k}_\mu = \tfrac{2}{a}\sin(\tfrac{1}{2}ak_\mu)), \qquad (246)$$

$$\Pi_{\mu\nu}(k) = a^4\sum_x e^{ik\cdot x}\langle j_\mu(x)\, j_\nu(0)\rangle + a\delta_{\mu\nu}\langle s_\nu(0)\rangle \qquad (247)$$

where the conserved vector current and the point-split scalar operator take the form

$$j_\mu(x) = \tfrac{1}{2}\big(\bar{\psi}(x+a\mu)(1+\gamma_\mu)U_\mu^{-1}(x)\psi(x) - \bar{\psi}(x)(1-\gamma_\mu)U_\mu(x)\psi(x+a\mu)\big). \qquad (248)$$

$$s_\nu(x) = \tfrac{1}{2}\big(\bar{\psi}(x+a\hat{\nu})(1+\gamma_\nu)U_\nu^{-1}(x)\psi(x) + \bar{\psi}(x)(1-\gamma_\nu)U_\nu(x)\psi(x+a\nu)\big). \qquad (249)$$

Eq. (246) corresponds in configuration space to

$$\sum_\mu \partial_\mu^*\langle j_\mu(x)j_\nu(0) + a^{-3}\delta_{\mu\nu}\delta_{x,0}s_\nu(0)\rangle = 0 \quad \forall x, \qquad (250)$$

which shows that the second term takes care of removing a quadratically divergent contact term. No summation over ν is implied in Eq. (247) and (250).

4.4 Lattice perturbation theory

The perturbative calculations of thermal spectral functions and Euclidean correlators are reviewed in section (3.5). Here we describe the results of free field calculations performed in lattice perturbation theory (see [138] for a general review of this subject). The motivation is to quantify the size of discretization errors for standard lattice actions and discretizations of the local operators in a controlled framework, namely leading order perturbation theory. Thus these calculations allow one to make an informed decision in choosing a discretization, and also allow one to estimate what lattice spacing it will be necessary to reach in order to achieve a certain accuracy. We will consider correlators in the mixed representation where they depend on time t and spatial momentum $\boldsymbol{k}$. This representation has the advantage that the correlator is 'on-shell'. The approach to the continuum of on-shell correlators is considerably simpler than that of off-shell correlators because the latter involve an integration over the contact region [105]. For a given lattice spacing $a = 1/(TN_t)$, there will thus be a range of time separations t and spatial momenta $\boldsymbol{k}$ for which the discretization errors is below a prescribed level, say 3%.

As an example, it is interesting to quantify how badly the breaking of translation invariance on the lattice affects the conservation of energy and momentum as measured by a discretization of T_{00} and T_{0k}. Indeed, the correlators $G_{00,00}(t,\boldsymbol{k}=\boldsymbol{0})$ and $G_{03,03}(t,\boldsymbol{k}=\boldsymbol{0})$ are t independent in the continuum, but on the lattice they suffer of discretization errors which vanish as $\sim a^2$ for a fixed t. Fig. (19) illustrates this point. It also shows that the discretization errors are numerically large, particularly in the energy correlator. A possible explanation for this large discretization effect is that the flattening results from a delicate cancellation of contributions which by power counting diverge as $1/t^5$ for small t.

The resolution in the Euclidean time variable is obviously important to constrain the spectral function. But the computational cost of decreasing the lattice spacing grows very rapidly (see section (4.8). The situation may

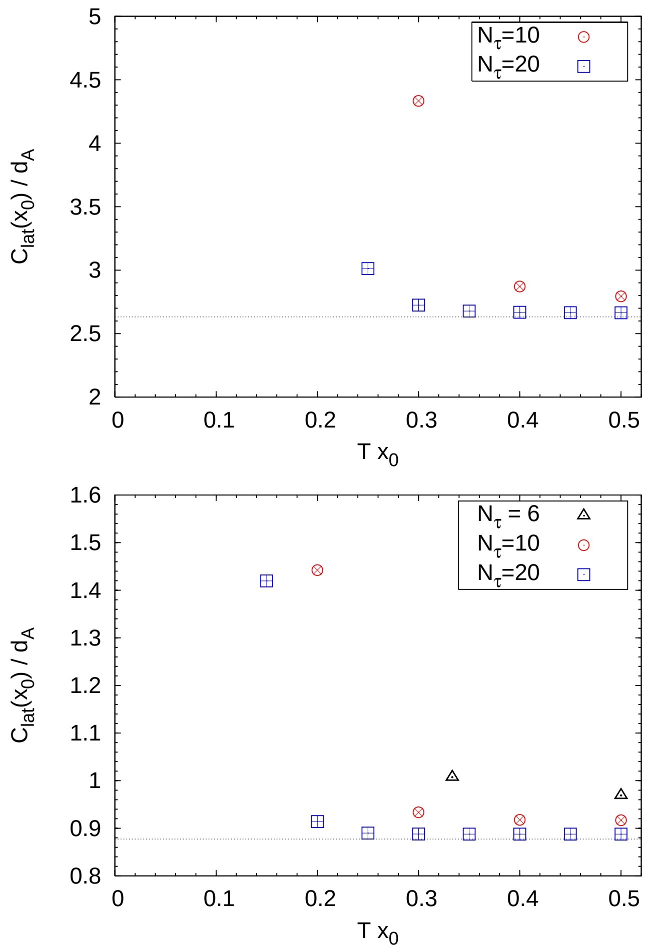

Fig. 19. Top: the treelevel $G_{00,00}(x_0, \mathbf{0})$ correlator at finite lattice spacing on the isotropic lattice in SU(3) gauge theory. The horizontal line is the continuum treelevel prediction, $4\pi^2/15$. **Bottom**: the treelevel $G_{03,03}(x_0, 0)$ correlator at finite lattice spacing on the isotropic lattice. The horizontal line is the continuum trelevel prediction, $4\pi^2/45$ [137].

potentially be improved by choosing an anisotropic lattice, where the temporal lattice spacing is smaller by a factor ξ than the spatial lattice spacing. This strategy has been followed in certain thermodynamic studies [139] and in studies of quarkonium in the deconfined phase of SU(3) gauge theory [140]. In perturbation theory it is observed that the discretization errors on thermodynamic potentials and on time-dependent correlators are more sensisitive to the value of the temporal lattice spacing than on the spatial one by a significant factor. At the same time the cost of producing independent configurations only scales as $1/a_\tau$, whereas reducing the lattice spacing on the isotropic lattice would scale as $1/a^4$. This constitutes the main motivation to use an anisotropic lattice. An example is given in Fig. (20), which displays the cutoff effect affecting the shear channel correlator $G_{13,13}(t, \boldsymbol{k} = \mathbf{0})$ in the $\mathrm{SU}(N_c)$ theory at maximum separation $t = \beta/2$. Clearly, reducing the temporal lattice spacing overall reduces the discretization error, although it changes sign for a particular value of the anisotropy near 2. The figure suggests that reducing the temporal lattice spacing by a factor 2 is almost as good as reducing the lattice spacing in each direction by the same amount.

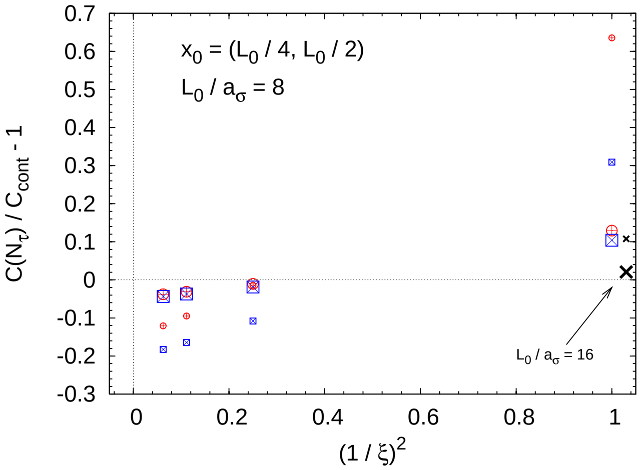

Fig. 20. The cutoff effects on the tensor correlator for $x_0 = \beta/4$ and $\beta/2$, corresponding to small and large symbols respectively [137]. The spatial lattice spacing a_σ is held fixed, the temporal lattice spacing a_τ is varied between a quarter and one times a_σ. The $\Box$'s refer to T_{12} and the $\otimes$'s to $\frac{1}{2}(T_{11} - T_{22})$. In addition, the two crosses at $\xi = 1$ indicate the reduction of the cutoff effect on the $\frac{1}{2}(T_{11} - T_{22})$ correlators when increasing β/a_σ from 8 to 16.

The results described above are obtained at tree level, and renormalization effects only set in at the next order. A drawback of the anisotropic action is that it requires a tuning of certain bare parameters in addition to the gauge coupling and the quark masses. In the pure gauge theory, the only such additional parameter is the bare anisotropy factor ξ_0 that enters the action. In effect it must be tuned in order to maintain a constant renormalized anisotropy ξ as the spatial lattice spacing is varied. The calculation of $\xi(\xi_0, g_0)$ has been carried out using various methods for the Wilson action [141,142]. Including the quarks, there are additional dimension-four operators whose coefficients need to be tuned. Methods have been developed to achieve this in the context of hadron spectroscopy [143]. In addition the anisotropic lattice complicates the normalization of local operators used in calculating thermodynamic properties or correlation functions. A possible strategy is then to determine the renormalization factors of a particular discretization based on the renormalization of the anisotropy ξ; this discretization can thereafter be used to calibrate other discretization.

The discretization effects in high-temperature meson correlators and spectral functions at nonzero-momentum and fermion mass were investigated by Aarts and Martinez-Resco in [66]. In this case the spectral function can be analyzed straightforwardly at finite lattice spacing because the transfer matrix expression of the meson correlators is simple [103]. We give as an example the Euclidean correlator of a quark bilinear $\bar{\psi}\Gamma\psi$ for (unimproved) Wilson fermions:

$$G_H(t,\boldsymbol{p}) = \frac{4N_c}{L^3}\sum_{\boldsymbol{k}} \mathrm{Tr}\,\{S(t,\boldsymbol{k})\mathit{\Gamma} S(-t,\boldsymbol{p}+\boldsymbol{k})\mathit{\Gamma}\} \tag{251}$$

$$= \frac{4N_c}{L^3}\sum_{\boldsymbol{k}} \Big[\; a_H^{(1)} S_4(t,\boldsymbol{k})S_4^\dagger(t,\boldsymbol{p}+\boldsymbol{k}) \tag{252}$$

$$-a_H^{(2)} S_i(t,\boldsymbol{k})S_i^\dagger(t,\boldsymbol{p}+\boldsymbol{k})$$

$$-a_H^{(3)} S_u(t,\boldsymbol{k})S_u^\dagger(t,\boldsymbol{p}+\boldsymbol{k})\Big]\,,$$

where for $t \neq 0$

$$S_4(t,\boldsymbol{k}) = \frac{\sinh(E_{\boldsymbol{k}}/\xi)}{2\mathcal{E}_{\boldsymbol{k}}\cosh(E_{\boldsymbol{k}}/2T)}\cosh(E_{\boldsymbol{k}}(t-\tfrac{\beta}{2}))\,, \tag{253}$$

$$S_i(t,\boldsymbol{k}) = \frac{1}{\xi}\,\frac{i\sin k_i}{2\mathcal{E}_{\boldsymbol{k}}\cosh(E_{\boldsymbol{k}}/2T)}\,\sinh(E_{\boldsymbol{k}}(t-\tfrac{\beta}{2}))\,,$$

$$S_u(t,\boldsymbol{k}) = -\frac{1-\cosh(E_{\boldsymbol{k}}/\xi)+\mathcal{M}_{\boldsymbol{k}}}{2\mathcal{E}_{\boldsymbol{k}}\cosh(E_{\boldsymbol{k}}/2T)}\sinh(E_{\boldsymbol{k}}(t-\tfrac{\beta}{2}))$$

and (r is the 'Wilson parameter' [104], usually set to unity)

$$\xi\,\mathcal{M}_{\boldsymbol{k}} = r\sum_{i=1}^{3}(1-\cos k_i) + m\,, \tag{254}$$

$$\xi\mathcal{K}_{\boldsymbol{k}} = \sum_{i=1}^{3}\gamma_i \sin k_i\,, \tag{255}$$

$$\cosh(E_{\boldsymbol{k}}/\xi) = 1 + \frac{\mathcal{K}_{\boldsymbol{k}}^2+\mathcal{M}_{\boldsymbol{k}}^2}{2(1+\mathcal{M}_{\boldsymbol{k}})}\,, \tag{256}$$

$$\mathcal{E}_{\boldsymbol{k}} = (1+\mathcal{M}_{\boldsymbol{k}})\sinh(E_{\boldsymbol{k}}/\xi)\,. \tag{257}$$

Due to the UV cutoff, the spectral function on the lattice vanishes for frequencies larger than the energy of the largest momentum in the Brillouin zone, $\boldsymbol{p} = \frac{\pi}{a}(1,1,1)$. This frequency is roughly

$$\omega_{\max} = \frac{2}{a}\log\Big(1+\frac{6+am}{\xi}\Big). \tag{258}$$

In addition, the spectral function admits several cusps corresponding to the edges of the Brillouin zone. For smaller frequencies, the finite lattice spacing affects predominantly the mismatch between the continuum and lattice light-cone, which can be substantial [66].

From a practical point of view, the conservative way to proceed is to extrapolate the Euclidean correlator to the continuum, see for instance [144,145]. Then the question of the analytic continuation takes place entirely in the continuum [145]. This way of proceeding has the advantage that analytic studies of the spectral function in the continuum, where perturbative calculations can be pushed more easily to higher orders, can be used directly.

4.5 The Electric Conductivity

As reviewed in section (3.2.1), the electric conductivity is phenomenologically important in that it determines the soft photon emission by the quark-gluon plasma, and it can be extracted from the vector current correlator via a Kubo formula. The early calculations of finite-temperature vector correlation functions were carried out with Kogut-Susskind fermions. The correlators from two such calculations, by S. Gupta [146] (up to $N_t = 12$) and Aarts et al [147] (up to $N_t = 24$), are displayed in Fig. (21). As is seen most clearly from the bottom plot, there are effectively two channels contributing, corresponding respectively to the vector current $\bar\psi\gamma_i\psi$ and the quark bilinear $\bar\psi\gamma_0\gamma_5\gamma_i\psi$; the contribution of the latter comes with a + sign on odd time-slice and a - sign on the even ones [147]. Due to this effect, the analysis proceeds separately on the even and on the odd sites, effectively resulting in a loss of resolution in the time variable by a factor 2. For this reason most recent calculations have been based on Wilson-type fermions.

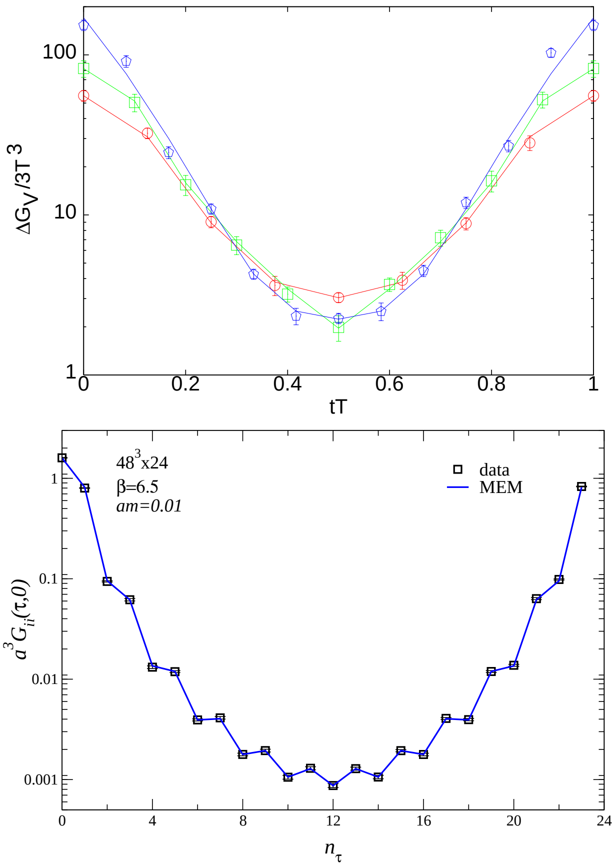

Fig. 21. Vector current correlation functions calculated with Kogut-Susskind fermions on quenched lattices at zero spatial momentum. Top: $T = 2T_c$, with $N_t = 8$ (circles), 10 (squares) and 12 (pentagons) [146]. Bottom: $T \approx 0.6T_c$ with $N_t = 24$ [147]. On both plots the curves are the result of Bayesian fits.

A very recently published calculation using O(a) improved Wilson fermions is displayed in Fig. (22), with temporal extents up to $N_t = 48$ [148]. The Euclidean correlator of the spatial components of the vector current at $1.45T_c$ has been normalized by its value in the non-

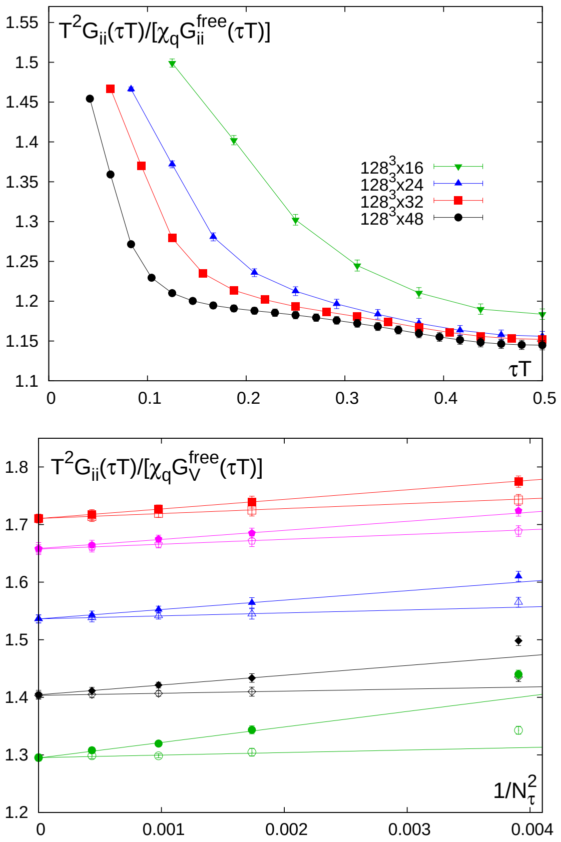

Fig. 22. Top: Vector current correlation function calculated with O(a) improved Wilson fermions on quenched lattices at zero spatial momentum [145] and $T \simeq 1.45T_c$. Bottom: from the same publication, the vector correlation function, $G_{ii}(\tau, T)$, normalized by the quark number susceptibility and the free vector correlation function calculated in the continuum (full symbols) and on lattices with temporal extent N_t (open symbols). The results of five values of Euclidean time are displayed, $\tau T = 0.1875$, 0.25, 0.3125, 0.375 and 0.5 (top to bottom), on lattices with temporal extent $N_t = 16$, 24, 32 and 48.

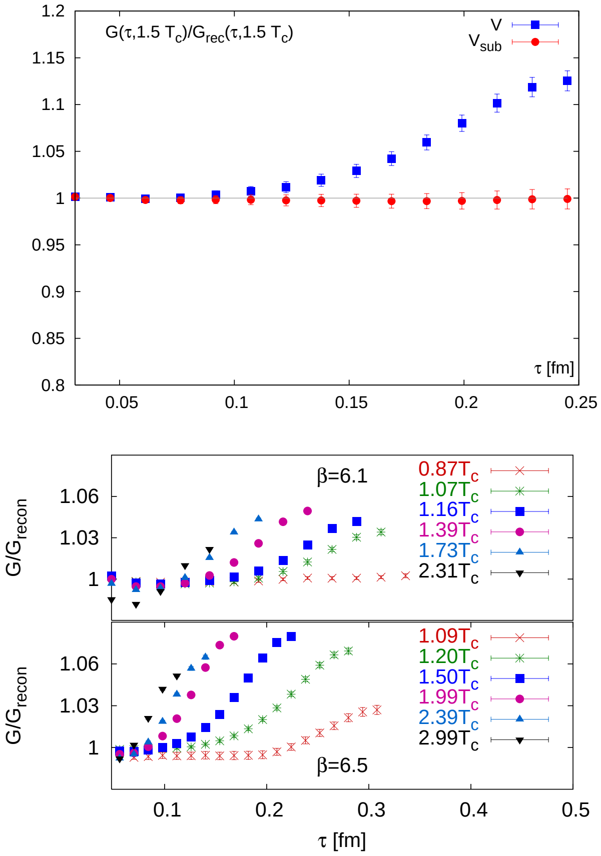

Fig. 23. Vector charm current correlation functions in quenched QCD. The ratio to the reconstructed correlator from the confined phase is taken. Top: O(a) improved Wilson fermions on isotropic lattices at $1.5T_c$ [148]. The correlator in the denominator is reconstructed from $0.75T_c$. In '$V_{\rm sub}$', the contribution of the transport peak has been subtracted. Bottom: anisotropic Fermilab lattice formulation ($\xi = 4$) at several temperatures ([140], fig. from [149]). The correlator in the denominator is reconstructed from a very low temperature. The enhancement over the reconstructed correlator is significant and is likely due to the contribution of a transport peak.

interacting limit, as well as by the quark number susceptibility. The latter normalization factor has the benefit of cancelling out the normalization of the vector current. On the bottom panel, this data is extrapolated to the continuum. One notices that normalizing by the free correlator computed at the corresponding value of N_t reduces the slope of the extrapolation, without completely eliminating it. The figure thus shows that a continuum extrapolation is mandatory for a precision analysis of Euclidean correlators. The achieved accuracy is below 1%. The continuum extrapolated data provides a solid basis for a study of the corresponding spectral function, which we will discuss in section (5.4).

The Euclidean correlator of the charm current has also been investigated extensively, with the primary motivation to study the 'melting' of charmonium states in the quark-gluon plasma. This effect is expected on general grounds at sufficiently high temperature [150], and is described in detail by resummed perturbative calculations, see in particular [151,152]. From the point of view of these studies, the presence of a transport peak of width $\sim T^2/M$, see Eq. (137), represents an undesirable contribution [153,154], which can approximately be subtracted by taking the difference of the correlator at two Euclidean-time points[155,148]. The functional form of the transport peak was calculated in [63] based on the Langevin equation, and the result is reviewed in section (3.3). If the charm quark is heavy enough to be well described by the static approximation, then the parameters of the transport peak can be obtained from a correlator calculated in heavy-quark effective theory (see the next section).

Figure (23) displays the ratio of the Euclidean correlator at $1.5T_c$ to the reconstructed correlator taken at $0.75T_c$. The latter was obtained by first solving for $\rho(\omega, 0.75T_c)$, and then applying the definition (58). The top panel presents data obtained on an isotropic lattice [148], while the lower one uses an anisotropic lattice with $a_\sigma/a_\tau = 4$ [140]. These

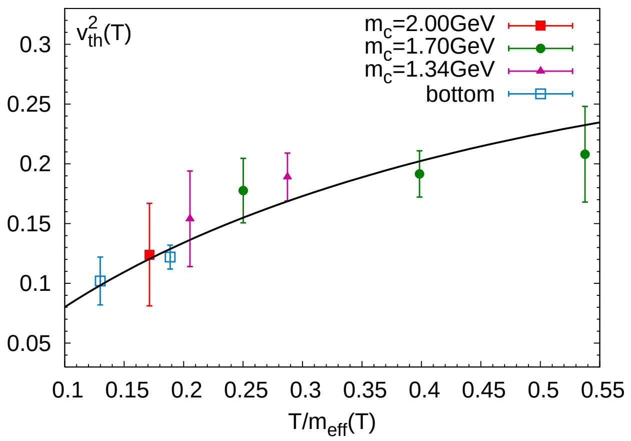

Fig. 24. Thermal velocity of the heavy quarks as a function of temperature, as extracted from the area under the transport peak in the vector current correlator [155].

calculations are performed in the quenched approximation using 'clover' improved Wilson fermions. Similar studies had been carried out earlier [156]. An important result of these analyses is that once the transport peak contribution is removed from the high-temperature correlator, the subtracted correlator at $1.5T_c$ is indistinguishable from the correlator at $0.75T_c$ to the present accuracy (top panel of Fig. 23).

At vanishing spatial momentum, the transport peak appearing in the density-density correlator is an exact delta function, and its weight is the static susceptibility χ_s. The transport peak appearing in the current-current correlator on the other hand acquires a width of order T^2/M. Its area is $\chi_s\langle v_p^2\rangle$ (see section 3.3). Therefore the thermal velocity of the heavy quarks can be extracted from the ratio. The main task consists in separating the low-frequency from the high-frequency contribution in the current correlator. An interesting analysis was carried out in [155] assuming that for $\omega > 2M$, the spectral density is unchanged from $T = 0$, which is consistent with the lattice data. Subtracting this high-frequency contribution from the Euclidean current correlator, what remains is an essentially t-independent function. Its ratio to the static susceptibility yields an estimate of the thermal velocity, displayed in Fig. (24). These results are compared to a prediction based on kinetic theory. Equating expression (136) with the susceptibility measured on the lattice defines an effective (temperature-dependent) quark mass [155]; inserting this effective mass into the equipartition prediction $\frac{1}{3}\langle v^2\rangle = \frac{T}{M}$ leads to the black curve in Fig. (24). Note that this curve is obtained without using the current correlator, and clearly the agreement with the data is excellent. This is evidence that the kinetic description works. The velocity appears to be solely a function of $\frac{T}{M}$, rather than T and M separately.

The transport peak has a width given by η, the drag coefficient (see Eq. (137)) which is of order $1/M$. Because of the smoothness of the kernel relating the spectral density to the Euclidean correlator, it is difficult to separately determine the width and height of the peak in the longitudinal current correlator from Euclidean data. This is crucial, since the height corresponds to the diffusion constant D. However, one can use heavy-quark effective theory to determine the momentum diffusion coefficient κ, in terms of which D and η can be expressed as $\eta = \kappa/(2MT)$ and $D = 2T^2/\kappa$ in the heavy quark limit. This is the subject of the next section.

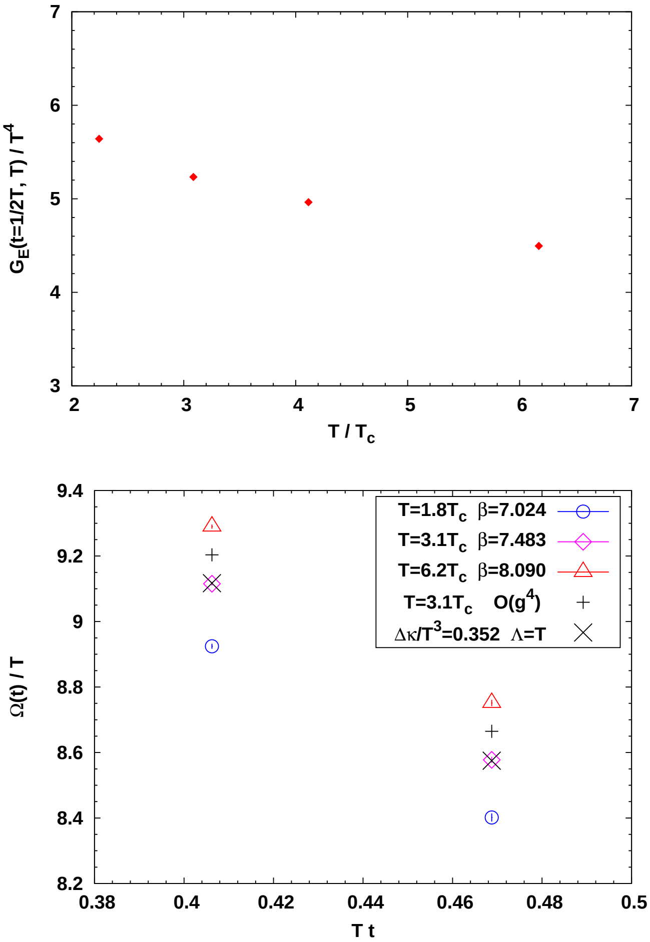

Fig. 25. Top: the Euclidean force-force correlator at $t = 1/2T$ from simulations with the Wilson action at $\beta = 7.483$ and $N_t = 8, 12, 16, 22$ [157]. The absolute normalization has been determined by matching the data at $tT = \frac{1}{4}$ and $T = 3.1T_c$ with the NLO result of Burnier et al [65]. Bottom: the quantity $\Omega(t)$, defined in Eq. (259). The '+' denote the $O(g^4)$ prediction at $3T_c$ [65]. The '×' denote the function $\Omega(t)$ that results from adding the low-frequency contribution $\Delta\rho(\omega) = \frac{1}{\pi}\Delta\kappa\tanh(\omega/2T)\theta(\Lambda-|\omega|)$ to the O(g^4) spectral function, with parameters $\Delta\kappa$ and Λ given in the caption.

4.6 Heavy Quark Diffusion

In the current correlator of a heavy quark flavor, the tail of the transport peak contains the information on the momentum diffusion coefficient κ, see Eq. (139). Here we review a first calculation of the HQET correlator (142) in the SU(3) gauge theory [157], from which κ can be extracted from the Kubo-type formula (143). The classical interpretation of the correlator is that it measures the (Lorentz) force correlator along the worldline of a heavy quark.

On the lattice the chromo-electric field is not protected from renormalization (unlike in the continuum). Since this normalizing factor has not yet been calculated, the next-to-leading order perturbative calculation of Burnier et al [65] was used to normalize the lattice correlator. The condition that the lattice correlator agree with the perturbative correlator at relatively short distances ($tT = \frac{1}{4}$) and $T = 3.1T_c$ was used. The resulting values of the Euclidean correlator at the maximal separation of $t = \frac{\beta}{2}$ are displayed in Fig. (25). The temperature was varied by changing N_t from 8 to 22 at fixed $6/g_0^2 = 7.483$. The temperature variation between $2T_c$ and $6T_c$ is on the order of 20%. The sign of the variation is the same as predicted by the perturbative expression: the magnitude of the force-force correlator in the gluon plasma increases as the temperature is decreased.

A quantity that measures the relative fall-off of the Euclidean correlator is the quantity $\Omega(t) \geq 0$ defined by

$$\frac{G_E(t-a/2)}{G_E(t+a/2)} = \frac{\cosh\left[\Omega(t)(\beta/2-(t-a/2))\right]}{\cosh\left[\Omega(t)(\beta/2-(t+a/2))\right]} \qquad (259)$$

It has a continuum limit, in which $\Omega \tanh \Omega(\beta/2 - t) = -\frac{d}{dt}\log G_E(t)$. One can interpret $\Omega(t)$ as the location of a delta function in the spectral function which by itself reproduces the local fall-off of the Euclidean correlator. The function $\Omega(t)$ is displayed in Fig. (25, bottom panel) for three different temperatures, where the temperature is varied this time by varying the bare coupling g_0^2 at fixed $N_t = 16$. Because the statistical samples of the numerator and the denominator in Eq. (259) are highly correlated, the numerical results for these ratios have uncertainties at the few-permille level. Figure 25 also displays the perturbative prediction at $3.1T_c$ [65]; it is based directly on Eq. (259) rather than on the continuum version of this equation, to allow for a more direct comparison with the lattice data. The lattice $\Omega(t)$ differs from the perturbative one only by a few percent, namely the latter falls off slightly more steeply. Since the difference is so small, it could partly be due to discretization effects. To reduce their influence, only the largest values of t were considered. One may ask nonetheless, how large a difference in the transport coefficient κ could this discrepancy possibly correspond to. An estimate is obtained by adding a low-frequency correction to the perturbative spectral function,

$$\Delta\rho(\omega) = \frac{1}{\pi}\cdot \Delta\kappa \, \tanh(\omega/2T)\,\theta(\Lambda - |\omega|). \qquad (260)$$

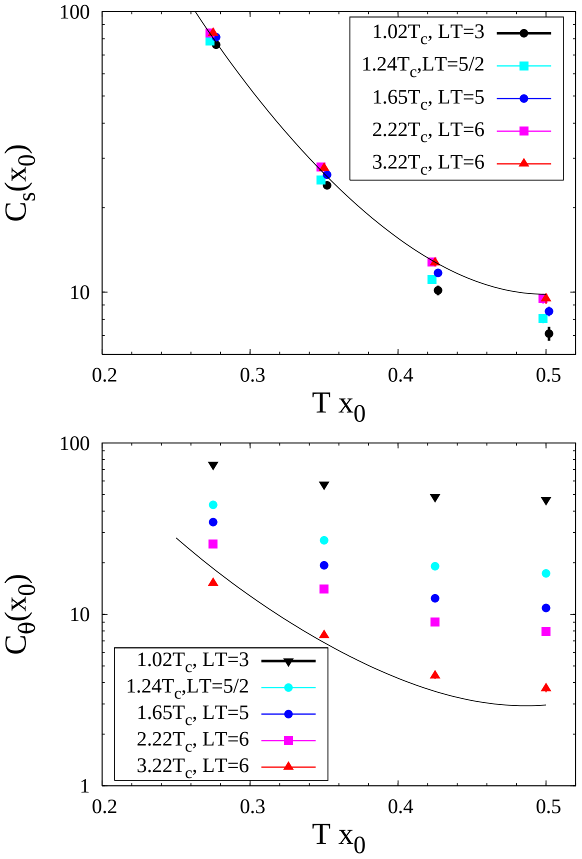

Fig. 26. Euclidean correlation function $G_E(x_0)$ of T_{12} (top) and $T_{\mu\mu}$ (bottom) in the SU(3) gauge theory, at zero spatial momentum and several temperatures in the deconfined phase with $N_t = 8$ [144,159]. The solid curves represent the treelevel correlators.

Other functional forms than (260), such as a Breit-Wigner curve, would perhaps be more realistic, but would not change the conclusions in any significant way. Adding such a term to the spectral function has the effect of making the Euclidean correlator flatter, and indeed, by adjusting $\Delta\kappa$, one can obtain good agreement for the largest two t values between the perturbative prediction modified by Eq. (260) and the lattice data. At $T = 3.1T_c$, for $\Lambda = T$ and $\Delta\kappa/T^3 = 0.352(38)$, agreement is obtained with the lattice data at the two largest t values. This represents a substantial enhancement of κ over the leading-order perturbative value. An equally good agreement is obtained if one chooses $\Lambda = 2T$, which leads to $\Delta\kappa/T^3 \approx 0.204(22)$. While it is too early to draw phenomenological conclusions, this increase appears to be not quite sufficient to explain the experimentally observed elliptic flow of heavy quarks [20,21,158].

One of the applications of this type of calculation in the HQET framework is that it can provide the parameters of the transport peak in bottomium, and perhaps even charmonium correlators. We refer the reader to section (3.3) for a review of this connection [64]. This could be instrumental in the analysis of the ‘melting’ of quarkonia states.

4.7 Shear and Bulk Viscosities

The calculation of the shear viscosity is of the greatest importance for heavy ion phenomenology. But for techni-

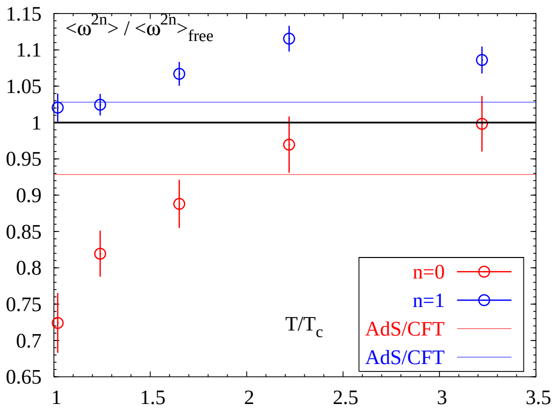

Fig. 27. The lowest two moments $n = 0$ and 1 defined in Eq. 55, normalized to their treelevel values [162]. For comparison, the same quantities computed in the strongly coupled $\mathcal{N} = 4$ SYM theory are displayed [56].

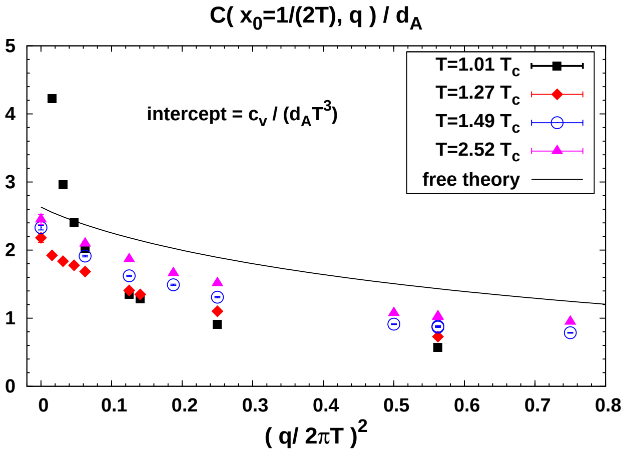

Fig. 28. The Euclidean energy density correlator for fixed $t = \frac{\beta}{2}$, as a function of the spatial momentum $\boldsymbol{q}$ [164]. In these calculations, the lattice size is 12×48^3 at the two lower temperatures and 10×20^3 at the two higher temperatures. The lattice is anisotropic, $a_\sigma / a_\tau = 2$. At $1.01T_c$ the intercept is as high as 13.6(1.9).

cal reasons the associated spectral function is also probably the hardest to constrain by using lattice simulations. Therefore results have only been obtained in the SU(3) gauge theory (see also the SU(2) results investigating the behavior of correlators near the second-order phase transition [160]).

The Euclidean correlators in the shear and in the bulk channels are displayed in Fig. (26). They are given as function of Euclidean time t and are evaluated at vanishing spatial momentum, $\boldsymbol{k} = 0$. The lattices used in these calculations are isotropic and have $N_t = 8$. The treelevel correlator is displayed as a solid black line. Clearly the departure from this curve is small. This is due to the large contribution from the ultraviolet frequencies, which results in a $1/t^5$ behavior at short distances and dominates the Euclidean correlator for all t. The data was obtained with a two-level algorithm [124,161], which exploits the locality of the action and the operator $T_{\mu\nu}$, both of which are formed of color-traces of 1x1 plaquettes. The algorithm averages out the short-wavelength fluctuations of the two operators separately before evaluating their correlation. In this way, the 'statistics' accumulated for each of them multiplies with the statistics accumulated for the other. These stochastic sub-averages do not lead to a bias in the final expectation value [123]. As a consequence of using this algorithm, the relative statistical uncertainty on the data points is roughly independent of t.

In order to see the departure from the free-field behavior, one has to inspect the correlator in greater detail. The moments (55) are directly computable on the lattice. The first two moments of the shear correlator, which amount to the value and the curvature of the Euclidean correlator at $t = \frac{\beta}{2}$, are displayed in Fig. (27) as a function of temperature. They were computed on $N_t = 8$ lattices and are normalized to their treelevel values, which can be obtained straightforwardly by integrating the spectral functions (161). While below $T = 2T_c$ one observes a clear departure of the lowest moment from the non-interacting limit, a higher accuracy (both statistical and systematic) would be needed to see a statistically significant departure from the non-interacting limit at the higher temperatures. The next moment is overall closer to the non-interacting limit, as one would expect on the basis that it weights the higher frequencies more strongly than the lowest moment. Before interpreting the departure of less than 10% from the free value, the discretization errors would need to be brought under a control comparable to the statistical errors. Note, the strong statistical correlations between Euclidean data points result in a strong reduction in the statistical error for the second derivative. The figure also displays the ratio of the $\mathcal{N} = 4$ SYM moments, calculated at infinite and zero coupling [56,80]. This confirms how numerically insensitive the Euclidean correlator is to interactions among the constituents of the plasma. It also shows that the size and magnitude of the deviations from the free approximation is the same in both theories. The numerical insensitivity of the Euclidean correlator to the transport properties was pointed out in [163] (weak coupling regime) and in [56] (strong coupling regime).

The conservation of the EMT, $\partial_\mu T_{\mu\nu} = 0$, implies in particular, for $\boldsymbol{q} = q\hat{e}_3$ and with Euclidean sign conventions,

$$\omega^4 \rho_{00,00}(\omega, \boldsymbol{q}) = -\omega^2 q^2 \rho_{03,03}(\omega, \boldsymbol{q}) = q^4 \rho_{33,33}(\omega, \boldsymbol{q}),$$
$$-\omega^2 \rho_{01,01}(\omega, \boldsymbol{q}) = q^2 \rho_{13,13}(\omega, \boldsymbol{q}) \,. \qquad (261)$$

In order to be more sensitive to the infrared part of the shear and sound channels, it is useful to combine the information from all the Euclidean correlators that belong to these channels [67]. Indeed the spectral function for the energy density correlator goes like $\boldsymbol{q}^4$ at high frequencies instead of ω^4. Similarly, the momentum density spectral function goes like $\omega^2 \boldsymbol{q}^2$ at high frequencies.

The energy-density correlator at non-zero spatial momentum $\boldsymbol{q}$ is particularly interesting. Its main contribution

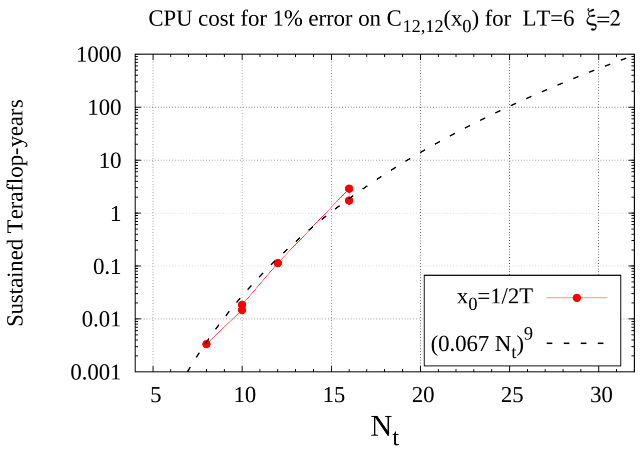

Fig. 29. Computational cost scaling for the shear channel correlator [164].

comes from the sound peak, Eq. (116). The area under this peak is to leading order the specific heat, c_v. At second order in (conformal) hydrodynamics, the position of the peak also depends on the relaxation time of the medium (Eq. 123). Figure (28) displays the Euclidean correlator at the fixed time $t = \frac{\beta}{2}$ and as a function of $\boldsymbol{q}$. The correlator falls off fairly slowly, by about a factor 2 between $\boldsymbol{q} = 0$ and $|\boldsymbol{q}| = \pi T$. This is in qualitative agreement with the free field expectation. The main difference between the free field prediction, displayed as a black curve, and the lattice data is the value of the specific heat which gives the intercept in Fig. (28). In section (5.6), we describe an attempt to fit simultaneously several sound channel correlators as a function of both t and $\boldsymbol{q}$.

Very close to the phase transition, a much steeper fall as a function of $\boldsymbol{q}$ is observed. The phase transition is weakly first order in the SU(3) gauge theory. However the specific heat is very large just above T_c [165], and this is confirmed by Fig. (28). However for perturbations of wave-vector $|\boldsymbol{q}| \simeq \frac{1}{2}\pi T$, the correlator is of the same typical magnitude as at the higher temperatures. This sharp fall-off of the energy-density correlator between $|\boldsymbol{q}| = 0$ and $\frac{1}{2}\pi T$ means that the area under the sound peak falls off rapidly in this wave-vector interval. This could be due to a corresponding fall-off in the static susceptibility of T_{00} as a function of the wavelength of the perturbation. In any case, the Euclidean correlator is incompatible with the leading-order form of the spectral function (116). Possibly, the fluctuations of the order parameter (the Polyakov loop) have to be treated as slow modes in hydrodynamics (see for instance [166]). We will return to the closely related question of the bulk channel near T_c in section (5.6).

4.8 Computational Cost Scaling

An important question for the field is how computationally expensive it is to improve our knowledge of the spectral functions. A first step is to look at the computational cost scaling of the Euclidean correlators.

Let us consider the correlator of T_{12} in the SU(N) gauge theory, out of which the shear viscosity can in principle be extracted. As long as we are in the deconfined phase, the correlator behaves as in a scale-invariant theory, up to small deviations. In other words, once the overall dimensionality is scaled out by an appropriate power of the temperature T, the correlator is to a good approximation a function of the variable tT. At the level of the lattice simulation, it is of course a function of N_t, N_s and the bare coupling g_0. The statement of scale-invariance translates into the lattice correlator being approximately independent of g_0, as long as the system is in the high-temperature phase. The observable, normalized to be finite both in the continuum and infinite-volume limit, reads

$$\lim_{L\to\infty}\lim_{a\to0}\frac{\beta^5}{L^3}\Big\langle \int \mathrm{d}\boldsymbol{x}\, T_{12}(t,\boldsymbol{x}) \int \mathrm{d}\boldsymbol{y} T_{12}(0,\boldsymbol{y})\Big\rangle_{\rm conn}. \tag{262}$$

Using a straightforward algorithm to compute this observable, the root of the variance is approximately

$$\frac{\beta^5}{L^3}\, L^3\Big\langle \int \mathrm{d}\boldsymbol{y}\, T_{12}(0,\boldsymbol{y}) T_{12}(0,\boldsymbol{y})\Big\rangle_{\rm conn} \propto {N_t}^5. \tag{263}$$

Therefore the number of independent ‘measurements’ needed scales as $N_s^0 N_t^{10}$. This is a very poor scaling indeed, and it means that reducing the lattice spacing by a factor two at a fixed temperature requires about three orders of magnitude as much statistics. Note also that both the observable (262) and the root of the variance are independent of the volume (in the large volume regime).

The scaling is however dependent on the way the gauge fields are sampled. The fields can be sampled in two levels, and we denote by $[\dots]$ an average done at the lower level of the algorithm [123, 161]. Specifically, the estimator in a two-level algorithm reads

$$\frac{\beta^5}{L^3}\Big\langle \big[\textstyle\int \mathrm{d}\boldsymbol{y}\, T_{12}(t,\boldsymbol{y})\big]\,\big[\textstyle\int \mathrm{d}\boldsymbol{x}\, T_{12}(0,\boldsymbol{x})\big]\Big\rangle_{\rm conn}. \tag{264}$$

The root of its variance is approximately

$$\sqrt{2}\frac{\beta^5}{L^3}\, L^3\Big\langle \big[\textstyle\int \mathrm{d}\boldsymbol{x} T_{12}(0,\boldsymbol{x})\big]^2\Big\rangle_{\rm conn} \tag{265}$$

which scales in the same way as the observable. Therefore the number of measurements at the higher level of the algorithm is independent of N_t and N_s. On the other hand, the number of measurements at the lower level of the algorithm must grow like N_t^5 in order to yield a good estimate of the sub-average $\big[\int \mathrm{d}\boldsymbol{x}\, T_{12}(0,\boldsymbol{x})\big]$. Therefore the scaling of the number of measurements, all levels confounded, is $N_s^0 N_t^5$.

Based on these power-counting estimates, the two-level algorithm yields a reduction of the number of measurements needed for a given statistical error by five powers of N_t. In both cases, the number of measurements must be multiplied by the volume, $N_t N_s^3$, to obtain the computational cost scaling. At the very least then, ignoring any critical slowing down, the computational cost scales as $N_t^6 N_s^3$ with the two-level algorithm.

The prefactors of a scaling law are obviously important, too. Fig. (29) displays the actually performed number of flops for a given statistical error in SU(3) gauge theory calculations [164]. These calculations were performed on anisotropic lattices $\xi = 2$, t is set equal to $\frac{\beta}{2}$, and the parameter $LT = N_s/N_t = 6$ is kept constant along the curve. Therefore one expects a scaling with N_t^9, which is consistent with the empirically observed variance of the observable, although the range of N_t is not long enough to exclude other scaling laws.

A recent calculation of the isovector vector current correlator at $1.5T_c$ in quenched QCD [145] shows that, at equal statistics, the error bars of the correlator at a fixed time separation only weakly depends on the lattice spacing. Since the configurations used were separated by a large number of update sweeps, one can assume that this reflects the behavior of the variance with the lattice spacing. It is clearly very different from the behavior in a flavor-singlet channel discussed above. This can be understood on the basis of the fact that the variance can be interpreted in partially quenched QCD. The cutoff dependence of the variance is then dominated by the operators of lowest dimension entering the operator-product expansion of the four-point function. The relevant operator product is $j_{\rm iso}(y)\tilde{j}_{\rm iso}(0)$, where $j_{\rm iso}$ is the isovector current and $\tilde{j}_{\rm iso}$ is a 'replica' thereof involving two unrelated flavors $\tilde{u}$ and $\tilde{d}$. Because of the non-trivial flavor quantum numbers, no operator of dimension less than 6 can contribute to the OPE, and therefore the variance is UV-finite by power-counting. When the correlator is calculated with the 'point-to-all' technique, neither the observable nor the variance have a volume dependence in leading order. The only source of increase in computational requirements as the lattice spacing is lowered is therefore the increase in the condition number of the Dirac operator, roughly $\propto N_t$ in the deconfined phase, and the obvious $N_s^3 N_t$ increase in cost for handling a larger lattice.

4.9 A variational method?

One lesson of linear response theory is that the operator B used to perturb the Hamiltonian need not be the same operator as the operator A, whose relaxation one wants to study. It is sufficient for it to have the same quantum numbers as A. One can even study the correlation of a whole set of operators B with A. Let us take $A \doteq n(t,\boldsymbol{k}) = \int \mathrm{d}\boldsymbol{x}\, e^{i\boldsymbol{k}\cdot\boldsymbol{x}} n(x)$ for illustration. Each of the correlators $G^{AB}(t)$ must decay with the same exponent $\exp -D\boldsymbol{k}^2 t$, only the coefficient is given by the static susceptibility $\chi_s^{AB} \equiv G_R^{AB}(i\epsilon)$, which depends on B:

$$G^{AB}(t) \overset{t\to\infty}{\sim} \chi_s^{AB}\,\Gamma\, e^{-\Gamma t}, \qquad \Gamma(\boldsymbol{k}) = D\boldsymbol{k}^2. \qquad (266)$$

The susceptibility χ_s^{AB} expresses how well the operator B is able to induce an excitation of the particle number density with wavelength $2\pi/k$. If one were able to find an operator B such that $G^{AB}(t)$ is a pure decaying exponential *even at short times*, then one could determine separately the static susceptibility χ_s^{AB} and the decay rate $\Gamma = D\boldsymbol{k}^2$. What functional form of the Euclidean correlator one should try to achieve by choosing an appropriate B operator is given by Eq. (54). Since the exponential (266) is the slowest decaying mode, the search for B amounts to finding the operator B whose Euclidean correlation with A decays as slowly as possible. This suggests a variational procedure to find the optimal B operator. Since this procedure can be repeated for every $\boldsymbol{k}$, one can check that the decay rate Γ is quadratic in $\boldsymbol{k}$, thus confirming that one is in the regime described by hydrodynamics. We note that a variational approach to the calculation of charmonium spectral function has been proposed recently (in a different form) [167].

5 Euclidean Correlators and the Analytic Continuation Problem

In this section, we discuss the problem of determining the spectral function $\rho(\omega)$ from Euclidean correlators. This question arises either when performing analytic calculations in Euclidean space before continuing them to real frequencies; or when Monte-Carlo calculations are done in Euclidean space, and one wants to determine the main features of the spectral function. Unless explicitly indicated, we will restrict ourselves to the two-point function of a Hermitian operator. Therefore the spectral function is a real, odd function of frequency, and it is given by the imaginary part of the retarded correlator.

As a historical note, this problem was first studied in the context of lattice QCD by Karsch and Wyld in the mid-eighties [168]. In non-relativistic systems, the problem had already been formulated and different numerical methods had been proposed to perform the analytic continuation [169,170,102]. A regularization of the inverse problem based on smoothness was introduced in [171]. The idea to impose a sum rule constraint was also used in [171]. In the early nineties, the maximum entropy method was introduced [172] and reviewed in [173] in the context of the many-body problem, as well as in [174] in the context of nuclear physics. The recent Ref. [175] compares different methods to extract the optical conductivity. There are still new methods that are being proposed [176], see notably the stochastic method introduced in [177].

Let $\tilde{G}_E(\omega_\ell) \equiv G_E^{(\ell)}$ be the frequency-space Euclidean correlator. It is initially calculated for the Matsubara frequencies $\omega_\ell = 2\pi T\ell$. However, since it is analytic, it can be continued into the complex plane. In particular, based on Eq. (48), the retarded correlator can be obtained by performing the substitution

$$G_R(\omega) = \tilde{G}_E(\omega_\ell \to -i[\omega + i\epsilon]), \qquad (267)$$

and then using Eq. (41) one arrives at the spectral function,

$$\rho(\omega) = \frac{1}{\pi}\,\mathrm{Im}\, G_R(\omega). \qquad (268)$$

Examples of spectral function calculations performed in this way can be found in [178,31,64,65]. The uniqueness of the solution is guaranteed by the Carlson theorem. This theorem of complex analysis implies that the only function f that is analytic in the upper half plane, is bounded at infinity by $e^{|cz|}$ with $|c| < \pi$, and vanishes at $z = in$ for $n \geq 0$ is $f = 0$. The condition $|c| < \pi$ is obviously necessary, because $\sinh \pi z$ fulfills the other conditions. The analytic continuation, as a mathematical problem, has been studied in detail in [179].

5.1 Formulation of the problem in configuration and in frequency space

Here we will be mostly concerned with the numerical version of the problem. The first question one may want to address is in what form to formulate the problem. Both on the Euclidean side and on the Minkowski side, one has a choice of working in frequency space or in coordinate space. If one chooses frequency space on both sides, the naive procedure (based on Eq. 267) consists in fitting an analytic function to the retarded correlator G_R at the discrete Matsubara frequencies along the imaginary axis, and then evaluate the function for frequencies just above the real axis. One can also work entirely in coordinate space, in which case the kernel relating the Minkowski-time correlator and the Euclidean correlator is given in Eq. (54). One then makes an ansatz for the Minkowski-time correlator and fits it to the Euclidean data. The formulation of the problem that has been used almost exclusively is the formulation based on the coordinate-space Euclidean correlator $G_E(t)$ and the frequency-space Minkowski correlator, which are related by the relation (see Eq. (50),

$$G_E(t) = \int_0^\infty d\omega\, \rho(\omega)\, \frac{\cosh \omega(\beta/2 - t)}{\sinh \omega\beta/2}. \qquad (269)$$

We are primarily interested in the low-frequency part of the spectral function. This leads to significant shortcuts. In the fully frequency-space based approach, the odd derivatives of the spectral function at the origin can be obtained from the derivatives of the retarded correlator along the imaginary axis, see Eq. (53). Since the transport properties can be extracted in this way via Kubo formulae, there is no need to literally evaluate the retarded correlator for an argument along the real axis. In the fully coordinate-space based approach, the low-frequency behavior of the spectral function is encoded in the late-time exponential fall-off of the Minkowski-time correlator, which allows one to extract for instance a diffusion coefficient ($G(t, k) \sim e^{-Dk^2 t}$) without having to explicitly perform the passage to frequency space. Finally, in the formulation (269), the transport properties are read off the spectral function using the Kubo formulae.

Working in frequency space, one thus has to interpolate between the Matsubara frequencies to obtain an estimate of the slope of the retarded correlator at the origin, yielding the transport coefficient. If one uses the coordinate-space Euclidean correlator as a starting point, one has to solve an integral equation numerically, either Eq. (269) or Eq. (54). In all three cases, the task represents a numerically ill-posed problem. In the interpolation case, one may see this by noticing that in practice, only frequencies up to a certain magnitude are numerically available. In that situation, a polynomial which vanishes at $\omega = i\ell \cdot 2\pi T$ for $\ell = 0, \ldots, \ell_{\max}$ can always be added with an arbitrary coefficient to a given tentative solution of the problem without spoiling the agreement with the available data. The slope at the origin is then modified by an arbitrary amount. Of course, such a high-degree polynomial can be excluded if one takes into account the information that the retarded correlator grows at most with a certain power (in an asymptotically free theory, or in theories satisfying non-renormalization theorems such as $\mathcal{N} = 4$ SYM, this power is given by dimensional analysis).

5.2 A numerically ill-posed problem

To illustrate the ill-posed nature of the problem more quantitatively, let us consider the problem at zero temperature, when it reduces to the well-studied problem of inverting the Laplace transform,

$$G_E(t) = \int_0^\infty d\omega\, e^{-\omega t} \rho(\omega). \qquad (270)$$

Bertero, Boccacci and Pike [180] proved the following property. The input 'data' $G_E^{\rm data}(t) = G_E(t) + \delta G_E(t)$ is necessarily imperfect, but is assumed to satisfy the quality criterion

$$\int_0^\infty dt\, |\delta G_E(t)|^2 \leq \epsilon^2. \qquad (271)$$

Let $\delta\rho$ be the function of frequency of which $\delta G_E(t)$ is the Laplace transform. Then the size of the set $\{\delta\rho\}$, in the sense of the $L^2(0, \infty)$ norm, is infinite. Suppose however we introduce a limit on the 'oscillations' of $\delta\rho(\omega)$ in the form

$$\int_0^\infty d\omega\, \omega |\delta\rho'(\omega)|^2 \leq E^2. \qquad (272)$$

Let S be the set of $\delta\rho$ satisfying this bound. Then a lower bound on the L^2-size of S can be given for small ϵ/E,

$$\sup_{\delta\rho \in S} ||\delta\rho|| \gtrsim \frac{\pi E}{2|\log(\epsilon/E)|}. \qquad (273)$$

From here one clearly sees that (a) letting E be arbitrarily large results in an infinite L^2-uncertainty on $\delta\rho$ and (b) for a given E, the L^2-uncertainty only decreases logarithmically in ϵ. When $G_E^{\rm data}(t)$ comes from a Monte-Carlo simulation, improving the accuracy is thus exponentially computationally expensive in the desired L^2-accuracy of the spectral function.

While this fact may seem discouraging, the authors of [180] also prove that the situation improves drastically if the spectral function is known to satisfy certain analyticity properties. Suppose that ρ is analytic in the sector

$\omega e^{i\phi}$, $\forall|\phi| < \alpha$ around the real axis, and that ρ is square-integrable along the direction ϕ. Then they provide the estimate

$$\sup_{\delta\rho\in S}||\delta\rho|| \propto \epsilon^{\beta}, \qquad \beta = \frac{2\alpha}{\pi + 2\alpha}. \qquad (274)$$

In words, the uncertainty decreases much faster in this case. As a very favorable example, in the $\mathcal{N} = 4$ SYM vector channel spectral function (169), $\alpha = \frac{\pi}{4}$.

5.3 Linear methods

We start by describing a class of linear methods to solve Eq. (269). A Fredholm equation of this type can trivially be modified by multiplying the kernel $K(t,\omega) = \frac{\cosh\omega(\beta/2-t)}{\sinh\omega\beta/2}$ by a function of t times a function of ω,

$$\tilde{G}_E(t) = \int_0^\infty \mathrm{d}\omega\, \tilde{\rho}(\omega)\tilde{K}(t,\omega), \qquad (275)$$

$$\tilde{G}_E(t) = \phi(t)G_E(t), \quad \tilde{\rho}(\omega) = \rho(\omega)/m(\omega), \qquad (276)$$

$$\tilde{K}(t,\omega) = \phi(t)m(\omega)K(t,\omega). \qquad (277)$$

Since Eq. (275) has the same form as Eq. (269), we will assume in the following that this ‘preconditioning’ has been done and that the kernel is regular everywhere. The twiddle over G_E, ρ and K will be dropped.

We assume that the input data in the inversion problem is a set of N points of the Euclidean correlator, $\{G_i \equiv G_E(t_i)\}_{i=1}^N$, along with their covariance matrix

$$S_{ii'} = \langle\delta G_i \delta G_{i'}\rangle. \qquad (278)$$

For any linear method, the estimator of the spectral function can be written in the form

$$\widehat{\rho}(\omega) = \sum_{i=1}^N q_i(\omega)G_i, \qquad (279)$$

where the $q_i(\omega)$ form a set of functions that depends on the specific method. Ignoring for now the statistical fluctuations affecting the values G_i, we can substitute for it expression (275) into Eq. (279) and obtain the relation between the estimator $\widehat{\rho}(\omega)$ and $\rho(\omega)$,

$$\widehat{\rho}(\omega) = \int_0^\infty \mathrm{d}\omega'\, \widehat{\delta}(\omega,\omega')\rho(\omega'), \qquad (280)$$

$$\delta(\omega,\omega') = \sum_{i=1}^N q_i(\omega)K(t_i,\omega'). \qquad (281)$$

Clearly, in view of Eq. (280) the goal is to have the *resolution function* $\widehat{\delta}(\omega,\omega')$ as close as possible to a delta function (by a measure which is relevant to the problem). The finiteness of N results in a loss of ‘sharpness’ in relation (280) between the estimator and the genuine spectral function. The estimator $\widehat{\rho}$ can thus be thought of as a ‘fudged’ version of the true spectral function. As the number of points N increases, the resolution function becomes more sharply peaked, as illustrated below.

As the simplest approach, one may choose a set of N linearly independent functions $u_\ell(\omega)$, and write $\widehat{\rho}$ as a linear combination of them, with coefficients to be determined,

$$\widehat{\rho}(\omega) = \sum_{\ell=1}^N a_\ell u_\ell(\omega). \qquad (282)$$

We also define

$$G_\ell(t) \equiv \int_0^\infty \mathrm{d}\omega\, K(t,\omega)\, u_\ell(\omega)\,. \qquad (283)$$

The coefficients a_ℓ in Eq. (282) can be worked out explicitly. The condition that $\widehat{\rho}$ reproduces the Euclidean correlator amounts to

$$\sum_{\ell=1}^N G_{i\ell}a_\ell = G_i, \quad i = 1,\dots,N \qquad (284)$$

where we have set $G_{i\ell} \equiv G_\ell(t_i)$. A standard way to proceed is to invert the matrix $G_{i\ell}$ using the singular-value decomposition,

$$G = UwV^t, \qquad (285)$$

where U and V satisfy $U^tU = VV^t = V^tV = \mathbf{1}$, and $w = \mathrm{diag}(w_1,\dots,w_N)$. We assume the w_ℓ to be ordered, $w_1 > w_2 > \dots$. One then obtains the solution of the linear problem,

$$q_i(\omega) = \sum_{\ell=1}^N \sum_{\ell'=1}^N U_{i\ell'} \frac{1}{w_{\ell'}} V_{\ell\ell'} u_\ell(\omega), \quad i = 1\dots N, (286)$$

Eq. (286, 279) provide an estimator $\widehat{\rho}$ of the spectral function which reproduces exactly the input data points G_i when inserted into the integral equation (275).

5.3.1 Regularization

So far we have ignored the finite accuracy with which the Euclidean correlator is known. The next question to address is therefore how accurately the Euclidean correlator $G_E(t)$ must be known in order to determine the coefficients a_ℓ with good accuracy. If $S_{ii'}$ is the covariance matrix of the Euclidean correlator points, then the covariance matrix of $\widehat{\rho}(\omega)$ and $\widehat{\rho}(\omega')$ reads

$$\sigma(\omega,\omega') = \sum_{i,i'=1}^N q_i(\omega)S_{ii'}q_{i'}(\omega), \qquad (287)$$

with $q_i(\omega)$ given by Eq. (286). The problem that arises is that the w_ℓ fall off very rapidly as the mode number ℓ increases. In practice, the direct application of Eq. (286, 279) then typically leads to a wildly oscillating function $\widehat{\rho}$ with 100% uncertainty.

It is the coefficients of modes of higher ℓ that are hardest to pin down. Therefore the simplest cure to this instability problem is to restrict ℓ to run from 1 to $M < N$ in Eq. (282). Since there are now fewer unknowns than input data, one performs an ordinary, linear fit to a lattice correlator, where the χ^2 reads

$$\chi^2[a] = \sum_{i,i'=1}^{N} (G_i - \widehat{G}_i)(S^{-1})_{ii'}(G_{i'} - \widehat{G}_{i'}), \quad (288)$$

$$\widehat{G}_i \equiv \int_0^\infty \mathrm{d}\omega\, K(t_i,\omega)\,\widehat{\rho}(\omega). \quad (289)$$

However this straighforward way of proceeding is sometimes unsatisfactory, because the transition (as M is increased) between having an unacceptably large χ^2 value and having a poorly conditioned system (leading to large uncertainties in $\widehat{\rho}$) is quite rapid. Therefore it is preferable to have a continuous parameter which allows one to balance the stability of the procedure against a faithful description of the Euclidean data. This is achieved by minimizing a function obtained by adding a regulating term to the χ^2 (288), multiplied by a 'Lagrange multiplier' λ:

$$\mathcal{F} = \chi^2 + \lambda R. \quad (290)$$

The minimization of $\mathcal{F}$ with respect to the fit parameters a_ℓ can now be interpreted as the minimization of the χ^2 under the condition that R take a given value. For $\lambda = 1/\mu$, it is also equivalent to the problem of minimizing $R+\mu\chi^2$, which means minimizing R at a fixed value of the χ^2. There is a significant amount of freedom in choosing R.

If one has an *a priori* idea of the functional form of the spectral function, then R can be chosen to measure the departure of $\widehat{\rho}$ from that functional form. Typically the expected functional form is *smooth*, so that the regulating term R tends to make the estimator $\widehat{\rho}$ less wildly oscillating. This kind of regulator is used also in nonlinear methods, such as the Maximum Entropy Method (see Eq. 316). A typical example would be a 'kinetic energy' term $R = \int_0^\infty \mathrm{d}\omega \left(\frac{\mathrm{d}\widehat{\rho}}{\mathrm{d}\omega}\right)^2 g(\omega)$, where $g(\omega) > 0$ is a weight function.

A different kind of regulator directly aims at reducing the *statistical variance* of $\widehat{\rho}$, for instance

$$R = \int_0^\infty \mathrm{d}\omega \int_0^\infty \mathrm{d}\omega'\, D(\omega,\omega')\sigma(\omega,\omega') \quad (291)$$

for some symmetric weighting function $D(\omega,\omega')$. If the goal is to minimize the variance of $\widehat{\rho}$ at the origin, one chooses $D(\omega,\omega') = \delta(\omega)\delta(\omega')$. This sort of regularization is employed e.g. in the Backus-Gilbert method (see [181] and Refs. therein), and has also been proposed in the context of the analytic continuation of Euclidean correlators in [177].

5.3.2 Choosing an appropriate basis of functions

For concreteness we give a specific realization of the general procedure outlined above. Both in t-space and in ω space, one should first specify a scalar product, which is given by a measure. In t-space, the inverse covariance matrix $(S^{-1})_{ii'}$ provides a natural measure, see for example expression (288). In frequency space, we define a scalar product via a symmetric kernel $D(\omega,\omega')$ as in Eq. (291). We will see that this kernel ultimately allows one to adjust what part of the spectral function one would like to reduce the statistical uncertainty on, and also what shape one wants the resolution function to have.

We define the symmetric frequency-space kernel

$$H(\omega,\omega') = \sum_{i,i'=1}^{N} (S^{-1})_{i,i'} K(t_i,\omega)K(t_{i'},\omega')\,. \quad (292)$$

There are functions with positive eigenvalues that satisfy the following generalized eigenvalue problem,

$$\int_0^\infty \mathrm{d}\omega'\, H(\omega,\omega')u_\ell(\omega') \quad (293)$$
$$= w_\ell^2 \int_0^\infty \mathrm{d}\omega'\, D(\omega,\omega')u_\ell(\omega')\,,$$

and their orthogonality and completeness properties take the form

$$\int_0^\infty \mathrm{d}\omega\, u_\ell(\omega)D(\omega,\omega')u_{\ell'}(\omega') = \delta_{\ell\ell'}\,, \quad (294)$$

$$\sum_{\ell=1}^{\infty} u_\ell(\omega) \int_0^\infty \mathrm{d}\omega''\, D(\omega',\omega'')u_\ell(\omega'') = \delta(\omega-\omega'). \quad (295)$$

We order the eigenfunctions so as to make the sequence $\omega_1 > \omega_2 \dots$ monotonically decreasing. The motivation for choosing this basis is that the functions with largest w_ℓ contribute most to the correlator, as seen in Eq. (298) below. Therefore it is natural to determine the components of $\widehat{\rho}(\omega) = \sum_{\ell=1}^{M} a_\ell u_\ell(\omega)$ in the linear subspace that the correlator is overall most sensitive too.

With $G_{i\ell} \equiv G_\ell(t_i)$, one easily checks that

$$w_\ell^{-1} w_{\ell'}^{-1} \sum_{i,i'=1}^{N} G_{i\ell}(S^{-1})_{ii'}G_{i'\ell'} = \delta_{\ell\ell'}. \quad (296)$$

In other words, if $S = L_s L_s^t$ is the Cholesky decomposition of S, the $N \times M$ matrix

$$U_{i\ell} \equiv \sum_{i'=1}^{N} (L_s^{-1})_{ii'} G_{i'\ell}\, \frac{1}{w_\ell} \quad (297)$$

is orthogonal, $U^t U = \mathbf{1}$. We now restrict ourselves to $M \doteq N$. The solution to Eq. (284) then yields a spectral function of the form Eq. (279), with

$$q_i(\omega) = \sum_{i'=1}^{N} (S^{-1})_{ii'} \sum_{\ell=1}^{N} \frac{1}{w_\ell^2} \cdot G_{i'\ell}\, u_\ell(\omega). \quad (298)$$

The resolution function (281) is given here by

$$\widehat{\delta}(\omega,\omega') = \sum_{\ell=1}^{N} u_\ell(\omega) \int_0^\infty \mathrm{d}\omega'' D(\omega',\omega'')u_\ell(\omega''). \quad (299)$$

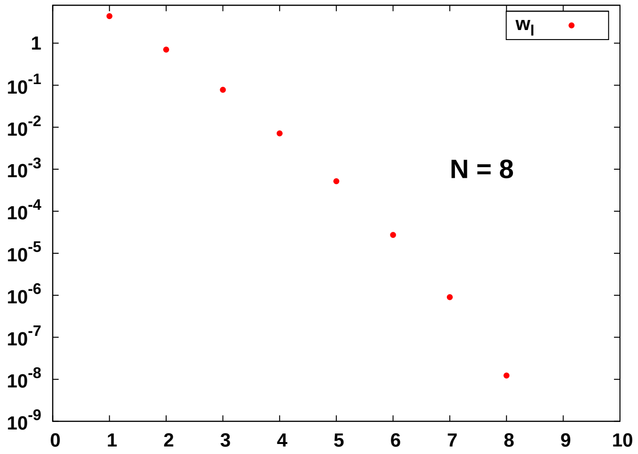

Fig. 30. Non-vanishing eigenvalues w_ℓ corresponding to operator $H(\omega,\omega')$ (Eq. 305 with $K(t,\omega)=\frac{\cosh\omega(\frac{\beta}{2}-t)}{\cosh\omega\beta/2}$) for $N=8$ and $Tt_i=\frac{1}{2}-\frac{i}{20}$, $i=0\dots N-1$.

If $S_{ii'}$ is the covariance matrix of the Euclidean correlator points, then the covariance matrix of the coefficients a_ℓ is given by

$$\sigma_{\ell,\ell'}=\frac{1}{w_\ell w_{\ell'}}\delta_{\ell\ell'}. \tag{300}$$

Since the eigenvalues w_ℓ appear in the denominator of Eq. (300), the contribution of mode ℓ is guaranteed to be well determined (in terms of statistical uncertainty) if w_ℓ is not too small. Finally, one can convert the covariance of the coefficients a_ℓ into the covariance between two values of $\widehat{\rho}$, weighted by the kernel D,

$$\int_0^\infty \mathrm{d}\omega\int_0^\infty \mathrm{d}\omega'\, D(\omega,\omega')\sigma(\omega,\omega')=\sum_{\ell=1}^{N}\frac{1}{w_\ell^2}. \tag{301}$$

To interpret Eq. (299) and (301), it is easiest to set $D(\omega,\omega')=f(\omega)\delta(\omega-\omega')$. Then these formulae become

$$\widehat{\delta}(\omega,\omega')=\sum_{\ell=1}^{N}u_\ell(\omega)f(\omega')u_\ell(\omega'), \tag{302}$$

$$\int_0^\infty \mathrm{d}\omega\, f(\omega)\sigma^2(\omega,\omega)=\sum_{\ell=1}^{N}\frac{1}{w_\ell^2}. \tag{303}$$

Thus one sees that if f is chosen to be peaked at some frequency ω_0, the resolution function $\delta(\omega_0,\omega')$ will be more concentrated around that point. But this comes at the cost of the whole variance $\sum_{\ell=1}^{N}\frac{1}{w_\ell^2}$ being concentrated around ω_0. Suppose that the spectral function is expected to have a narrow peak at ω_0. To balance the two effects against eachother, one can maximize the figure-of-merit $S/\sqrt{\sigma^2+B}$, where S is the area under the peak, $\sigma\doteq\sigma(\omega_0,\omega_0)$ and B is the area under the 'smooth' part of the spectral function. The task is reminiscent of choosing a bin size in experimental particle physics when trying to extract a signal S from a background B.

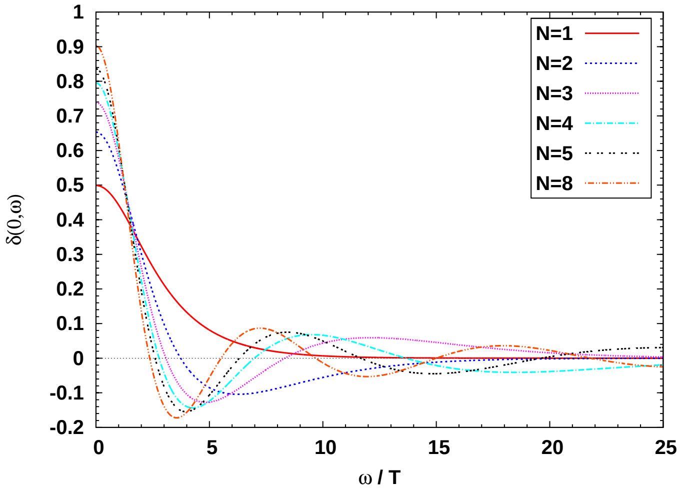

Fig. 31. Resolution function $\delta(\omega',\omega)=\sum_{\ell=1}^{N}u_\ell(\omega)u_\ell(\omega')$ at the origin ($\omega'=0$), for different values of N. The $u_\ell(\omega)$ are eigenfunctions of $H(\omega,\omega')$ (Eq. 305 with $K(t,\omega)=\frac{\cosh\omega(\frac{\beta}{2}-t)}{\cosh\omega\beta/2}$).

To regularize the problem, an option is to minimize $\chi^2+\lambda R$, with R given by Eq. (291,287), but with

$$q_i(\omega)=\sum_{i'=1}^{N}(S^{-1})_{ii'}\sum_{\ell=1}^{N}z_\ell\cdot G_{i'\ell}\,u_\ell(\omega), \tag{304}$$

and the z_ℓ are treated as the fit parameters.

5.3.3 Illustration and an example from the literature

For illustration, a possible set of orthogonal functions is formed by the N non-zero modes of the kernel

$$H(\omega,\omega')=\sum_{i=1}^{N}K(t_i,\omega)K(t_i,\omega'). \tag{305}$$

Upon discretizing the frequency variable, $\omega_j=j\delta\omega$, these modes can be obtained conveniently from the singular-value decomposition of the matrix $K_{ij}\equiv\sqrt{\delta\omega}K(t_i,\omega_j)$, $K^t=UwV^t$.

The eigenvalues w_ℓ are displayed in Fig. (30) for the case $m(\omega)=\tanh(\omega/2T)$. Note that these eigenvalues are now solely a property of the kernel $K(t,\omega)$. Unfortunately, they fall off very rapidly as ℓ increases. This means that already the fourth or fifth normalized eigenfunction $u_\ell(\omega)$ make only a small contribution to the Euclidean correlator (recall Eq. (296)), in other words the correlator has little sensitivity to it.

The resolution function centered around the origin is displayed in Fig. (31). It is clear that it becomes more strongly peaked as N increases, but that it takes quite a large N for it to become narrow on the scale of the temperature T.

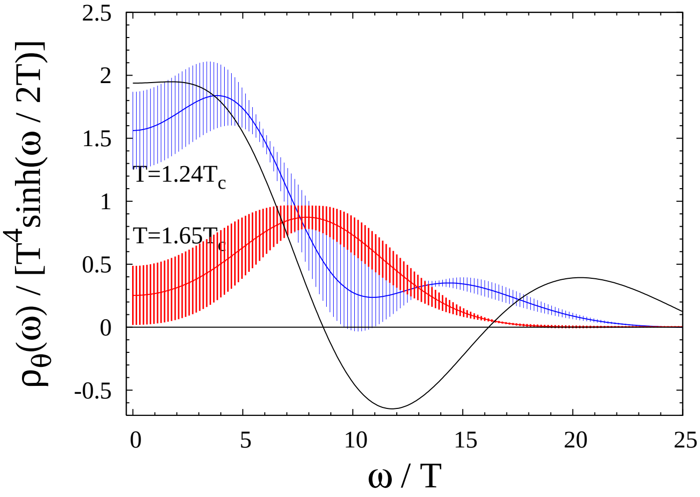

Fig. 32. The spectral function $\widehat{\rho}(\omega,T)$ in the bulk channel of SU(3) gauge theory reconstructed by a linear method from $N_t = 12$ lattices at two different temperatures [144]. The bulk viscosity is estimated by $\zeta/T^3 = (\pi/18)\times$intercept. The oscillating curve is the (rescaled) resolution function $\widehat{\delta}(0,\omega)$.

In [144], the bulk channel was studied, more precisely the $\boldsymbol{p}=0$ correlation function of θ. The spectral function was parametrized as

$$\rho(\omega) = m(\omega)[1+\sum_{\ell=1}^{N} a_\ell u_\ell(\omega)] \qquad (306)$$

with

$$m(\omega) = \frac{A\omega^4}{\tanh(\frac{\beta}{4}\omega)\tanh^2(c\beta\omega)}. \qquad (307)$$

The constant A is given by leading order perturbation theory, Eq. (161. The sensitivity of the final result to the parameter c was probed by varying it by a factor 2 around the value $\frac{1}{4}$. The $u_\ell(\omega)$ were the eigenmodes of the operator (305), with $K(t,\omega) = m(\omega)\frac{\cosh\omega(\frac{\beta}{2}-t)}{\sinh\frac{\beta}{2}\omega}$ and $m(\omega)$ given by Eq. (307). Since N was only 4, the determination of the coefficients a_ℓ did not require invoking a regulating term. The resulting spectral function, as well as the resolution function associated with this reconstruction, are displayed in Fig. (32). Due to the large UV tail of $m(\omega)$, the resolution function $\widehat{\delta}(0,\omega)$ is rather broad in units of temperature. This clearly signals that only the gross features of $\widehat{\rho}(\omega)$ are reliable. The actual spectral function may well contain more rapidly varying features which are washed out in this analysis, due to the paucity of the data.

5.3.4 The method of Cuniberti, de Micheli and Viano

The analytic structure of Minkowski and Euclidean correlators was studied thoroughly in [179]. The basic quantities defined there are the one-sided sum

$$\mathcal{G}^+(\tau,\cdot) \equiv T\sum_{\omega_n\geq 0}\tilde{\mathcal{G}}(\omega_n,\cdot)e^{-i\omega_n\tau}, \qquad (308)$$

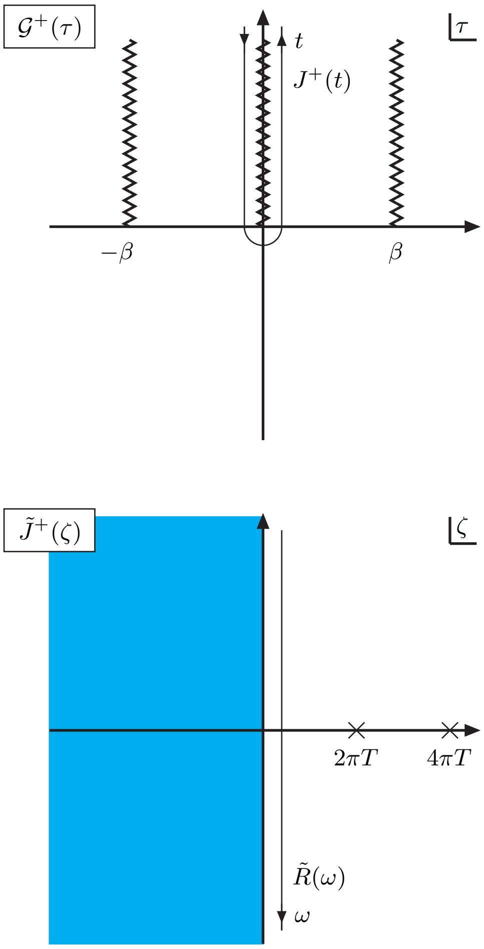

Fig. 33. The complex planes, basic functions, and analytic structures (figure from [182]).

which is analytic for $\mathrm{Im}\,\tau<0$ but has cuts in the upper half-plane; its discontinuity across the cut starting at the origin,

$$J^+(t,\cdot) \equiv i\big[\mathcal{G}^+(\epsilon+it,\cdot)-\mathcal{G}^+(-\epsilon+it,\cdot)\big], \qquad (309)$$

$t>0$, $\epsilon=0^+$, which equals the retarded real-time correlator, $\mathcal{R}(t,\cdot)$; as well as its Laplace transform

$$\tilde{J}^+(\zeta,\cdot) \equiv \int_0^\infty \mathrm{d}t\, e^{-\zeta\, t} J^+(t,\cdot), \qquad (310)$$

which is analytic for $\mathrm{Re}\,\zeta>0$. For $\zeta=\omega_n$, $\tilde{J}^+(\zeta,\cdot)$ reduces to the Fourier components $\tilde{\mathcal{G}}(\omega_n,\cdot)$, and therefore constitutes the desired analytic continuation to a complex half-plane. The value of $\tilde{J}^+(\zeta,\cdot)$ along the axis $\zeta=\epsilon-i\omega$, $\omega\in\mathbb{R}$, yields the Fourier transform of the retarded correlator, $\tilde{\mathcal{R}}(\omega,\cdot)$, whose imaginary part in turn equals the spectral function. The basic analytic structure is illustrated in Fig. 33.

Cuniberti et al. [179] also proposed a practical procedure to analytically continue the Euclidean correlator. It was recently reviewed and tested in a realistic example by Burnier et al. [182]. Here we follow the notation and treatment of the latter publication. From our point of view the most important result of Cuniberti et al. is that the retarded correlator $G(t)$ can be obtained as a series in Laguerre polynomials (normalized so that $L_\ell(0)=1$),

$$G(t) = \exp\big[-\exp(-2\pi T t)\big]\sum_{\ell=0}^{\infty} a_\ell\, L_\ell(2e^{-2\pi T t}), \qquad (311)$$

$$a_\ell \equiv 2(-1)^\ell \sum_{n=0}^{\infty}\frac{(-1)^n}{n!} G_E^{(n+1)}\; {}_2F_1(-\ell, n+1; 1; 2) \qquad (312)$$

Here ${}_2F_1$ is the hypergeometric function; Burnier et al. provide a recurrence relation to compute the combination appearing in Eq. (312). From here the spectral function can be obtained by Fourier transformation of $G(t)$, Eq. (32), exploiting if applicable the symmetry properties of $G(t)$ Eq. (28,29). However, if the goal is to determine transport properties, they can also be read off directly from the $t\to\infty$ behavior of $G(t)$ (see e.g. Eq. 213 and 214). Finally we note that formula (311) is valid for $G_E(t)$ continuous at $t = 0 \bmod \beta$. In relativistic theories this property will in general only be fulfilled after a subtraction of the hardest UV contributions.

Since the required input into formula (311) is the Euclidean correlator in frequency-space, we may assume that the latter has been calculated on the lattice for the N first Matsubara frequencies. The practical recipe that the result (312) suggests is to truncate the sum (311) at some $\ell = \ell_{\max}$ [182]. Various criteria can be used to motivate the choice of $\ell_{\max}$. In the original proposal, based on mathematical arguments the suggestion was to look for a plateau in $\sum_{\ell=1}^{\ell_{\max}} |a_\ell|^2$ as a function of $\ell_{\max}$. An alternative, more physical condition put forward in [182] is to require that $G(t) \overset{t\to\infty}{\to} 0$ [35], which is equivalent to $\sum_{\ell=1}^{N} a_\ell = 0$. We remark that through the dependence of $\ell_{\max}$ on the data, one introduces a non-linearity of the spectral function on the input data.

In the case that the channel under consideration admits a diffusion pole, the asymptotic behavior of $G(t)$ is (disregarding non-linear effects that generically lead to power-law tails [101]),

$$G(t) \sim \chi D\boldsymbol{k}^2\, e^{-D\boldsymbol{k}^2 t}. \qquad (313)$$

It is interesting to see how this behavior arises from a formula such as (311). At large times, $e^{-2\pi T t}$ will be very close to zero, and therefore the Laguerre polynomials are evaluated near the origin in this regime. Since the leading term, $\sum_\ell a_\ell$, must vanish for the retarded correlator to vanish at infinity, the exponential fall-off must arises from the derivative of the Laguerre polynomials at the origin. It is thus clear that the expression with a finite number of terms will always fall off as $e^{-2\pi T t}$ for sufficiently large t. However, this asymptotic behavior can of course be different when all the terms are included. Specifically, we note the formula

$$x^\beta = \Gamma(\beta+1)\sum_{i=0}^{\infty}(-1)^i \binom{\beta}{i} L_i(x), \qquad (314)$$

which for $x = 2e^{-2\pi T t}$ and $\beta = D\boldsymbol{k}^2/2\pi T$ allows one to express the diffusion constant D directly in terms of the large-ℓ behavior of a_ℓ.

Burnier et al. performed a practical test of the method on a UV-subtracted Euclidean correlator. With N equally spaced data points in Euclidean time, they tested the accuracy of the reconstructed spectral function, assuming a relative accuracy of 10^{-3} or better on the Euclidean mock data. In this case, for the kind of test spectral function used, the accuracy achieved on $\rho(\omega)$ is better than 50%. Another lesson is that doubling N from 24 to 48 only moderately improves the result, and the accuracy must be drastically improved to benefit from the additional points. We expect the latter to be a general qualitative conclusion.

5.4 The Maximal Entropy Method

The Maximal Entropy Method (MEM) was first applied to the determination of spectral functions in lattice QCD in [183]. The method is described in detail in [184] (see also the older review [173]). Some technical improvements have been introduced more recently ([185,186]). It is noteworthy that the method is also currently being used to study the spectral function in non-relativistic systems [187].

From a pragmatic point of view, this method is also based on the minimization of $\chi^2 + \lambda R$, where R acts as a regulator. But the difference with linear methods is that neither the χ^2 nor R are any longer quadratic in $\widehat{\rho}$. Using a more standard notation the quantity that is maximized is thus not simply $e^{-\frac{1}{2}\chi^2}$, but rather

$$P \propto \exp\left\{-\frac{1}{2}\chi^2 + \alpha S\right\}, \qquad (315)$$

$$S[g] = \int_0^\infty \mathrm{d}\omega\, \left[\widehat{\rho}(\omega) - m(\omega) - \widehat{\rho}(\omega)\log\frac{\widehat{\rho}(\omega)}{m(\omega)}\right]. \qquad (316)$$

For Gaussian distributed data, minimizing the χ^2 corresponds to the condition of maximum likelihood of the parameters, given the observed data. The functional S is called the Shannon-Jaynes entropy, and measures the departure of the reconstructed $\rho(\omega)$ from the prior function $m(\omega)$. The relative weight given to the ‘prior knowledge’, encoded by S, and the observed data, encoded by the χ^2, is fixed by the parameter α. We shall return to the question of how to set its value shortly.

Similar to the linear methods, the singularity of the kernel should be removed by multiplying it by a function which is proportional to ω at small frequencies, and compensating by dividing $\rho(\omega)$ by this function [185,186].

The spectral function $\rho(\omega)$ is assumed to be positive. It is parametrized as follows,

$$\widehat{\rho}(\omega) = m(\omega)\,\exp f(\omega), \qquad (317)$$

where $m(\omega)$ is the same ‘prior’ function as in Eq. (316). The exponent f is parametrized using a similar basis of functions as described in (5.3),

$$f(\omega) = \sum_{\ell=1}^{M} a_\ell u_\ell(\omega) \qquad (318)$$

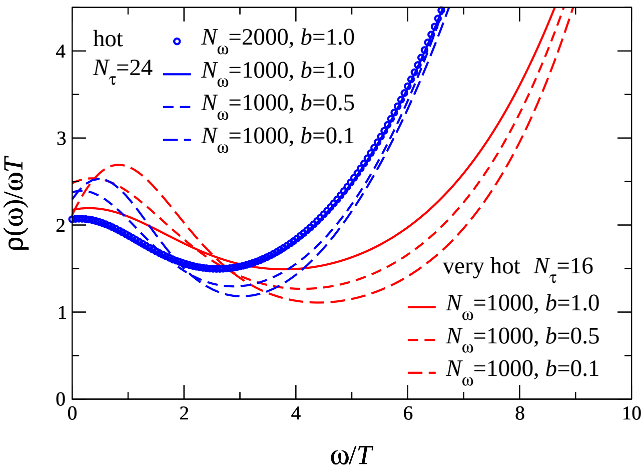

Fig. 34. The spectral function $\widehat{\rho}(\omega,T)$ in the vector channel of quenched QCD obtained by a MEM analysis [185]. The normalization of the spectral function differs by a factor 2π from ours; the conductivity σ is $\frac{T}{6}\times$ the intercept. The prior used for ρ/ω was $m(\omega)\propto(bN_t+\frac{\omega}{T})$.

where $u_\ell(\omega)$ are the M eigenfunctions of highest eigenvalue of the eigenvalue problem (293), with $M\leq N$. In the recent literature, the basis was obtained by performing the singular-value decomposition of the matrix $K_{ij}\equiv K(t_i,\omega_j)$, $K^t=UwV^t$. This corresponds to choosing $H(\omega,\omega')=\sum_{i=1}^N K(t_i,\omega)K(t_i,\omega')$ and $D(\omega,\omega')=\delta(\omega-\omega')$ in Eq. (293). The solution to the minimization of $\frac{1}{2}\chi^2-\alpha S$ is then obtained iteratively, for example with the Marquardt-Levenberg algorithm [181].

A reasonable value of the parameter α is one for which the χ^2 per degree of freedom is of order unity. More refined ways of choosing α, or more generally averaging over it, can be found in [184]. To calculate the error on the spectral function, a simple and robust approach is to use the jacknife method. Splitting the data into batches has the advantage of giving some information on the spread of $\widehat{\rho}$, and has been found to yield somewhat more stable results [187]. One may also quote the error not on a particular value of $\widehat{\rho}(\omega)$, but rather on its average over a chosen frequency interval [184], which has a stabilizing effect. An example of a spectral function in the vector channel of quenched QCD obtained from a MEM analysis is reported in Fig. (34). See the recent reference [145] for further examples.

The choice of non-quadratic regulator (316) has an information-theoretic justification. An argument for this form of S is given in [184]. The argument is based on the Bayesian idea that one has an *a priori* expectation for the outcome of $\widehat{\rho}$, which is encoded in the function $m(\omega)$. The idea is then to construct the most probable spectral function by maximizing the conditional probability $P[\widehat{\rho}|D\,H]$, where D denotes the data and H the prior information.

Generally speaking, non-linear regulators have an advantage over linear regulators when the spectral density exhibits sharp peaks over a slowly varying 'background' [181]. This is quite easy to understand in the case of MEM, since it is the exponent in Eq. (317) that is expanded in a basis of functions, and therefore a modest increase of this linear combination can lead to a strong increase in $\widehat{\rho}(\omega)$ itself. For this reason, the maximum entropy method is probably the best currently available method to analyze quarkonium correlators, where rapid changes of the spectral function are expected around threshold.

5.5 Frequency-space method

Here we describe an approach to determining transport coefficients proposed in [58] starting from the Euclidean correlator in frequency space. The idea is based on Eq. (53), which relates derivatives of the retarded correlator in the imaginary frequency direction to derivatives of the spectral function along the real axis; and (48), which relates the retarded correlator for frequencies along the positive imaginary axis to the Euclidean correlator. By the Carlson theorem, the exact knowledge of the Euclidean correlator at the Matsubara frequencies, where it can be calculated by Euclidean path integral methods, determines its analytic continuation to all frequencies, since physical correlation functions can grow at most with a power-law at large frequencies. At the point ω it then coincides with the retarded correlator evaluated at $i\omega$, so that

$$\frac{d\tilde{G}_E(\omega)}{d\omega}\overset{\omega=0}{=}-\pi\frac{d\rho}{d\omega},\tag{319}$$

$$\frac{d^3\tilde{G}_E(\omega)}{d\omega^3}\overset{\omega=0}{=}\pi\frac{d^3\rho}{d\omega^3},\quad\text{etc.}\tag{320}$$

This allows one, in principle, to determine the transport properties, since the right-hand side of Eq. (319) is precisely the expression appearing in the Kubo formulae. To illustrate this point, it is useful to note that the contribution of a diffusion pole $\rho=\chi_s\frac{D\boldsymbol{k}^2}{\omega^2+(D\boldsymbol{k}^2)^2}$ to the Euclidean correlator takes the form

$$\tilde{G}_E(\omega,\boldsymbol{k})=\frac{\chi_s D\boldsymbol{k}^2}{|\omega|+D\boldsymbol{k}^2}.\tag{321}$$

Thus one sees that a non-zero value of $\rho(\omega)/\omega$ near the origin translates into a non-analyticity of the Euclidean correlator in ω^2 around the origin.

For a function known at $\omega_\ell=2\pi T\ell\equiv\omega_M\cdot\ell$, one can write a polynomial of degree n going through the $n+1$ first points $\{G_E^{(\ell)}\}_{\ell=0}^n$. It has a slope at the origin given by

$$\tilde{G}'_E(\omega=0)_{\rm eff}\equiv-\frac{n!}{\omega_M}\sum_{\ell=1}^n\frac{(-1)^\ell}{\ell!(n-\ell)!}\,\frac{G_E^{(\ell)}-\tilde{G}_E^{(0)}}{\ell}\,.\tag{322}$$

When expressed in terms of dispersion integrals as in Eq. (56-57), the degree of convergence in the UV of this expression improves with the order of the polynomial: with some combinatorics one can show that it is asymptotically $\rho(\omega)/\omega^{n+3}$ for n even and $\rho(\omega)/\omega^{n+2}$ for n odd. For instance, the slope at the origin of the $n=2$ polynomial is given by

$$-\frac{1}{2\omega_M}(3\tilde{G}_E^{(0)}-4G_E^{(1)}+G_E^{(2)})\tag{323}$$

$$=-6\omega_M^3\int_{-\infty}^{\infty}d\omega\,\frac{\rho(\omega)}{\omega}\,\frac{1}{(\omega^2+\omega_M^2)\,(\omega^2+4\omega_M^2)}\,,$$

where the linear combination (57) appears. Thus the slope of the quadratic polynomial is negative-definite, just as the actual slope of the retarded correlator $\frac{d}{d\omega}\tilde{G}_R(i\omega)$. One might be tempted to use it as a Euclidean estimator for the transport coefficient (for instance the diffusion coefficient D). However, if the spectral function admits a diffusion pole of width $D\boldsymbol{k}^2 \ll \omega_M$, expression (323) amounts to $-\frac{3}{2}\chi_s/\omega_M$, while actually $\frac{d}{d\omega}\tilde{G}_R(i\omega) = -\frac{\chi_s}{D\boldsymbol{k}^2}$. It is clear why that is: a polynomial interpolating between the Euclidean points is only a good approximation to the retarded correlator if the latter does not contain a scale $\omega_0 = D\boldsymbol{k}^2 \ll \omega_M$ over which it varies significantly.

However, one knows *a priori* that the number density correlator must exhibit a diffusion pole. Therefore it is appropriate to ‘help’ the determination of the slope by including a term of the form (321) in a fit to the Euclidean data set $\{G_E^{(\ell)}\}$. The remainder can be assumed to analytic in ω^2 near the origin. We note that the idea of parametrizing the frequency-space Euclidean correlator by a rational function, and then obtaining the spectral function from its discontinuity across the real axis was one of the first proposed [170]. Extracting a derivative along the imaginary axis should be comparatively more stable.

No attempt has been made yet to use this method in practice, mainly because the calculation of off-shell correlators such as $G_E^{(\ell)}$ is technically more complicated than working in coordinate space. The attractiveness of this method is that one does not need to reconstruct explicitly the whole spectral function, and this is a special feature of the transport properties – as opposed to, for instance, determining the width of a quarkonium state. Recently, the method has been tested to determine the optical conductivity in a Hubbard model and found to work quite well in this case ([175], see section 5.7).

5.6 Combining Numerical Euclidean Data with Analytic Results

In attacking the inverse problem of determining the spectral function, one can take a ‘purist’ approach, and apply a ready-to-use formula which is exact in the limit of perfect Euclidean data, such as (311) or (322). At the other extreme, if one has control over the functional form of the spectral function, then a fit with a small number of free parameters is appropriate. However in practice and for the foreseeable future the first approach is bound to be of limited use due to imperfect data, while in QCD it seems unlikely that one will have good enough control over the functional form over the whole real axis of frequencies. Therefore it will remain useful to exploit prior knowledge about the spectral function, such as the parametric location of a diffusion or sound pole, even when a ‘purist’ approach is adopted. Here we wish to collect the kind of analytic information one may want to make use of.

	$1.58T_c$	$2.32T_c$	free gluons	$\lambda=\infty$ SYM
$(\eta+\frac{3}{4}\zeta)/s$	0.20(3)	0.26(3)	∞	$\frac{1}{4\pi}\approx 0.080$
$2\pi T\tau_\Pi$	3.1(3)	3.2(3)	∞	$2-\log 2\approx 1.31$
$\frac{\eta+\frac{3}{4}\zeta}{Ts\tau_\Pi}$	0.40(5)	0.51(5)	0.17	0.38

Table 1. Sound channel spectral function at $2.3T_c$. In the Table, lattice results are compared to free gluons [188] and to the strongly coupled SYM results [16, 59]. Stat. errors only are given. We expect ζ to be negligible at these temperatures.

Knowing even partially the functional form of the spectral function is of course a great advantage. Information about the functional form is provided by ‘straightforward’ perturbation theory at frequencies $\omega \gg T$. Power corrections are predicted by the operator-product expansion. In QCD at zero chemical potential, the leading power corrections at finite temperature are suppressed by four powers of the frequency, because that is the dimension of the lowest-dimensional gauge-invariant operators (the mass operator $\bar{\psi}\psi$ comes accompanied by one power of the quark mass, since it is a chirally non-invariant contribution). At low frequencies and momenta on the other hand, hydrodynamics is expected to predict the pole structure of the correlators correctly, see section (3.2). The main unknown is the domain filling the gap between these two asymptotic regimes. This interval is precisely the region that the Euclidean correlator at the first few Matsubara frequencies is most sensitive too.

Sum rules can be used as a constraint on the spectral function, if the RHS of the sum-rule is known. One example is the difference of vector and axial-vector current correlators (Eq. 197-199). Because the difference of the vector and axial-vector spectral functions falls off rapidly at large frequencies, the difference should be easier to parametrize and be more sensitive to the low-frequency region. The shear and bulk channels also obey sum rules once the $T=0$ correlators have been subtracted, Eq. (196) and (194) respectively. In all these cases a subtraction is necessary in order to make the spectral integral converge. This entails the loss of the positivity of the function one is trying to reconstruct. This is clearly a drawback, since the positivity property has a stabilizing effect. It has to be decided on a case-by-case basis whether it is preferable to deal with non-positivity or with a large ultraviolet contribution to the signal. This is the major added difficulty one faces in relativistic field theories as compared to non-relativistic systems.

Exploiting the fact that different correlators at finite $(\omega, \boldsymbol{k})$ are related by Ward identities can help to constrain the unknown spectral function. This observation is particularly useful in the sound channel, where the energy-density correlator is most sensitive to the sound peak, while the longitudinal pressure correlator is much more sensitive to the UV tail of the sound-channel spectral function.

Thanks to the known tensor structure of the vector and energy-momentum tensor correlators (see section 2.5), one can exploit a richer set of Euclidean data if one is willing to analyze two channels simultaneously. For instance, letting $\theta_{\rm q}$ be the polar angle of $\boldsymbol{q}$, one can exploit also momenta

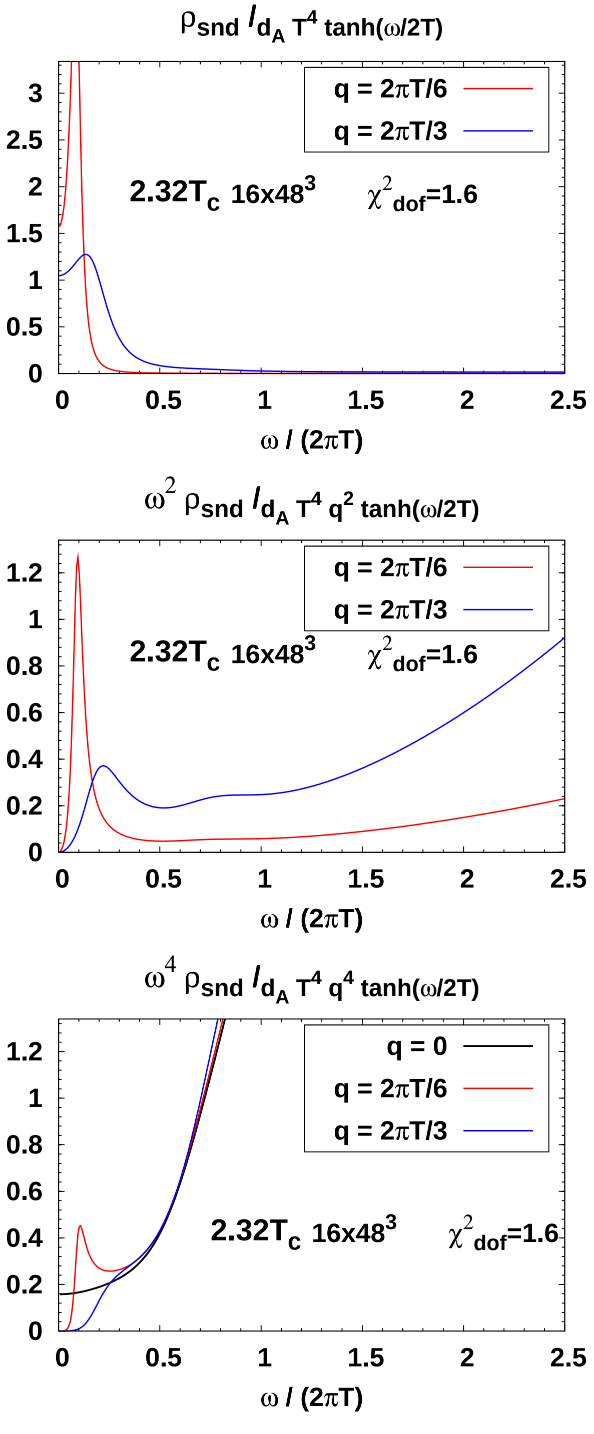

Fig. 35. The spectral function obtained from the fit (325) [164].

that are not aligned along a lattice axis via [164]

$$G_E^{03,03}(t,\boldsymbol{q}) = \int_0^\infty d\omega \frac{\cosh\omega(\frac{1}{2}\beta-t)}{\sinh\frac{1}{2}\beta\omega}\cdot \Big\{\rho_{\rm snd}(\omega,\boldsymbol{q})\,\cos^2\theta_{\rm q}+\rho_{\rm sh}(\omega,\boldsymbol{q})\,\sin^2\theta_{\rm q}\Big\}. \qquad (324)$$

Here $\rho_{\rm sh}$ and $\rho_{\rm snd}$ are the shear and sound channel spectral functions, using the notation $\rho_{\rm snd}(\omega,\boldsymbol{q}) \equiv -\rho_{03,03}(\omega,\boldsymbol{q})$ and $\rho_{\rm sh}(\omega,\boldsymbol{q}) \equiv -\rho_{01,01}(\omega,\boldsymbol{q})$. On the anisotropic lattice, the correct normalization of all components of the energy-momentum tensor involves many independent normalization factors. Apart from reproducing the correct thermodynamic properties, they must obey the Ward identities. This has been used to determine some of the normalization constants in the SU(3) gauge theory [164]. In the latter reference, an attempt was made to fit the sound-channel correlators with the ansatz

$$\rho_{\rm snd} = \rho_{\rm low} + \rho_{\rm med} + \rho_{\rm high}, \qquad (325)$$

where

$$\begin{aligned}\frac{\rho_{\rm low}(\omega,q,T)}{\tanh(\omega/2T)} &= \frac{2\widehat{\varGamma}_s}{\pi}\,\frac{(e+P)\,\omega^2q^2}{(\omega^2-c_s^2(q)q^2)^2+(\widehat{\varGamma}_s\omega q^2)^2}\,\frac{1+\sigma_1\omega^2}{1+\sigma_2\omega^2}\\ \frac{\rho_{\rm med}(\omega,q,T)}{\tanh(\omega/2T)} &= \omega^2q^2\tanh^2(\frac{\omega}{2T})\frac{\ell\,\sigma}{\sigma^2+(\omega^2-q^2-M^2)^2}\,,\\ \frac{\rho_{\rm high}(\omega,q,T)}{\tanh(\omega/2T)} &= \omega^2q^2\tanh^2(\frac{\omega}{2T})\frac{2d_A}{15(4\pi)^2}\,, \end{aligned} \qquad (326)$$

and $c_s(q^2)$ is given by Eq. (123). In the present specific example 7 parameters are fitted to a total of 48 data points, obtained at $T = 2.3T_c$ on a 16×48^3 lattice with anisotropy $a_\sigma/a_\tau = 2$. The parameters are $\widehat{\varGamma}_s,\sigma_1,\sigma_2,\tau_\varPi,\ell,\sigma,M$. Figure (35) displays the reconstructed sound spectral function based on lattice data at $2.3T_c$, and the results for the fit parameters of interest are given in Tab. (5.6). In this fit, the contribution of the δ-function to the T_{33} correlator at $\boldsymbol{q}=0$ according to (187) was not properly taken into account. This neglect leads to an overestimation of the sound attenuation length $\varGamma_s = \frac{\frac{4}{3}\eta+\zeta}{e+p}$ (although the error bars on the T_{33} correlator being significantly larger than on the T_{03} correlator, the effect may be small).

The fit yields an acceptable correlated χ^2 value per degree of freedom, $\chi^2/{\rm d.o.f} = 1.6$. An interesting point is that no prominent features are needed to fit the Euclidean data apart from the hydrodynamics structure at low frequencies and the perturbative UV tails at high frequencies. In this sense the result is reminiscent of the strongly coupled SYM spectral functions displayed in Fig. (15). Based on the perturbative calculation [68], at $2.3T_c$ the bulk viscosity is expected to be negligible compared to the shear viscosity. The values of the shear viscosity are numerically quite small, and the 'relaxation time' $\tau_\varPi$ is quite well constrained by the fit. This comes from the sensitivity of the Euclidean correlator to the precise location of the sound pole. We note that the ratio $\frac{\varGamma_s}{\tau_\varPi}$ is strongly constrained by the requirement of causality [189], namely

$$\frac{\varGamma_s}{\tau_\varPi} \leq 1-c_s^2. \qquad (327)$$

The values of the parameters given in Tab. (5.6) are close to but consistent with this upper limit.

A different strategy was adopted in [58] to interpret the bulk channel Euclidean correlator using a maximum amount of analytic information. The temperatures studied were 1.02, 1.24 and $1.65T_c$ in the SU(3) gauge theory. The first step is to switch to the Euclidean correlator of the operator $\mathcal{O}_\star \propto \left(T_{\mu\mu} + (3c_s^2 - 1)T_{00}\right)$ defined in Eq. (192). This removes the delta function at the origin from the infinite-volume spectral function of $T_{\mu\mu}$. Secondly, the difference between the finite-temperature and zero-temperature spectral functions was taken, which corresponds to Eq. (60) in terms of the Euclidean correlators. While this removes the bulk of the UV contribution, which represents an undesirable background when determining the low-frequency part of the spectral function, it also introduces the (delta-function) contributions of the stable glueballs with negative weight. A property characteristic of SU(N) gauge theories is that the mass gap m is numerically large, as compared to T_c. In particular, the subtracted spectral function $\Delta\rho(\omega,T) \equiv \rho(\omega,T) - \rho(\omega,0)$ is still positive for $\omega < m$. The lightest two scalar glueball (G) masses are known quite well, and also the matrix element $f_G \equiv \langle\text{vac}|\mathcal{O}_\star|G\rangle$ for the lightest glueball has been calculated [190,191]. Therefore is would be desirable to compensate for these contributions by forming $\Delta\rho(\omega,T)+f_G^2\delta(\omega-m)+f_{G'}^2\delta(\omega-m')$. This linear combination is then still positive up to the two-glueball threshold $2m$, which is about 3GeV. However, due to the imperfect knowledge of the glueball matrix elements, the subtraction of the one-particle contributions was not carried out explicitly.

The asymptotic UV behavior of the difference of spectral functions is given by the operator-product expansion, Eq. (181). Numerically, the OPE was assumed to be reliable starting at $\omega \approx 4.8$GeV. The formula (181) then predicts $\Delta\rho$ to be very small beyond that frequency. This sets a boundary value for the spectral function beyond which it essentially vanishes.

The bulk sum rule in the form Eq. (194) provides one global constraint on the subtracted spectral function in terms of thermodynamic quantities,

$$\frac{2}{e+p}\int_0^\infty \frac{d\omega}{\omega}\,\Delta\rho_\star(\omega,T) = 3(1-3c_s^2) - 4\frac{e-3p}{e+p}\,. \quad (328)$$

Secondly the value of the subtracted Euclidean correlator at maximum time separation $t = \frac{\beta}{2}$ was used,

$$\frac{T^4}{e+p}\left[G_E(t,T) - G_E^{\rm rec}(t,T)\right]_{t=\beta/2}\,, \quad (329)$$
$$= \frac{1}{e+p}\int_0^\infty \frac{d\omega}{T}\,\frac{\Delta\rho_\star(\omega,T)}{\sinh\frac{\omega}{2T}}.$$

Expression (329) turns out to be positive while expression (328) is negative. Since both receive the same contribution from low frequencies, but the higher frequencies contribute practically only to (Eq. 328), one infers that the subtracted spectral function must be positive at small frequencies and negative at higher frequencies. This can be quantified as follows. The frequency axis was divided into three intervals, defined by the separation points $\omega_1 \approx m$ and $\omega_2 = 4.8$GeV. In each interval, the subtracted spectral function is assumed to to be a quadratic polynomial in ω, and the function is required to be continuous and differentiable at the boundary points. Beyond ω_2, it is assumed to be given by the operator-product expansion prediction. Based on the two pieces of information (328) and (329), the parametrization of the subtracted spectral function obtained in [58] is displayed in Fig. (36).

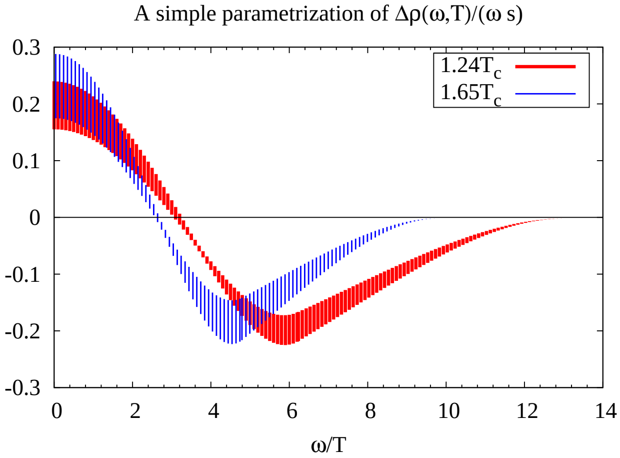

Fig. 36. A smooth parametrization of the subtracted bulk-channel spectral function in SU(3) gauge theory, $\Delta\rho_\star(\omega,T)/(\omega\cdot s)$, compatible with the bulk sum rule and the lattice correlator at $t = \beta/2$[58]. Recall that the ratio ζ/s is given by $\frac{\pi}{9}\times$ the intercept of this function.

This calculation thus provides evidence for the depletion of the spectral density in the region of those glueballs that are stable or lie slightly above the two-particle threshold, and secondly for the appearance of a positive spectral weight for $\omega < m$. The analysis proceeded by maximizing the use of available analytic information on the spectral function.

5.7 Comparison of different methods

It is of interest to know how well different inverse problem methods compare, even if the outcome of such a comparison depends to some extent on the character of the spectral function one is trying to reconstruct from a Euclidean correlator. Such a comparison was recently done by Gunnarsson, Haverkort and Sangiovanni[175]. They started from the spectral function

$$\sigma(\omega) \equiv \frac{\pi\rho(\omega)}{\omega} = \Big[\frac{W_1}{1+(\omega/\Gamma_1)^2} + \frac{W_2}{1+((\omega-\epsilon)/\Gamma_2)^2} + \frac{W_2}{1+((\omega+\epsilon)/\Gamma_2)^2}\Big]\frac{1}{1+(\omega/\Gamma_3)^6}, \quad (330)$$

a superposition of Lorentzians weighted by an overal factor. The values of the parameters were chosen to be

$$\frac{\Gamma_1}{2\pi T} = 0.71, \qquad \frac{\Gamma_2}{2\pi T} = 2.9, \qquad \frac{\Gamma_3}{2\pi T} = 9.5, \quad (331)$$
$$\frac{\epsilon}{2\pi T} = 7.1, \qquad W_1 = 0.3, \qquad W_2 = 0.2\,. \quad (332)$$

in this example. To put this in perspective, Moore and Saremi [192] obtained the spectral function in the shear channel of SU(3) gauge theory and found a transport peak of width roughly $\Gamma \approx 0.05g^4T$. For an intermediate 't Hooft coupling value of $\lambda_H = 10 - 12$ thought to be relevant at a temperature of a few T_c [193], this corresponds to $\frac{\Gamma_1}{2\pi T}$ =0.09 .. 0.12. Thus the width (331) should be considered to be quite large and for such a smooth spectral function (on the scale of $2\pi T$) one would expect the inverse problem to be a fairly controlled procedure. We remark that there are also channels where the QCD spectral functions do not have kinetic theory peaks, for instance the tensor channel of the energy-momentum tensor or the transverse channel of the vector current. So a subtracted spectral function in a strongly interacting gauge theory may in fact bear some resemblance with this form, displayed as a solid red curve in Fig. (37).

After obtaining the frequency-space Euclidean correlator via (52) and giving them uncorrelated Gaussian noise of relative standard deviation σ_0, four different methods were used to reconstruct the spectral function. The four panels of Fig. (37) display these results. We briefly summarize what these four methods are, and refer the reader to the original article [175] for the details.

1. The Padé approximation is one of the oldest methods used in this problem [169]. The procedure consists in fitting a rational function ansatz to the Euclidean data (i.e. at imaginary frequencies), and then evaluating the imaginary part of the function along the real axis.
2. the second method is very similar to the method described in section (5.3), except that it is based on Euclidean-frequency data. The spectral function is expanded in a set of functions which are eigenfunctions of $K^\dagger K$, if K is the kernel of the transform (52) modified by a weighting factor to take advantage of the finite (effective) support of the spectral function. The eigenvalues of $K^\dagger K$ become small rapidly and a cutoff n_ν on their number is introduced.
3. the sampling method: this is similar to the Maximum Entropy Method, where however instead of using a default model the spectral function is given by an average weighted by $P[\sigma|G_E]$.
4. the Maximum Entropy Method with a flat prior distribution of the parameter α and a featureless prior function $m(\omega)$ displayed in Fig. (37d). We note that the data is divided into batches and the result of MEM in each of them is averaged over.

See Fig. (37) for the outcome of this test. The sensitivity of the results to variations in the parameters was also investigated by doubling Γ_1 and by reducing σ_0 by an order of magnitude. The authors conclude that the Padé approximation is somewhat less reliable than the three others, while no clear winner was found among the SVD, MEM, and MEM sampling methods. For the spectral function studied, all three provide a decent approximation in the range of parameters they investigated. Using several methods has the advantage of giving some indication of which features are genuine and which are artefacts of a particular method.

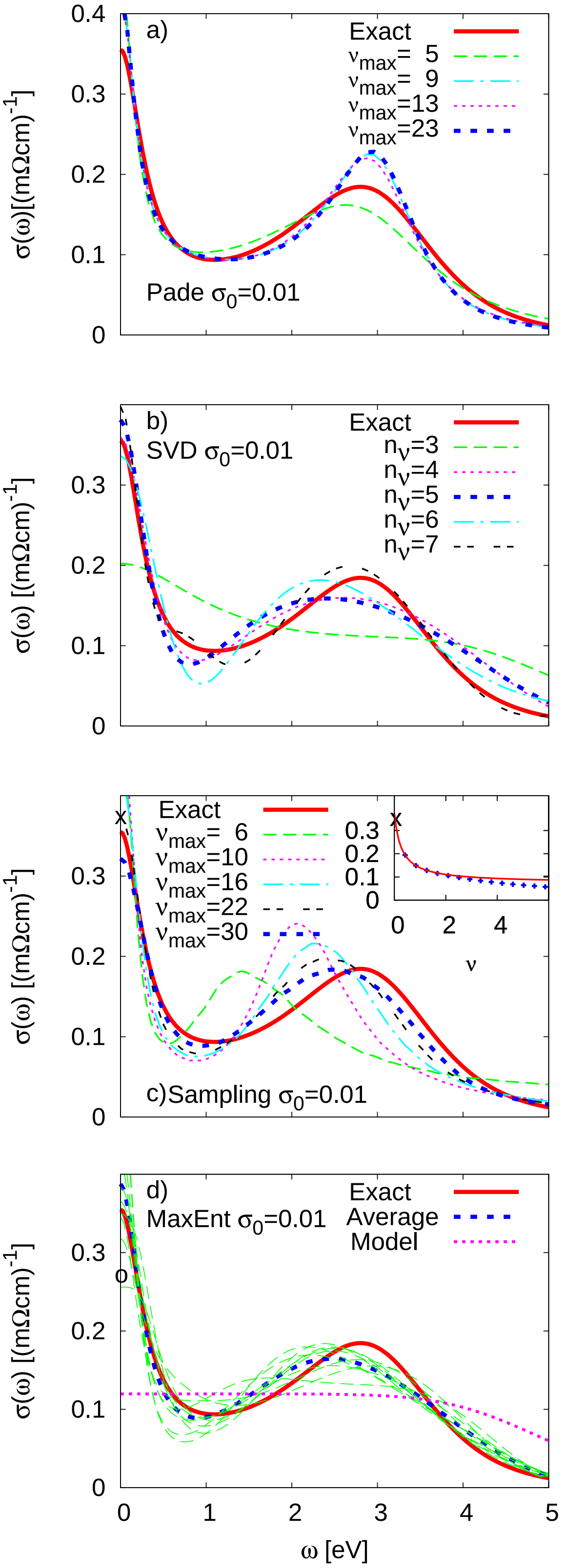

Fig. 37. Comparison of different methods to reconstruct a known spectral function from the frequency-space Euclidean correlator. See the text for a description of the methods. Study and figure from [175]. The temperature is 0.067eV.

In addition, the method of extrapolating the Euclidean frequency-space correlator to $\omega = 0$ described in section (5.5) provides a rather good estimate of the conductivity, $\sigma(0)$, in this example. This is illustrated in the inset of figure (37c). It is a good method if one is only interested in the transport part of the spectral function.

6 Summary and Outlook

We started this review by presenting the motivation to study the transport coefficients of the quark-gluon plasma in heavy-ion collisions and in cosmology. We then summarized the theoretical framework which underlies the determination of spectral functions from Euclidean-space Monte-Carlo simulations. We reviewed the analytic methods that have been used to study the spectral functions in various kinematic regimes, such as the hydrodynamic expansion and kinetic theory at low frequencies, and perturbation theory and the operator-product expansion at high frequencies. The recent lattice QCD calculations of Euclidean correlators in the vector, shear and sound channels were reviewed in section (4).

In section (5), we summarized the main methods used to infer information about spectral functions from Euclidean correlation functions. Whatever conclusion one draws about the spectral function must be shown to be a property of QCD as opposed to a combination of QCD and model information. In most cases that were described in this review, the functional form of the spectral function is known both far in the ultraviolet $\omega \gg T$ (from perturbation theory) and deep in the infrared, $\omega \ll \tau_R^{-1}$ (from hydrodynamics), where τ_R is the longest relaxation time in the system. However practically no solid information is available for the frequencies between these two extremes for temperatures relevant to heavy-ion collisions. In addition the onset of the validity of perturbation theory and of hydrodynamics is not known a priori, adding to the uncertainty of the ansatz one should use.

We highlighted the differences between linear and non-linear methods to solve Eq. (269). The main advantages of the former is that it allows one to predict straightforwardly the maximum resolution one may possibly achieve in frequency space for a given kind of input data, *before the data is available*, and secondly that the solution is found directly by inverting a matrix rather than by an iterative procedure. An attractive feature of the maximum entropy method (MEM) is that it is based on a generalization of the maximum likelihood principle to the situation where one has prior knowledge on the spectral function. In addition, it conveniently enforces the positivity of the spectral function by writing its estimator as the exponential of a real function. The functional form of the ansatz means that one can more readily describe a spectral function that contains both sharp 'peaks' and smooth 'backgrounds', but the difficulty of determining both the width and height of narrow peaks remains.

In view of the inherent difficulty of any analytic continuation, it is also worth trying to develop methods that circumvent this step, such as finite-volume and variational techniques. We have only briefly described some aspects of these research directions in Sections (3.8) and (4.9). For instance, one should study what signature a diffusion process occurring in a finite volume leaves on current correlators.

Nonetheless, what have we learnt about QCD spectral functions from the corresponding Euclidean correlators? Fit ansätze motivated by hydrodynamics at low frequencies and by perturbation theory at high frequencies are able to describe the Euclidean correlators, see for instance Fig. (35) where the estimated relaxation time was $\tau_\Pi \simeq 3.1/2\pi T$ at $1.58T_c$. Recently, the isovector vector current correlator (extrapolated to the continuum) was successfully fitted by an ansatz composed of the free-field contribution, plus a Breit-Wigner peak centered at the origin. The relaxation time corresponding to the width of the peak is well constrained by the fit and about $5.6/2\pi T$ at $1.45T_c$. These values certainly suggest that the relaxation times are not long on the thermal time scale, as kinetic theory parametrically predicts $(1/g^4T)$. On the other hand, they are not as small as their value in the $\mathcal{N} = 4$ SYM in the strong coupling limit, where $\tau_\Pi \approx 1.3/2\pi T$. The fact that the relaxation time is longer for the vector current is natural in perturbation theory, since the color charge carried by the quarks is smaller than the charge carried by the gluons [6]. While the ordering of scales characteristic of a weakly coupled plasma is not respected at temperatures relevant to heavy-ion collisions (we knew this already from static quantities), some remnant of the kinetic theory transport peak would thus appear to be present, at least in the vector channel (see Fig. 34). These observations should be regarded as preliminary; one's confidence in them would increase if $\tau_R T$ was seen to become progressively larger as the temperature is raised. By the methods used, it cannot be excluded at present that the longest relaxation times in the system are in reality much longer than these values, and that the spectral function has a more complicated structure than the fit ansätze allow. The quoted results merely provide the 'simplest' explanation for the lattice data.

One of the goals of this review is to indicate the prospects for decisive progress in the field using lattice QCD methods. This exercise splits up into two separate questions. The first is, what accuracy is necessary on the Euclidean correlator in order to impact our knowledge of the spectral functions. And secondly, how much computing time is necessary to obtain Euclidean correlators with that precision. We can illustrate this set of questions with the case of the force-force correlator that determines how fast a heavy quark diffuses in the quark-gluon plasma (see section 4.6). Addressing the first question, we want to determine the form of the spectral function at small frequencies, and it is important that one is really interested in a subtracted spectral function where the ultraviolet $\sim \omega^3$ tail has been removed. An important aspect here is that even in the weak-coupling limit, no narrow features are predicted to occur in the spectral function. The analysis of [182], where the narrowest feature of the (resummed perturbative) spectral function has width $\approx \pi T$, then shows that one needs a relative error at least as small as 10^{-3} on the UV-subtracted Euclidean correlator and $N_t = 24$ to reconstruct semi-quantitatively the spectral function. In this estimate, no physically motivated ansatz is made, it is a truncation of an exact mathematical formula.

---

[6] Comparing the widths of the transport peaks in Fig. (9) and (10), the ratio of relaxation times is approximately given by the ratio of the Casimir operators in their irreducible representations, C_F/C_A, which amounts to 4/9 for the SU(3) color group.

What amount of computing time is then necessary to determine the Euclidean correlator to this high degree of accuracy? Recently, the force-force correlator was calculated in the SU(3) gauge theory on lattices with N_t between ranging from 8 to 22 [157]. An $N_t = 16$ simulation around $6T_c$ cost about 2Gflop years (see Fig. 25). The cost increases rapidly with N_t: to achieve the same accuracy at $N_t = 22$ as at $N_t = 16$, an increase in CPU-time by a factor 20–25 is necessary. From this data, we estimate that it would take about half a month on a machine that sustains 100Tflops to achieve the relative accuracy of 10^{-3} on the shape of the UV-subtracted correlator at $N_t = 22$. In addition to the statistical errors, it is important to control the systematic errors at the same level. Thus one needs to check for finite-volume effects, and (probably more importantly in this particular case) for discretization errors. This requires varying the lattice spacing within a significant range. We note however that the overall normalization of the correlator does not need to be known to better than a few percent: it is the 'shape' of the correlator that must be controlled to very high accuracy in order to constrain the spectral function.

The example above shows that when detailed analytic information is available, and that relatively efficient numerical techniques can be used, the problem of determining the spectral function and in particular the transport coefficient say at the 30% level can be tackled with currently existing computing resources, albeit at the high end. It appears likely that the calculations will continue to be performed in the pure Yang-Mills theory for some time, since they are much faster and the crucial dynamics in any case appears to be associated with the gluons. Thus with a dedicated effort it is likely that in the next five to ten years, decisive progress will be made in this direction. Fortunately this is also the time scale on which heavy-ion collision experiments are approved for, in particular the CBM experiment at FAIR. The only assumption (backed up by resummed perturbation theory) made in this analysis on the spectral function is that it does not vary strongly on a frequency intervals of about πT. Even before such a model-independent reconstruction of the spectral function becomes possible, one may be able to draw interesting lessons already when the Monte-Carlo data quality is lower, for instance by making weak-coupling or strong-coupling (AdS/CFT) inspired fits.

The isovector vector channel for light quarks is another case where we expect significant progress to be made, because the cost does not increase as fast with N_t, and the spectral function increases more mildly, as ω^2, at large frequencies. On the other hand, the spectral function has a narrow transport peak at small frequencies in the weak coupling regime (parametrically, the width is g^4T and numerically, $0.4T$ to $0.6T$ for intermediate coupling values [192]), and determining separately the width and height of the transport peak is extremely difficult in that regime. The difficulty may be overcome with extremely accurate data, and possibly exploiting small but non-vanishing momenta by using twisted boundary conditions [194,195].

Given the observation of elliptic flow at RHIC [4,5,6, 7] and most recently at the LHC [9] the shear viscosity is undoubtedly the most important transport coefficient for heavy-ion phenomenology. The shear and sound channels are presumably the hardest to tackle by Euclidean methods, because they both exhibit a parametrically narrow transport peak at weak coupling, they have a very hard UV contribution (ω^4 in the spectral function), and the variance is strongly UV-divergent. The multi-level algorithm [161] only partly alleviates the latter problem by reducing the power with which the variance diverges. So far these major difficulties have only partly been overcome by fitting a particular ansatz (motivated by hydrodynamics and perturbation theory) simultaneously to several correlators related by Ward identities (see section 5.6).

The methods discussed here may be of interest to physicists in other fields where quantum Monte-Carlo simulations are used. In particular we have in mind cold Fermi gases, with which very controlled experiments can be made. When tuned to 'unitarity', the atoms have a divergent scattering length in the s-channel, and the system is strongly interacting. The shear viscosity to entropy density ratio has been estimated to be below unity, thus making this system an excellent fluid (see the review [8]). On the theory side, the spectral functions of a Fermi gas have recently been studied in kinetic theory [196]. An important technical simplification over the relativistic case discussed in this review is that the shear spectral function goes to zero at high frequencies [197,198], which implies that the Euclidean correlator is far more sensitive to the low-frequency part of the spectral function relevant to transport properties.

Acknowledgements

I thank Gert Aarts, Douglas Beck, Jorge Casalderrey-Solana, Philippe de Forcrand, Elias Kiritsis, Mikko Laine, Martin Lüscher, Guy Moore, John Negele, Peter Petreczky, Krishna Rajagopal, Alexi Vuorinen, Paul Romatschke, Thomas Schäfer, Dam Thanh Son, Misha Stephanov, Derek Teaney, Laurence Yaffe and Urs Wiedemann for many stimulating and illuminating discussions on the subject of this review over the past four years. Any misstatements or errors are of course the sole responsibility of the author.

References

1. C. DeTar and U. M. Heller, *QCD Thermodynamics from the Lattice*, *Eur. Phys. J.* **A41** (2009) 405–437, [`arXiv:0905.2949`].
2. Y. Bai, *Anisotropic Flow Measurements in STAR at the Relativistic Heavy Ion Collider*, . Ph.D. thesis (2007).
3. D. A. Teaney, *Viscous Hydrodynamics and the Quark Gluon Plasma*, `arXiv:0905.2433`.
4. **PHENIX** Collaboration, K. Adcox *et. al.*, *Formation of dense partonic matter in relativistic nucleus nucleus collisions at RHIC: Experimental evaluation by the PHENIX collaboration*, *Nucl. Phys.* **A757** (2005) 184–283, [`nucl-ex/0410003`].
5. **STAR** Collaboration, J. Adams *et. al.*, *Experimental and theoretical challenges in the search for the quark gluon plasma: The STAR collaboration's critical assessment of the evidence from RHIC collisions*, *Nucl. Phys.* **A757** (2005) 102–183, [`nucl-ex/0501009`].
6. B. B. Back *et. al.*, *The PHOBOS perspective on discoveries at RHIC*, *Nucl. Phys.* **A757** (2005) 28–101, [`nucl-ex/0410022`].
7. **BRAHMS** Collaboration, I. Arsene *et. al.*, *Quark gluon plasma and color glass condensate at RHIC? The perspective from the BRAHMS experiment*, *Nucl. Phys.* **A757** (2005) 1–27, [`nucl-ex/0410020`].
8. T. Schafer and D. Teaney, *Nearly Perfect Fluidity: From Cold Atomic Gases to Hot Quark Gluon Plasmas*, *Rept.Prog.Phys.* **72** (2009) 126001, [`arXiv:0904.3107`].
9. **The ALICE** Collaboration, K. Aamodt *et. al.*, *Elliptic flow of charged particles in Pb-Pb collisions at 2.76 TeV*, `arXiv:1011.3914`.
10. P. Romatschke and U. Romatschke, *Viscosity Information from Relativistic Nuclear Collisions: How Perfect is the Fluid Observed at RHIC?*, *Phys. Rev. Lett.* **99** (2007) 172301, [`arXiv:0706.1522`].
11. K. Dusling and D. Teaney, *Simulating elliptic flow with viscous hydrodynamics*, *Phys. Rev.* **C77** (2008) 034905, [`arXiv:0710.5932`].
12. H. Song and U. W. Heinz, *Suppression of elliptic flow in a minimally viscous quark- gluon plasma*, *Phys. Lett.* **B658** (2008) 279–283, [`arXiv:0709.0742`].
13. D. Teaney and L. Yan, *Triangularity and Dipole Asymmetry in Heavy Ion Collisions*, `arXiv:1010.1876`.
14. P. Arnold, G. D. Moore, and L. G. Yaffe, *Transport coefficients in high temperature gauge theories. I: Leading-log results*, *JHEP* **11** (2000) 001, [`hep-ph/0010177`].
15. P. Arnold, G. D. Moore, and L. G. Yaffe, *Transport coefficients in high temperature gauge theories. II: Beyond leading log*, *JHEP* **05** (2003) 051, [`hep-ph/0302165`].
16. G. Policastro, D. T. Son, and A. O. Starinets, *The shear viscosity of strongly coupled $N = 4$ supersymmetric Yang-Mills plasma*, *Phys. Rev. Lett.* **87** (2001) 081601, [`hep-th/0104066`].
17. P. Kovtun, D. T. Son, and A. O. Starinets, *Viscosity in strongly interacting quantum field theories from black hole physics*, *Phys. Rev. Lett.* **94** (2005) 111601, [`hep-th/0405231`].
18. M. Luzum and P. Romatschke, *Conformal Relativistic Viscous Hydrodynamics: Applications to RHIC results at s(NN)**(1/2) = 200-GeV*, *Phys.Rev.* **C78** (2008) 034915, [`arXiv:0804.4015`].
19. B. Mueller, *Theoretical challenges posed by the data from RHIC*, *Prog. Theor. Phys. Suppl.* **174** (2008) 103–121.
20. **STAR** Collaboration, B. I. Abelev *et. al.*, *Transverse momentum and centrality dependence of high- p_T non-photonic electron suppression in Au+Au collisions at $\sqrt{s}$ = 200 GeV*, *Phys. Rev. Lett.* **98** (2007) 192301, [`nucl-ex/0607012`].
21. **PHENIX** Collaboration, A. Adare *et. al.*, *Energy Loss and Flow of Heavy Quarks in Au+Au Collisions at $\sqrt{s}$ = 200 GeV*, *Phys. Rev. Lett.* **98** (2007) 172301, [`nucl-ex/0611018`].
22. G. D. Moore and D. Teaney, *How much do heavy quarks thermalize in a heavy ion collision?*, *Phys. Rev.* **C71** (2005) 064904, [`hep-ph/0412346`].
23. **PHENIX** Collaboration, K. Adcox *et. al.*, *Suppression of hadrons with large transverse momentum in central Au+Au collisions at $\sqrt{s}$ = 130-GeV*, *Phys. Rev. Lett.* **88** (2002) 022301, [`nucl-ex/0109003`].
24. **STAR** Collaboration, C. Adler *et. al.*, *Centrality dependence of high p_T hadron suppression in Au+Au collisions at $\sqrt{s}$ = 130-GeV*, *Phys. Rev. Lett.* **89** (2002) 202301, [`nucl-ex/0206011`].
25. U. A. Wiedemann, *Jet Quenching in Heavy Ion Collisions*, `arXiv:0908.2306`.
26. F. Iocco, G. Mangano, G. Miele, O. Pisanti, and P. D. Serpico, *Primordial Nucleosynthesis: from precision cosmology to fundamental physics*, *Phys. Rept.* **472** (2009) 1–76, [`arXiv:0809.0631`].
27. Y. Aoki, G. Endrodi, Z. Fodor, S. Katz, and K. Szabo, *The Order of the quantum chromodynamics transition predicted by the standard model of particle physics*, *Nature* **443** (2006) 675–678, [`hep-lat/0611014`].
28. R. Durrer, *Gravitational waves from cosmological phase transitions*, *J. Phys. Conf. Ser.* **222** (2010) 012021, [`arXiv:1002.1389`].
29. L. P. Csernai and J. I. Kapusta, *Nucleation of relativistic first order phase transitions*, *Phys.Rev.* **D46** (1992) 1379–1390.
30. T. Asaka, S. Blanchet, and M. Shaposhnikov, *The nuMSM, dark matter and neutrino masses*, *Phys. Lett.* **B631** (2005) 151–156, [`hep-ph/0503065`].
31. T. Asaka, M. Laine, and M. Shaposhnikov, *On the hadronic contribution to sterile neutrino production*, *JHEP* **06** (2006) 053, [`hep-ph/0605209`].
32. T. Asaka, M. Laine, and M. Shaposhnikov, *Lightest sterile neutrino abundance within the nuMSM*, *JHEP* **01** (2007) 091, [`hep-ph/0612182`].
33. S. Borsanyi, G. Endrodi, Z. Fodor, A. Jakovac, S. D. Katz, *et. al.*, *The QCD equation of state with dynamical quarks*, *JHEP* **1011** (2010) 077, [`arXiv:1007.2580`].
34. P. Arnold and L. G. Yaffe, *The NonAbelian Debye screening length beyond leading order*, *Phys. Rev.* **D52** (1995) 7208–7219, [`hep-ph/9508280`].
35. P. B. Arnold and L. G. Yaffe, *Effective theories for real time correlations in hot plasmas*, *Phys.Rev.* **D57** (1998) 1178–1192, [`hep-ph/9709449`].
36. M. Laine and M. Vepsalainen, *On the smallest screening mass in hot QCD*, *JHEP* **09** (2009) 023, [`arXiv:0906.4450`].
37. M. Cheng, S. Datta, A. Francis, J. van der Heide, C. Jung, *et. al.*, *Meson screening masses from lattice QCD with two light and the strange quark*, *Eur.Phys.J.* **C71** (2011) 1564, [`arXiv:1010.1216`].

38. S. Caron-Huot and G. D. Moore, *Heavy quark diffusion in perturbative QCD at next-to- leading order*, *Phys. Rev. Lett.* **100** (2008) 052301, [`arXiv:0708.4232`].
39. F. Jegerlehner and A. Nyffeler, *The Muon g-2*, *Phys.Rept.* **477** (2009) 1–110, [`arXiv:0902.3360`].
40. D. Bernecker and H. B. Meyer. Unpublished (2011).
41. Y. Aoki, Z. Fodor, S. D. Katz, and K. K. Szabo, *The QCD transition temperature: Results with physical masses in the continuum limit*, *Phys. Lett.* **B643** (2006) 46–54, [`hep-lat/0609068`].
42. Y. Aoki *et. al.*, *The QCD transition temperature: results with physical masses in the continuum limit II*, *JHEP* **06** (2009) 088, [`arXiv:0903.4155`].
43. **Wuppertal-Budapest** Collaboration, S. Borsanyi *et. al.*, *Is there still any Tc mystery in lattice QCD? Results with physical masses in the continuum limit III*, *JHEP* **09** (2010) 073, [`arXiv:1005.3508`].
44. A. Bazavov *et. al.*, *Equation of state and QCD transition at finite temperature*, *Phys. Rev.* **D80** (2009) 014504, [`arXiv:0903.4379`].
45. M. Cheng *et. al.*, *Equation of State for physical quark masses*, *Phys. Rev.* **D81** (2010) 054504, [`arXiv:0911.2215`].
46. E. Laermann and O. Philipsen, *Status of lattice QCD at finite temperature*, *Ann. Rev. Nucl. Part. Sci.* **53** (2003) 163–198, [`hep-ph/0303042`].
47. P. Romatschke, *New Developments in Relativistic Viscous Hydrodynamics*, *Int. J. Mod. Phys.* **E19** (2010) 1–53, [`arXiv:0902.3663`].
48. D. T. Son, *Hydrodynamics and gauge/gravity duality*, *Acta Phys. Polon.* **B39** (2008) 3173–3182.
49. S. S. Gubser and A. Karch, *From gauge-string duality to strong interactions: A Pedestrian's Guide*, *Ann.Rev.Nucl.Part.Sci.* **59** (2009) 145–168, [`arXiv:0901.0935`].
50. J. Casalderrey-Solana, H. Liu, D. Mateos, K. Rajagopal, and U. A. Wiedemann, *Gauge/String Duality, Hot QCD and Heavy Ion Collisions*, `arXiv:1101.0618`.
51. G. D. Moore, *Transport coefficients in hot QCD*, `hep-ph/0408347`.
52. P. K. Kovtun and A. O. Starinets, *Quasinormal modes and holography*, *Phys. Rev.* **D72** (2005) 086009, [`hep-th/0506184`].
53. J. I. Kapusta and C. Gale, *Finite-temperature field theory: Principles and applications*, . Cambridge, UK: Univ. Pr. (2006) 428 p.
54. J. Hong and D. Teaney, *Spectral densities for hot QCD plasmas in a leading log approximation*, *Phys. Rev.* **C82** (2010) 044908, [`arXiv:1003.0699`].
55. P. B. Arnold, G. D. Moore, and L. G. Yaffe, *Photon emission from ultrarelativistic plasmas*, *JHEP* **0111** (2001) 057, [`hep-ph/0109064`].
56. D. Teaney, *Finite temperature spectral densities of momentum and R- charge correlators in $N = 4$ Yang Mills theory*, *Phys. Rev.* **D74** (2006) 045025, [`hep-ph/0602044`].
57. P. Romatschke and D. T. Son, *Spectral sum rules for the quark-gluon plasma*, *Phys. Rev.* **D80** (2009) 065021, [`arXiv:0903.3946`].
58. H. B. Meyer, *The Bulk Channel in Thermal Gauge Theories*, *JHEP* **04** (2010) 099, [`arXiv:1002.3343`].
59. R. Baier, P. Romatschke, D. T. Son, A. O. Starinets, and M. A. Stephanov, *Relativistic viscous hydrodynamics, conformal invariance, and holography*, *JHEP* **04** (2008) 100, [`arXiv:0712.2451`].
60. G. D. Moore and K. A. Sohrabi, *Kubo Formulae for Second-Order Hydrodynamic Coefficients*, `arXiv:1007.5333`.
61. P. Romatschke, *Relativistic Viscous Fluid Dynamics and Non-Equilibrium Entropy*, *Class.Quant.Grav.* **27** (2010) 025006, [`arXiv:0906.4787`].
62. G. S. Denicol, J. Noronha, H. Niemi, and D. H. Rischke, *Origin of the Relaxation Time in Dissipative Fluid Dynamics*, *Phys.Rev.* **D83** (2011) 074019, [`arXiv:1102.4780`].
63. P. Petreczky and D. Teaney, *Heavy quark diffusion from the lattice*, *Phys. Rev.* **D73** (2006) 014508, [`hep-ph/0507318`].
64. S. Caron-Huot, M. Laine, and G. D. Moore, *A way to estimate the heavy quark thermalization rate from the lattice*, *JHEP* **04** (2009) 053, [`arXiv:0901.1195`].
65. Y. Burnier, M. Laine, J. Langelage, and L. Mether, *Colour-electric spectral function at next-to-leading order*, *JHEP* **08** (2010) 094, [`arXiv:1006.0867`].
66. G. Aarts and J. M. Martinez Resco, *Continuum and lattice meson spectral functions at nonzero momentum and high temperature*, *Nucl. Phys.* **B726** (2005) 93–108, [`hep-lat/0507004`].
67. H. B. Meyer, *Energy-momentum tensor correlators and spectral functions*, *JHEP* **08** (2008) 031, [`arXiv:0806.3914`].
68. P. Arnold, C. Dogan, and G. D. Moore, *The bulk viscosity of high-temperature QCD*, *Phys. Rev.* **D74** (2006) 085021, [`hep-ph/0608012`].
69. G. Baym, H. Monien, C. Pethick, and D. Ravenhall, *Transverse Interactions and Transport in Relativistic Quark-Gluon and Electromagnetic Plasmas*, *Phys.Rev.Lett.* **64** (1990) 1867–1870.
70. Z. Xu and C. Greiner, *Shear viscosity in a gluon gas*, *Phys.Rev.Lett.* **100** (2008) 172301, [`arXiv:0710.5719`].
71. J.-W. Chen, J. Deng, H. Dong, and Q. Wang, *How Perfect a Gluon Plasma Can Be in Perturbative QCD?*, *Phys.Rev.* **D83** (2011) 034031, [`arXiv:1011.4123`].
72. M. Laine, M. Vepsalainen, and A. Vuorinen, *Ultraviolet asymptotics of scalar and pseudoscalar correlators in hot Yang-Mills theory*, *JHEP* **1010** (2010) 010, [`arXiv:1008.3263`].
73. A. L. Kataev, N. V. Krasnikov, and A. A. Pivovarov, *Two-loop calculations for the propagators of gluonic currents*, *Nucl. Phys.* **B198** (1982) 508–518, [`hep-ph/9612326`].
74. A. A. Pivovarov, *Two-loop corrections to the correlator of tensor currents in gluodynamics*, *Phys. Atom. Nucl.* **63** (2000) 1646–1649, [`hep-ph/9905485`].
75. F. Karsch, M. Mustafa, and M. Thoma, *Finite temperature meson correlation functions in HTL approximation*, *Phys.Lett.* **B497** (2001) 249–258, [`hep-ph/0007093`].
76. A. Vuorinen, *Quark number susceptibilities of hot QCD up to g**6 ln g*, *Phys.Rev.* **D67** (2003) 074032, [`hep-ph/0212283`].
77. D. T. Son and A. O. Starinets, *Minkowski-space correlators in AdS/CFT correspondence: Recipe and applications*, *JHEP* **09** (2002) 042, [`hep-th/0205051`].
78. G. Policastro, D. T. Son, and A. O. Starinets, *From AdS/CFT correspondence to hydrodynamics*, *JHEP* **09** (2002) 043, [`hep-th/0205052`].

79. G. Policastro, D. T. Son, and A. O. Starinets, *From AdS/CFT correspondence to hydrodynamics. II: Sound waves*, *JHEP* **12** (2002) 054, [`hep-th/0210220`].
80. P. Kovtun and A. Starinets, *Thermal spectral functions of strongly coupled N = 4 supersymmetric Yang-Mills theory*, *Phys. Rev. Lett.* **96** (2006) 131601, [`hep-th/0602059`].
81. D. T. Son and A. O. Starinets, *Viscosity, Black Holes, and Quantum Field Theory*, *Ann. Rev. Nucl. Part. Sci.* **57** (2007) 95–118, [`arXiv:0704.0240`].
82. R. C. Myers, A. O. Starinets, and R. M. Thomson, *Holographic spectral functions and diffusion constants for fundamental matter*, *JHEP* **11** (2007) 091, [`arXiv:0706.0162`].
83. D. Z. Freedman, S. D. Mathur, A. Matusis, and L. Rastelli, *Correlation functions in the CFT(d) / AdS(d+1) correspondence*, *Nucl.Phys.* **B546** (1999) 96–118, [`hep-th/9804058`].
84. G. Chalmers, H. Nastase, K. Schalm, and R. Siebelink, *R current correlators in N=4 superYang-Mills theory from anti-de Sitter supergravity*, *Nucl.Phys.* **B540** (1999) 247–270, [`hep-th/9805105`].
85. M. Natsuume and T. Okamura, *Causal hydrodynamics of gauge theory plasmas from AdS/CFT duality*, *Phys.Rev.* **D77** (2008) 066014, [`arXiv:0712.2916`].
86. U. Gursoy and E. Kiritsis, *Exploring improved holographic theories for QCD: Part I*, *JHEP* **0802** (2008) 032, [`arXiv:0707.1324`].
87. S. S. Gubser, A. Nellore, S. S. Pufu, and F. D. Rocha, *Thermodynamics and bulk viscosity of approximate black hole duals to finite temperature quantum chromodynamics*, *Phys. Rev. Lett.* **101** (2008) 131601, [`arXiv:0804.1950`].
88. U. Gursoy, E. Kiritsis, L. Mazzanti, G. Michalogiorgakis, and F. Nitti, *Improved Holographic QCD*, *Lect.Notes Phys.* **828** (2011) 79–146, [`arXiv:1006.5461`].
89. A. Buchel, *Bulk viscosity of gauge theory plasma at strong coupling*, *Phys.Lett.* **B663** (2008) 286–289, [`arXiv:0708.3459`].
90. S. Weinberg, *The Quantum theory of fields. Vol. 1: Foundations*, . Cambridge, UK: Univ. Pr. (1995) 609 p.
91. S.-z. Huang and M. Lissia, *Constraining spectral functions at finite temperature and chemical potential with exact sum rules in asymptotically free theories*, *Phys. Rev.* **D52** (1995) 1134–1149, [`hep-ph/9412246`].
92. S. Caron-Huot, *Asymptotics of thermal spectral functions*, *Phys. Rev.* **D79** (2009) 125009, [`arXiv:0903.3958`].
93. M. Laine, M. Vepsalainen, and A. Vuorinen, *Intermediate distance correlators in hot Yang-Mills theory*, *JHEP* **1012** (2010) 078, [`arXiv:1011.4439`].
94. P. J. Ellis, J. I. Kapusta, and H.-B. Tang, *Low-energy theorems for gluodynamics at finite temperature*, *Phys. Lett.* **B443** (1998) 63–68, [`nucl-th/9807071`].
95. D. Kharzeev and K. Tuchin, *Bulk viscosity of QCD matter near the critical temperature*, *JHEP* **09** (2008) 093, [`arXiv:0705.4280`].
96. H. B. Meyer, *Lattice Gauge Theory Sum Rule for the Shear Channel*, *Phys.Rev.* **D82** (2010) 054504, [`arXiv:1005.2686`].
97. J. I. Kapusta and E. V. Shuryak, *Weinberg type sum rules at zero and finite temperature*, *Phys. Rev.* **D49** (1994) 4694–4704, [`hep-ph/9312245`].
98. L. Giusti and M. Luscher, *Chiral symmetry breaking and the Banks–Casher relation in lattice QCD with Wilson quarks*, *JHEP* **03** (2009) 013, [`arXiv:0812.3638`].
99. G. Ford, M. Kac, and P. Mazur, *Statistical Mechanics of Assemblies of Coupled Oscillators*, *J. Math. Phys.* **6** (1965) 604.
100. C. Gardiner and P. Zoller, *Quantum Noise*, . Springer-Verlag Berlin.
101. P. Kovtun and L. G. Yaffe, *Hydrodynamic fluctuations, long time tails, and supersymmetry*, *Phys.Rev.* **D68** (2003) 025007, [`hep-th/0303010`].
102. D. Scalapino and H.-B. Schuttler, *On the calculation of time correlation functions in quantum systems: Path integral techniques*, *Phys. Rev. Lett.* **55** (1985) 12041207.
103. M. Luscher, *Construction of a Selfadjoint, Strictly Positive Transfer Matrix for Euclidean Lattice Gauge Theories*, *Commun.Math.Phys.* **54** (1977) 283.
104. K. G. Wilson, *Confinement of quarks*, *Phys. Rev.* **D10** (1974) 2445–2459.
105. K. Symanzik, *Continuum Limit and Improved Action in Lattice Theories. 1. Principles and phi**4 Theory*, *Nucl. Phys.* **B226** (1983) 187.
106. M. Luescher, S. Sint, R. Sommer, and P. Weisz, *Chiral symmetry and O(a) improvement in lattice QCD*, *Nucl. Phys.* **B478** (1996) 365–400, [`hep-lat/9605038`].
107. M. Luscher, S. Sint, R. Sommer, P. Weisz, and U. Wolff, *Nonperturbative O(a) improvement of lattice QCD*, *Nucl.Phys.* **B491** (1997) 323–343, [`hep-lat/9609035`].
108. **ALPHA collaboration** Collaboration, K. Jansen and R. Sommer, *O(alpha) improvement of lattice QCD with two flavors of Wilson quarks*, *Nucl.Phys.* **B530** (1998) 185–203, [`hep-lat/9803017`].
109. **CP-PACS Collaboration, JLQCD Collaboration** Collaboration, S. Aoki *et. al.*, *Nonperturbative O(a) improvement of the Wilson quark action with the RG-improved gauge action using the Schrodinger functional method*, *Phys.Rev.* **D73** (2006) 034501, [`hep-lat/0508031`].
110. J. B. Kogut and L. Susskind, *Hamiltonian Formulation of Wilson's Lattice Gauge Theories*, *Phys.Rev.* **D11** (1975) 395.
111. M. Golterman, *Applications of chiral perturbation theory to lattice QCD*, `arXiv:0912.4042`.
112. D. B. Kaplan, *A Method for simulating chiral fermions on the lattice*, *Phys.Lett.* **B288** (1992) 342–347, [`hep-lat/9206013`].
113. Y. Shamir, *Chiral fermions from lattice boundaries*, *Nucl.Phys.* **B406** (1993) 90–106, [`hep-lat/9303005`].
114. H. Neuberger, *Exactly massless quarks on the lattice*, *Phys. Lett.* **B417** (1998) 141–144, [`hep-lat/9707022`].
115. S. Chandrasekharan and U. Wiese, *An Introduction to chiral symmetry on the lattice*, *Prog.Part.Nucl.Phys.* **53** (2004) 373–418, [`hep-lat/0405024`].
116. S. Duane, A. Kennedy, B. Pendleton, and D. Roweth, *Hybrid Monte Carlo*, *Phys.Lett.* **B195** (1987) 216–222.
117. M. Hasenbusch, *Speeding up the hybrid Monte Carlo algorithm for dynamical fermions*, *Phys.Lett.* **B519** (2001) 177–182, [`hep-lat/0107019`].
118. M. Luscher, *Schwarz-preconditioned HMC algorithm for two-flavour lattice QCD*, *Comput. Phys. Commun.* **165** (2005) 199–220, [`hep-lat/0409106`].
119. M. Clark and A. Kennedy, *Accelerating dynamical fermion computations using the rational hybrid Monte*

Carlo (RHMC) algorithm with multiple pseudofermion fields, *Phys.Rev.Lett.* **98** (2007) 051601, [`hep-lat/0608015`].

120. M. Luscher, *Lattice QCD and the Schwarz alternating procedure*, *JHEP* **0305** (2003) 052, [`hep-lat/0304007`].
121. M. Luscher, *Local coherence and deflation of the low quark modes in lattice QCD*, *JHEP* **0707** (2007) 081, [`arXiv:0706.2298`].
122. R. Babich, J. Brannick, R. Brower, M. Clark, T. Manteuffel, *et. al.*, *Adaptive multigrid algorithm for the lattice Wilson-Dirac operator*, *Phys.Rev.Lett.* **105** (2010) 201602, [`arXiv:1005.3043`].
123. M. Luscher and P. Weisz, *Locality and exponential error reduction in numerical lattice gauge theory*, *JHEP* **09** (2001) 010, [`hep-lat/0108014`].
124. H. B. Meyer, *Locality and statistical error reduction on correlation functions*, *JHEP* **01** (2003) 048, [`hep-lat/0209145`].
125. M. Luscher, *Computational Strategies in Lattice QCD*, `arXiv:1002.4232`.
126. M. Della Morte, R. Hoffmann, F. Knechtli, R. Sommer, and U. Wolff, *Non-perturbative renormalization of the axial current with dynamical Wilson fermions*, *JHEP* **0507** (2005) 007, [`hep-lat/0505026`].
127. M. Della Morte, R. Sommer, and S. Takeda, *On cutoff effects in lattice QCD from short to long distances*, *Phys.Lett.* **B672** (2009) 407–412, [`arXiv:0807.1120`].
128. S. L. Adler, J. C. Collins, and A. Duncan, *Energy-Momentum-Tensor Trace Anomaly in Spin 1/2 Quantum Electrodynamics*, *Phys.Rev.* **D15** (1977) 1712. Revised version.
129. K. Fujikawa, *Energy Momentum Tensor in Quantum Field Theory*, *Phys.Rev.* **D23** (1981) 2262.
130. H. B. Meyer and J. W. Negele, *Gluon contributions to the pion mass and light cone momentum fraction*, *Phys. Rev.* **D77** (2008) 037501, [`arXiv:0707.3225`].
131. M. Goeckeler *et. al.*, *Lattice Operators for Moments of the Structure Functions and their Transformation under the Hypercubic Group*, *Phys. Rev.* **D54** (1996) 5705–5714, [`hep-lat/9602029`].
132. J. Engels, F. Karsch, H. Satz, and I. Montvay, *Gauge Field Thermodynamics for the SU(2) Yang-Mills System*, *Nucl.Phys.* **B205** (1982) 545.
133. H. B. Meyer, *Finite Temperature Sum Rules in Lattice Gauge Theory*, *Nucl. Phys.* **B795** (2008) 230–242, [`arXiv:0711.0738`].
134. D. T. Son and M. A. Stephanov, *Real-time pion propagation in finite-temperature QCD*, *Phys. Rev.* **D66** (2002) 076011, [`hep-ph/0204226`].
135. P. Hasenfratz, S. Hauswirth, T. Jorg, F. Niedermayer, and K. Holland, *Testing the fixed point QCD action and the construction of chiral currents*, *Nucl.Phys.* **B643** (2002) 280–320, [`hep-lat/0205010`].
136. **QCDSF Collaboration** Collaboration, M. Gockeler *et. al.*, *Vacuum polarization and hadronic contribution to muon g-2 from lattice QCD*, *Nucl.Phys.* **B688** (2004) 135–164, [`hep-lat/0312032`].
137. H. B. Meyer, *Cutoff Effects on Energy-Momentum Tensor Correlators in Lattice Gauge Theory*, *JHEP* **06** (2009) 077, [`arXiv:0904.1806`].
138. S. Capitani, *Lattice perturbation theory*, *Phys.Rept.* **382** (2003) 113–302, [`hep-lat/0211036`].
139. **CP-PACS** Collaboration, Y. Namekawa *et. al.*, *Thermodynamics of SU(3) gauge theory on anisotropic lattices*, *Phys. Rev.* **D64** (2001) 074507, [`hep-lat/0105012`].
140. A. Jakovac, P. Petreczky, K. Petrov, and A. Velytsky, *Quarkonium correlators and spectral functions at zero and finite temperature*, *Phys. Rev.* **D75** (2007) 014506, [`hep-lat/0611017`].
141. T. R. Klassen, *The anisotropic Wilson gauge action*, *Nucl. Phys.* **B533** (1998) 557–575, [`hep-lat/9803010`].
142. J. Engels, F. Karsch, and T. Scheideler, *Determination of anisotropy coefficients for SU(3) gauge actions from the integral and matching methods*, *Nucl. Phys.* **B564** (2000) 303–324, [`hep-lat/9905002`].
143. R. Morrin, A. O. Cais, M. Peardon, S. M. Ryan, and J.-I. Skullerud, *Dynamical QCD simulations on anisotropic lattices*, *Phys.Rev.* **D74** (2006) 014505, [`hep-lat/0604021`].
144. H. B. Meyer, *A calculation of the bulk viscosity in SU(3) gluodynamics*, *Phys. Rev. Lett.* **100** (2008) 162001, [`arXiv:0710.3717`].
145. H.-T. Ding, A. Francis, O. Kaczmarek, F. Karsch, E. Laermann, *et. al.*, *Thermal dilepton rate and electrical conductivity: An analysis of vector current correlation functions in quenched lattice QCD*, *Phys.Rev.* **D83** (2011) 034504, [`arXiv:1012.4963`].
146. S. Gupta, *The electrical conductivity and soft photon emissivity of the QCD plasma*, *Phys. Lett.* **B597** (2004) 57–62, [`hep-lat/0301006`].
147. G. Aarts, C. Allton, J. Foley, S. Hands, and S. Kim, *Spectral functions at non-zero momentum in hot QCD*, *PoS* **LAT2006** (2006) 134, [`hep-lat/0610061`].
148. H. T. Ding, O. Kaczmarek, F. Karsch, H. Satz, and W. Soldner, *Charmonium correlators and spectral functions at finite temperature*, `arXiv:0910.3098`.
149. A. Bazavov, P. Petreczky, and A. Velytsky, *Quarkonium at Finite Temperature*, `arXiv:0904.1748`.
150. T. Matsui and H. Satz, *J/psi Suppression by Quark-Gluon Plasma Formation*, *Phys.Lett.* **B178** (1986) 416.
151. M. Laine, *How to compute the thermal quarkonium spectral function from first principles?*, *Nucl.Phys.* **A820** (2009) 25C–32C, [`arXiv:0810.1112`].
152. Y. Burnier, M. Laine, and M. Vepsalainen, *Heavy quarkonium in any channel in resummed hot QCD*, *JHEP* **0801** (2008) 043, [`arXiv:0711.1743`].
153. T. Umeda, *A constant contribution in meson correlators at finite temperature*, *Phys. Rev.* **D75** (2007) 094502, [`hep-lat/0701005`].
154. A. Mocsy and P. Petreczky, *Quarkonia correlators above deconfinement*, *Phys.Rev.* **D73** (2006) 074007, [`hep-ph/0512156`].
155. S. Datta and P. Petreczky, *Zero mode contribution in quarkonium correlators and in-medium properties of heavy quarks*, *J.Phys.G* **G35** (2008) 104114, [`arXiv:0805.1174`].
156. S. Datta, F. Karsch, P. Petreczky, and I. Wetzorke, *Behavior of charmonium systems after deconfinement*, *Phys. Rev.* **D69** (2004) 094507, [`hep-lat/0312037`].
157. H. B. Meyer, *The errant life of a heavy quark in the quark-gluon plasma*, *New J.Phys.* **13** (2011) 035008, [`arXiv:1012.0234`].

158. J. Casalderrey-Solana and D. Teaney, *Heavy quark diffusion in strongly coupled $N = 4$ Yang Mills*, *Phys. Rev.* **D74** (2006) 085012, [`hep-ph/0605199`].
159. H. B. Meyer, *A calculation of the shear viscosity in SU(3) gluodynamics*, *Phys. Rev.* **D76** (2007) 101701, [`arXiv:0704.1801`].
160. K. Huebner, F. Karsch, and C. Pica, *Correlation functions of the energy-momentum tensor in SU(2) gauge theory at finite temperature*, *Phys. Rev.* **D78** (2008) 094501, [`arXiv:0808.1127`].
161. H. B. Meyer, *The Yang-Mills spectrum from a 2-level algorithm*, *JHEP* **01** (2004) 030, [`hep-lat/0312034`].
162. H. B. Meyer, *Computing the viscosity of the QGP on the lattice*, *Prog. Theor. Phys. Suppl.* **174** (2008) 220–227, [`arXiv:0805.4567`].
163. G. Aarts and J. M. Martinez Resco, *Transport coefficients, spectral functions and the lattice*, *JHEP* **04** (2002) 053, [`hep-ph/0203177`].
164. H. B. Meyer, *Transport properties of the quark-gluon plasma from lattice QCD*, *Nucl. Phys.* **A830** (2009) 641c–648c, [`arXiv:0907.4095`].
165. G. Boyd *et. al.*, *Thermodynamics of SU(3) Lattice Gauge Theory*, *Nucl. Phys.* **B469** (1996) 419–444, [`hep-lat/9602007`].
166. T. Kunihiro and Y. Minami, *Toward Identifying the QCD Critical Point: Attenuation of the sound mode around the critical point*, *PoS* **CPOD2009** (2009) 014, [`arXiv:0908.2710`].
167. **WHOT-QCD Collaboration** Collaboration, H. Ohno *et. al.*, *An application of the variational analysis to calculate the meson spectral functions*, *PoS* **LATTICE2010** (2010) 209, [`arXiv:1011.1728`].
168. F. Karsch and H. W. Wyld, *Thermal Green's Functions and Transport Coefficients on the lattice*, *Phys. Rev.* **D35** (1987) 2518.
169. J. Serene and H. Vidberg, *Solving the Eliashberg equations by means of N-point Pad approximants*, *Journal of Low Temperature Physics* **29** (1977) 179–192.
170. D. Thirumalai and B. J. Berne, *On the calculation of time correlation functions in quantum systems: Path integral techniques*, *Journal of Chemical Physics* **79** (1983) 5029–5033.
171. M. Jarrell and O. Biham, *Dynamical approach to analytic continuation of quantum Monte Carlo data*, *Phys. Rev. Lett.* **63** (1989) 25042507.
172. J. Gubernatis, M. Jarrell, R. Silver, and D. Sivia, *Quantum Monte Carlo simulations and maximum entropy: Dynamics from imaginary-time data*, *Phys.Rev.* **B44** (1991) 6011–6029.
173. J. Gubernatis and M. Jarrell, *Bayesian inference and the analytic continuation of imaginary-time quantum Monte Carlo data*, *Physics Reports* **269** (1996) 133–195.
174. S. Koonin, D. Dean, and K. Langanke, *Shell model Monte Carlo methods*, *Phys.Rept.* **278** (1997) 1–77, [`nucl-th/9602006`].
175. O. Gunnarsson, M. W. Haverkort, and G. Sangiovanni, *Analytical continuation of imaginary axis data for optical conductivity*, *Phys. Rev. B* **82** (Oct, 2010) 165125.
176. A. S. Mishchenko, N. V. Prokof'ev, A. Sakamoto, and B. V. Svistunov, *Diagrammatic quantum monte carlo study of the fröhlich polaron*, *Phys. Rev. B* **62** (Sep, 2000) 6317–6336.
177. I. Krivenko and A. Rubtsov, *Analytical Continuation of Quantum Monte Carlo Data: Optimal Stochastic Regularization Approach*, `cond-mat/0612233`.
178. M. Laine, O. Philipsen, P. Romatschke, and M. Tassler, *Real-time static potential in hot QCD*, *JHEP* **03** (2007) 054, [`hep-ph/0611300`].
179. G. Cuniberti, E. De Micheli, and G. A. Viano, *Reconstructing the thermal Green functions at real times from those at imaginary times*, *Commun. Math. Phys.* **216** (2001) 59–83.
180. M. Bertero, P. Boccacci, and E. Pike, *On the Recovery and Resolution of Exponential Relaxation Rates from Experimental Data: A Singular-Value Analysis of the Laplace Transform Inversion in the Presence of Noise*, *Proceedings of the Royal Society of London* **383** (1982) 15–29.
181. W. H. Press, S. A. Teukolsky, W. T. Vetterling, and B. P. Flannery, *Numerical Recipes: The Art of Scientific Computing*, . Cambridge, UK: Univ. Pr. (2007).
182. Y. Burnier, M. Laine, and L. Mether, *A Test on analytic continuation of thermal imaginary-time data*, `arXiv:1101.5534`.
183. Y. Nakahara, M. Asakawa, and T. Hatsuda, *Hadronic spectral functions in lattice QCD*, *Phys. Rev.* **D60** (1999) 091503, [`hep-lat/9905034`].
184. M. Asakawa, T. Hatsuda, and Y. Nakahara, *Maximum entropy analysis of the spectral functions in lattice QCD*, *Prog. Part. Nucl. Phys.* **46** (2001) 459–508, [`hep-lat/0011040`].
185. G. Aarts, C. Allton, J. Foley, S. Hands, and S. Kim, *Spectral functions at small energies and the electrical conductivity in hot, quenched lattice QCD*, *Phys. Rev. Lett.* **99** (2007) 022002, [`hep-lat/0703008`].
186. J. Engels and O. Vogt, *Longitudinal and transverse spectral functions in the three-dimensional O(4) model*, *Nucl.Phys.* **B832** (2010) 538–566, [`arXiv:0911.1939`].
187. O. Gunnarsson, M. W. Haverkort, and G. Sangiovanni, *Analytical continuation of imaginary axis data using maximum entropy*, *Phys. Rev. B* **81** (Apr, 2010) 155107.
188. M. A. York and G. D. Moore, *Second order hydrodynamic coefficients from kinetic theory*, *Phys.Rev.* **D79** (2009) 054011, [`arXiv:0811.0729`].
189. S. Pu, T. Koide, and D. H. Rischke, *Does stability of relativistic dissipative fluid dynamics imply causality?*, *Phys.Rev.* **D81** (2010) 114039, [`arXiv:0907.3906`].
190. H. B. Meyer, *Glueball matrix elements: a lattice calculation and applications*, *JHEP* **01** (2009) 071, [`arXiv:0808.3151`].
191. Y. Chen *et. al.*, *Glueball spectrum and matrix elements on anisotropic lattices*, *Phys. Rev.* **D73** (2006) 014516, [`hep-lat/0510074`].
192. G. D. Moore and O. Saremi, *Bulk viscosity and spectral functions in QCD*, *JHEP* **09** (2008) 015, [`arXiv:0805.4201`].
193. N. Iqbal and H. B. Meyer, *Spatial correlators in strongly coupled plasmas*, *JHEP* **11** (2009) 029, [`arXiv:0909.0582`].
194. C. Sachrajda and G. Villadoro, *Twisted boundary conditions in lattice simulations*, *Phys.Lett.* **B609** (2005) 73–85, [`hep-lat/0411033`].
195. P. F. Bedaque, *Aharonov-Bohm effect and nucleon nucleon phase shifts on the lattice*, *Phys.Lett.* **B593** (2004) 82–88, [`nucl-th/0402051`].

196. J. Chao, M. Braby, and T. Schafer, *Viscosity spectral functions of the dilute Fermi gas in kinetic theory*, *New J.Phys.* **13** (2011) 035014, [`arXiv:1012.0219`].
197. E. Taylor and M. Randeria, *Viscosity of strongly interacting quantum fluids: spectral functions and sum rules*, *Phys.Rev.* **A81** (2010) 053610, [`arXiv:1002.0869`].
198. D. T. Son and E. G. Thompson, *Short-distance and short-time structure of a unitary Fermi gas*, *Phys.Rev.* **A81** (2010) 063634, [`arXiv:1002.0922`].